ALFRED-WEGENER-INSTITUT
HELMHOLTZ-ZENTRUM FÜR POLAR- UND MEERESFORSCHUNG

685
2015

Berichte
zur Polar- und Meeresforschung

Reports on Polar and Marine Research

The Expedition PS86 of the Research Vessel POLARSTERN to the Arctic Ocean in 2014

Edited by
Antje Boetius
with contributions of the participants

HELMHOLTZ GEMEINSCHAFT

Die Berichte zur Polar- und Meeresforschung werden vom Alfred-Wegener-Institut, Helmholtz-Zentrum für Polar- und Meeresforschung (AWI) in Bremerhaven, Deutschland, in Fortsetzung der vormaligen Berichte zur Polarforschung herausgegeben. Sie erscheinen in unregelmäßiger Abfolge.

Die Berichte zur Polar- und Meeresforschung enthalten Darstellungen und Ergebnisse der vom AWI selbst oder mit seiner Unterstützung durchgeführten Forschungsarbeiten in den Polargebieten und in den Meeren.

Die Publikationen umfassen Expeditionsberichte der vom AWI betriebenen Schiffe, Flugzeuge und Stationen, Forschungsergebnisse (inkl. Dissertationen) des Instituts und des Archivs für deutsche Polarforschung, sowie Abstracts und Proceedings von nationalen und internationalen Tagungen und Workshops des AWI.

Die Beiträge geben nicht notwendigerweise die Auffassung des AWI wider.

Herausgeber
Dr. Horst Bornemann

Redaktionelle Bearbeitung und Layout
Birgit Chiaventone

Alfred-Wegener-Institut
Helmholtz-Zentrum für Polar- und Meeresforschung
Am Handeshafen 12
27570 Bremerhaven
Germany

www.awi.de
www.reports.awi.de

The Reports on Polar and Marine Research are issued by the Alfred Wegener Institute, Helmholtz Centre for Polar and Marine Research (AWI) in Bremerhaven, Germany, succeeding the former Reports on Polar Research. They are published at irregular intervals.

The Reports on Polar and Marine Research contain presentations and results of research activities in polar regions and in the seas either carried out by the AWI or with its support.

Publications comprise expedition reports of the ships, aircrafts, and stations operated by the AWI, research results (incl. dissertations) of the Institute and the Archiv für deutsche Polarforschung, as well as abstracts and proceedings of national and international conferences and workshops of the AWI.

The papers contained in the Reports do not necessarily reflect the opinion of the AWI.

Editor
Dr. Horst Bornemann

Editorial editing and layout
Birgit Chiaventone

Alfred-Wegener-Institut
Helmholtz-Zentrum für Polar- und Meeresforschung
Am Handeshafen 12
27570 Bremerhaven
Germany

www.awi.de
www.reports.awi.de

Titel: Das Hybrid-ROV Nereid Under Ice (NUI) des Deep Submergence Laboratory am Ozeanographischen Institut in Woods Hole (WHOI, USA) vor einem Taucheinsatz (Foto von Christian Katlein, Alfred-Wegener-Institut, 21. Juli 2014).

Cover: The Hybrid ROV Nereid Under Ice (NUI) of the Deep Submergence Laboratory at the Oceanographic Institute in Woods Hole (WHOI, USA) before a dive mission (picture taken by Christian Katlein, Alfred Wegener Insitute, 21st of July 2014).

The Expedition PS86 of the Research Vessel POLARSTERN to the Arctic Ocean in 2014

Edited by

Antje Boetius

with contributions of the participants

Please cite or link this publication using the identifiers
hdl:10013/epic.44857 or http://hdl.handle.net/10013/epic.44857 and
doi:10.2312/BzPM_0685_2015 or http://doi.org/10.2312/BzPM_0685_2015

ISSN 1866-3192

PS86 (ARK-XXVIII/3)

7 July 2014 - 3 August 2014

Tromsø - Tromsø

Chief Scientist
Antje Boetius

Coordinator
Rainer Knust

Contents

1.	Zusammenfassung und Fahrtverlauf		2
	Summary and Itinerary		7
2.	Weather Conditions during PS86		11
3.	Hydroacoustics		15
	3.1	Bathymetry - Hydrosweep	15
	3.2	Sub-bottom profiling - Parasound	20
	3.3	Acoustic navigation - Posidonia	23
4.	Seismology		25
	4.1	Installation of seismometers on ice floes	26
	4.2	Deployment of an ocean bottom Seismometer under sea ice	28
5.	Heat Flow		33
6.	Marine Geology		40
	6.1	Sediments	40
	6.2.	Hard rocks	46
7.	Oceanography		49
8.	Biogeochemistry and Biology		56
	8.1.	Plume chemistry and microbiology	56
	8.2.	OFOS Mapping	59
	8.3.	Sediment biogeochemistry	67
9.	Sea Ice Observations		70
10.	Technology Development: Use Of HROV NUI For Under Ice Research		77
11.	Seabirds And Marine Mammals At Sea Distribution		97
APPENDIX			102
A.1	Teilnehmende Institute / Participating Institutions		103
A.2	Fahrtteilnehmer / Cruise Participants		105
A.3	Schiffsbesatzung / ship's crew		107
A.4	Stationsliste / Station List Ps 86		108
A.5	Marine Geology		115

1. ZUSAMMENFASSUNG UND FAHRTVERLAUF

Antje Boetius (AWI)

Die Expedition PS86 (ARK-XXVIII/3) AURORA ist der Untersuchung von geophysikalischen, geologischen, geochemischen und biologischen Prozessen an Hydrothermalquellen des Gakkelrückens gewidmet. Die ultralangsamen Spreizungszonen der Arktis und des Südwestindischen Rückens führen Vent-Systeme und sind seismisch aktiv. Die tektonischen, magmatischen und biogeochemischen Prozesse an beiden Rückensystemen sind aber bisher kaum verstanden, da sie in fernen und klimatisch schwierigen Arbeitsgebieten liegen. Unser Zielgebiet der Expedition AURORA (PS86) ist das Aurora Hydrothermalquellen Feld, das 2001 während der gemeinsamen AMORE Expedition mit zwei Eisbrechern, der FS *Polarstern* und der USCGC *Healy* entdeckt wurde. Das Aurora Feld liegt in 4.000 m Wassertiefe bei 82°53'N und 6°15'W am südlichen Ende der Westlichen Vulkanischen Zone. Hier wurden in 2001 in der Wassersäule Austritte hydrothermaler Fluide kartiert, ein frischer Schwefel-Schlot gedredgt und interessante Videosequenzen vom Meeresboden aufgezeichnet, die auf aktiven Hydrothermalismus sowie auf das Vorkommen von Vent-Ökosystemen hindeuten. Seit 2001 ist dieses vielversprechende Untersuchungsgebiet wegen der schwierigen Lage und starken Eisbedeckung aber nicht weiter untersucht worden. Unser Arbeitsprogramm zielt darauf ab, die Morphologie, seismische Aktivität, Geophysik, Biogeochemie, Petrologie und die faunistische Zusammensetzung des Aurora Feldes zu untersuchen. Ein erheblicher Anteil der geplanten Forschung trägt zum Programm „Geosphären-Biosphären Interaktion“ des Exzellenzcluster MARUM an der Universität Bremen bei. Wir sind ein Team von 47 Wissenschaftlern und Technikern aus acht verschiedenen Ländern, die zusammen sowohl an dem bisher unbekannten Hydrothermalquellensystem des Gakkelrückens arbeiten, wie auch den Zustand und die Änderung des Meereissystems der Region nördlich von Grönland untersuchen wollen. Eine besonderes Vorhaben zur Weiterentwicklung mariner Robotik ist der erste Einsatz des nagelneuen Hybridroboters des Woods Hole Oceanographic Institution (WHOI, USA). Das ROV NUI wurde dafür gebaut, physikalische, chemische und biologische Beobachtungen direkt unter den Eisschollen über größere räumliche Distanzen zu sammeln.

Die Expedition AURORA (PS86) begann am Morgen des 7. August in Tromsø, Norwegen, nach einer zweitägigen Verzögerung aufgrund von logistischen Problemen mit der Bereitstellung von Brennstoff für *Polarstern*. Von Tromsø aus dampften wir nordwärts entlang des Ostgrönländischen Schelfes, aufgrund einer breiten Öffnung der Polynya im Westen der Framstraße. Auf der Anfahrt zum Zielgebiet begann die Forschung zunächst mit Beobachtungen von Meeresvögeln und -Säugetieren durch das Labor für Polarökologie. Die Beobachtungen sind Teil einer Langzeitstudie seit 1988. In der Nacht des 9.-10. Juli erreichten wir bei etwa 78°N und 5°W die Eiskante und starteten die Eisbeobachtungen. Stündliche Meereisbeobachtungen von der Brücke beschreiben die aktuelle Situation und sichtbaren Eigenschaften des Meereises. Wir waren von mehrjährigem Eis mit einer Dicke von ca. 2 Metern umgeben, das Anfang Juli noch eine Schneedecke von durchschnittlich 15 cm aufwies. Es war durch wenige große und viele kleine Schollen charakterisiert und zeigte in unserem weiteren Arbeitsgebiet zwischen 82-83°N nur 80-90 % Eisbedeckung für den größten Teil der Reise (Abb. 1.1).

Die Stationsarbeiten begannen am Morgen des 11. Juli um 8:00 mit XCTD-Würfen (Station PS86/001; 81° 17'N, 9°W) in Wassertiefen ab 300 m. In engen Abständen über den Kontinentalrand von Grönland bis ins Arbeitsgebiet am Gakkelrücken wurden insgesamt 16 XCTDs geworfen, um die hydrographischen Bedingungen zusammen mit den oberflächennahen biogeochemischen Bedingungen zu erfassen. Im Laufe des 11. Juli testeten wir außerdem die Auslöser unserer Posidonia-Transponder in Tiefen von 2.500 m.

Abb. 1.1: Polarstern im grönländischen Eis (Quelle: S. Arndt).

Fig. 1.1: Polarstern in the Greenland ice (Source: S. Arndt).

Die CTD/Wasserschöpfer-Arbeiten begannen am 12. Juli, kurz nachdem wir das Zielgebiet, den Aurora Seeberg bei 82°54' N, 6°15' W und 4.000 m Wassertiefe erreicht hatten. Eine erste CTD-Station wurde am frühen Morgen des 13. Juli mit einem Tow-Yo-Survey fortgesetzt. Tow-Yo bedeutet für unsere Fahrt, dass die CTD im Bereich von 1.000 m über dem Meeresboden wiederholt gehievt und gefiert wird, um die Ausdehnung der hydrothermale Fahne zu verfolgen, die wir entsprechend der ersten Messung in 2001 auch wieder zwischen 3.600 und 3.100 m Wassertiefe entdecken. Unsere Messungen vom 14. -23. Juli mit an CTD und OFOS (Abb. 1.2) fixierten chemischen Sensoren zeigen, dass das Aurora Hydrothermalfeld noch aktiv ist. Zeitgleich mit den Arbeiten in 4 Kilometer Wassertiefe liefen auch die Helikopter-gestützte seismologische Forschung auf dem Eis und die Meereisbeobachtung auf Hochtouren, wann immer der Nebel über dem Eis sich aufklarte und Flüge möglich waren. Mehrere Landseismometer wurden in der ersten Woche der Stationsarbeiten auf Eisschollen platziert und drifteten in sicherer Entfernung um uns herum, um Erdbeben aufzuzeichnen. Die Eisarbeiten beinhalten vor allem Untersuchungen optischer Parameter und Schneedicken-Messungen, zudem werden drei Eismassenbilanz-Bojen ausgebracht. Am 15.7. setzen wir ein Ocean Bottom Seismometer (OBS) am Meeresboden in dieser eisbedeckten Region ab, und hoffen es vor Ende der Fahrt aus dem Eis bergen zu können.

Die ersten Auswertungen der Hydrosweep-Aufzeichnungen verbesserten die vorhandene Bathymetrie des Aurora Ventfeldes erheblich, wir konnten nun deutlich einen Seeberg von ca. 1x1.5 km Ausmaßen und einem Gipfel von 400 m über dem 4.200 m tiefen Meeresboden erkennen. Vom 16.7.- 18.7. fokussierten wir unsere Strategie der Suche nach dem aktiven Hydrothermalquellenfeld auf den Gipfel und die Flanken des Aurora Seeberges. Eine große hydrothermale Fahne ist vor allem südwestlich des Seeberges ausgeprägt gewesen, sie ist methanhaltig und partikelreich. Die OFOS Tauchgänge an den Fuß, die Flanken und den Gipfel des Seeberges zeigten teilweise sedimentierte Lavakissen, dicht bewachsen von verschiedenen Glasschwämmen und Seeanemonen. Die Temperaturlanze hatte dagegen nördlich des Seeberges einen Rekord an Wärmefluss gemessen, Stationen auf dem Seeberg sind unzugänglich wegen der geringen Sedimentauflage. Die mit TV MUC und Schwerelot beprobten Sedimente zeigen eine starke Stratifizierung und interessante farbige Ablagerungen, aus dem Becken konnten wir mehrere Meter Sediment gewinnen, auf dem Seeberg allerdings maximal einen Meter in der Senke und an seinen Flanken. Die *in-situ* Pumpen zeigten einen gelblichen Belag mit schwarzen Ablagerungen. Alle diese Geräte wurden im Wechsel eingesetzt, um den Ursprung der hydrothermalen Quelle zu erkennen.

Abb. 1.2: Das OFOS – Ocean Floor Observation System (AWI, Quelle: M. Molari) ist mit einer HD Photo- und Videokamera, einem Posidonia-Transponder sowie verschiedenen physikochemischen Sensoren bestückt.

Fig. 1.2: The OFOS – Ocean Floor Observation System (AWI, Source: M. Molari) is equipped with a HD Photo- and Video-camera, a Posidonia-Transponder, as well as various physicochemical sensors.

Das Hybrid-ROV Nereid Under Ice (NUI) des WHOI wurde erstmals am 18.7. für einen technischen Erprobungs-Tauchgang eingesetzt. Nereid Under Ice (NUI) ist das neueste Unterwasserroboter des „Deep Submergence Laboratory“ am Ozeanographischen Institut in Woods Hole (WHOI, USA), das in Zusammenarbeit mit der John Hopkins Universität in den

Vereinigten Staaten entwickelt wurde und dessen Einsatz auf unserer *Polarstern*-Expedition von NOAA und anderen amerikanischen Stiftungen unterstützt wurde (Abb. 1.3). Nach den ersten erfolgreichen Tests setzen wir es jeden zweiten Tag ein, um verschiedene optische, hydrographische und biogeochemische Messungen im Schmelzwasser direkt unter dem mehrjährigen Eis durchzuführen. Gleichzeitig wured die Eisscholle darüber fotografiert, vermessen und beprobt.

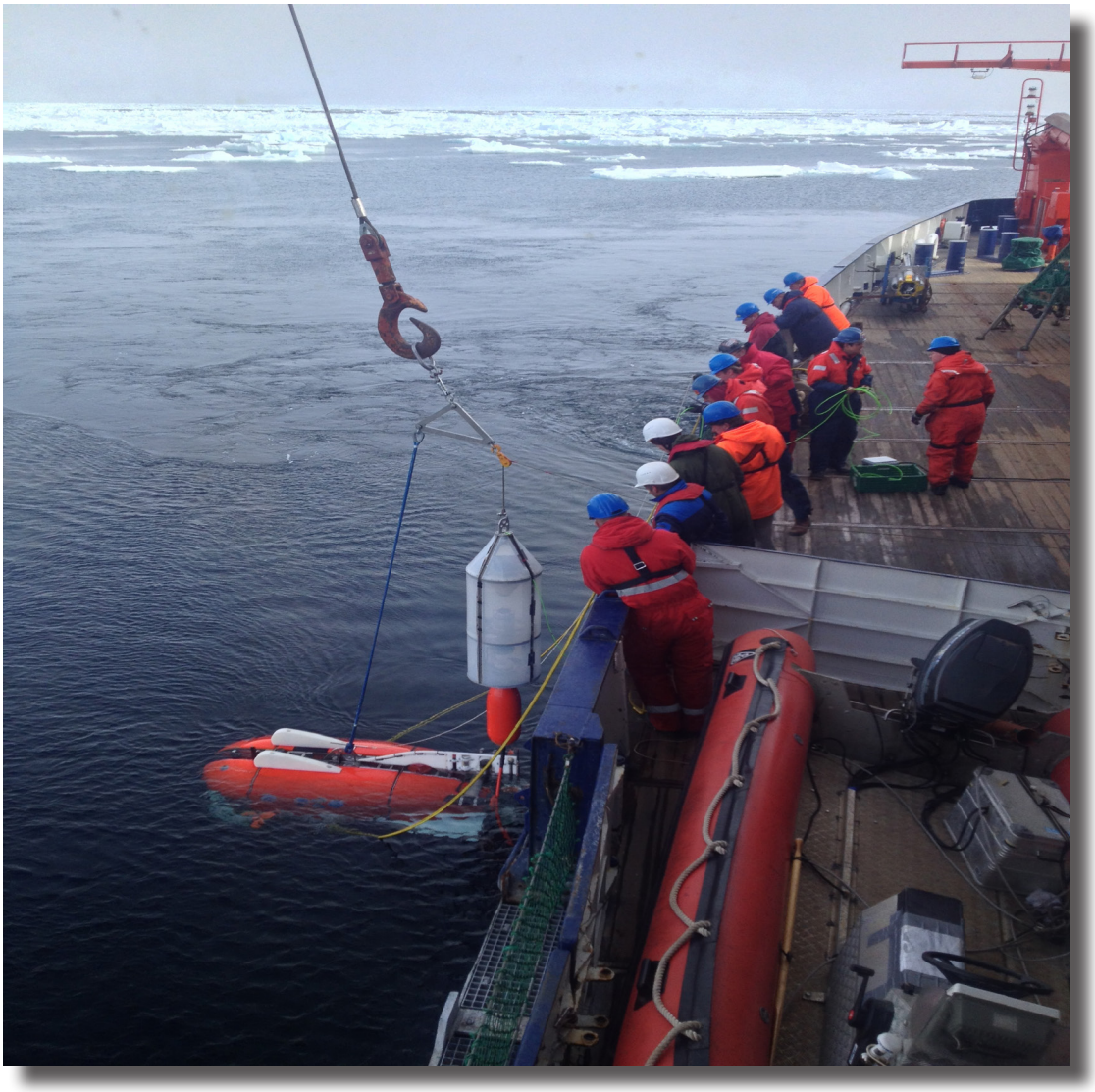

Abb. 1.3: Das Nereid Under Ice (NUI) des Woods Hole Oceanographic Institute (WHOI USA). Es ist mit einem haarfeinen Glasfaserkabel mit dem Schiff verbunden und überträgt hochauflösende Bilder sowie Multibeam Daten und Sensoren Messungen zwischen 3 und 40 m unter dem Eis.

Fig. 1.3: The Nereid Under Ice (NUI) from Woods Hole Oceanographic Institute (WHOI USA). The vehicle is connected to the vessel with a hair-thin fiber optic cable and transmits high-definition images, multibeam data, and sensor measurements from between 3 and 40 m under the ice.

Vom 19.-21. Juli besuchten wir noch zwei nördlich des Aurora-Feldes gelegene Seeberge bei 83° 00’ N und 83° 05’. Sie wurden mit dem Hydrosweep vermessen und ebenfalls mit CTD, OFOS, und Temperaturlanze beprobt. Wir fanden dort aber keine Hinweise auf rezente hydrothermale Aktivität: weder die physikochemischen Messungen mit CTD und Sensoren

noch die biologischen Beobachtungen mit dem OFOS zeigten erhöhte Faunadichten auf Felsen oder Sediment, ganz anders als am Aurora Seeberg. Die Landseismometer auf dem Eis wurden immer wieder umgesetzt, bevor sie aus dem Arbeitsgebiet herausdrifteten; das Eis bewegte sich zumeist mit einer Geschwindigkeit von 0.2-0.3 Knoten in südliche Richtung. Die Eisdrift-Richtung und -Geschwindigkeit änderte sich dabei fast täglich.

Direkt nach der Rückkehr in unser Hauptarbeitsgebiet am 22. Juli fokussierten wir uns vor allem auf den Südwesten des Aurora Seeberges, wo die meisten Temperaturanomalien in der Wassersäule und am Meeresboden zu beobachten sind. Im Wechsel der Surveys in der Wassersäule und am Meeresboden versuchten wir den Ursprung der Plume zu finden, deren Ausprägung für ein Feld aktiver schwarzer Raucher spricht. OFOS Tauchgänge vom 24.-25. Juli zeigten direkt unter dem steilen Südhang mehrere Meter breite und tiefe Krater, wie sie durch Gaseruptionen aus dem Sediment-bedeckten Meeresboden verursacht werden können. Am 26.7. unternahmen wir einen Transit in das Becken östlich vom Gakkelrücken, um eine Referenzmessung der Wärmeflüsse mit der Temperaturlanze durchzuführen und um mit einem CTD-Wasserschöpfer von vom Rücken nicht beeinflusste Proben zu erhalten. Bei Rückkehr zum Aurora Seeberg am 26. Juli fanden die nächsten auf den Süden des Seeberges ausgerichtete OFOS Tauchgänge erstmals inaktive, dicht besiedelte Schlote. Sie lagen knapp nördlich der Krater und waren über und über bewachsen mit verschiedenen Arten von Schwämmen. Die letzte Woche im Arbeitsgebiet war neben der Suche nach den Schwarzen Rauchern am Aurora Seeberg weiteren ROV Tauchgängen sowie dem Einsammeln von OBS und Landseismometern auf dem Eis gewidmet, glücklicherweise war die Eisbedeckung noch weiter zurückgegangen und auch das Wetter spielte mit. Vom 27.-29. Juli wurden die letzten Stationen nach Beendigung des Schwerelot, TV MUC und Temperaturlanzen Programms sowie nach dem letzten *in-situ* Pumpen-Einsatz auf das OFOS konzentriert, um systematisch die südliche Flanke in der Gegend um die Krater und die inaktiven Schlote abzusuchen. Erst der allerletzte OFOS Tauchgang in der Nacht vom 29. auf 30.7. brachte die erhofften Bilder: Wir fanden ein aktives Ventfeld, mit Sulfidschloten und schwarzen Rauchern am südlichen Ausläufer des Aurora Seeberges, nördlich der Krater und Canyons, unterhalb der inaktiven Schlote. Die Probennahme war am frühen Morgen des 30.07. beendet, wir traten die Rückreise durch die grönländische Polynya an, am 31. Juli kreuzten wir die Framstraße, um den Rest der Strecke nach Tromsø für die Vogel und Meeressäuger-Beobachtungen entlang des norwegischen Kontinentalrandes bei 500 m Wassertiefe abzufahren. Die letzte Station PS86/087 ist ein Test der Parasound und Hydrosweep Anlage am stark gas-emittierenden Haakon Mosby Schlammvulkan. Beide Anlagen zeigen deutlich in Tiefen von ca 1.250-500 m Wassertiefe die Gasfahnen des Schlammvulkans.

Der Transit zurück nach Bremerhaven dauerte bis zum frühen Morgen des 3. August und *Polarstern* machte um 6:00 an der Breivik Pier in Tromsø fest. Die Expedition war ein voller Erfolg, im Namen aller Fahrtteilnehmer bedanken wir uns beim Kapitän und der Crew der *Polarstern* für die hervorragende Unterstützung bei den Arbeiten auf See und die freundliche Zusammenarbeit während der Expedition AURORA (PS86).

Abb. 1.4: Gruppenfoto der Expedition AURORA (PS86). Quelle: B. Christian & S. Arndt.

Fig. 1.4: Group photo of the Expedition AURORA (PS86). Source: B. Christian & S. Arndt.

SUMMARY AND ITINERARY

The *Polarstern* expedition PS86 AURORA (ARK-XXVIII/3) aimed at studying geophysical, geological, geochemical and biological processes at hydrothermal vents of the Arctic Gakkel Ridge. Ultraslow spreading occurs at Gakkel Ridge and at the Southwest Indian Ridge, both are known to be seismically active, but little is known about their hydrothermal vent systems. Because of the remoteness and challenging climatic conditions of these study areas, the tectonic, magmatic and biogeochemical processes are poorly understood. The PS86 expedition targeted the Aurora hydrothermal vent field, which was discovered in 2001 during the AMORE expedition with the two icebreakers RV *Polarstern* and USCGC *Healy*. The Aurora vent field is located near the southern end of the Western Volcanic Zone (82°53'N, 6°15'W) at over 4,000 m water depth. The AMORE expedition detected the presence of hydrothermal fluids in the water column, recovered a fresh sulfide chimney by dredging, and recorded interesting video footage of the seabed, which indicate active hydrothermalism as well as the occurrence of vent ecosystems. Since 2001, this promising study area has not been further investigated because of its remoteness and the technical challenges of a thick ice cover. The programme of the AURORA mission aimed at investigating the morphology, seismic activity, geophysics, biogeochemistry, petrology and the faunal composition of the Aurora field. A significant part of the proposed research contributes to the programme "Geosphere-Biosphere Interaction" of the Cluster of Excellence MARUM at the University of Bremen. We were a team of 47 scientists and technicians from eight different countries working together to investigate the previously unknown hydrothermal vent systems of the Gakkel Ridge as well as the condition and change

of the sea ice cover in this region north of Greenland. Moreover, a part of the programme of this expedition was dedicated to the implementation of under-ice marine robotics, using the new hybrid robot of the Woods Hole Oceanographic Institution (WHOI, USA) for the first time. The ROV NUI was built to collect physical, chemical and biological observations directly under the ice floes and over great distances from the vessel.

The expedition AURORA (PS86) began on the morning of August 7 in Tromsø, Norway, after a two-day delay caused by logistical problems with the provision of fuel for *Polarstern*. From Tromsø we steamed northward along the East Greenland shelf, due to a wide opening of the polynya in the western Fram Strait. On the way to the target area, the research first began with observations of marine birds and mammals by the Laboratory for Polar Ecology. The observations are part of a long-term study since 1988. On the night of the 9th-10th July we reached the ice edge at about 78°N and 5°W and started the ice observations. Hourly sea ice observations from the bridge describe the current situation and visible properties of sea ice. We were surrounded by multi-year ice with a thickness of about 2 meters and a snow cover of on average 15 cm in early July. It was characterized by a few large and many small floes with a total ice coverage of only 80 to 90% in our work area (between 82 and 83°N) for most of the trip (Fig. 1.1).

The station work began on the morning of July 11 at 8:00 with XCTD deployments (station PS86/001, 81°17'N, 9°W) in water depths from 300 m. In total, 16 XCTDs were thrown at close intervals from the continental margin of Greenland to the working area on the Gakkel Ridge in order to capture the hydrographic conditions together with the subsurface biogeochemical conditions. During the July 11, we also tested the releasers of our Posidonia transponder at depths of 2,500 m.

The CTD and water sampling work began on July 12, shortly after we had reached the target area: the Aurora seamount at 82°54'N, 6°15'W and 4,000 m water depth. The first CTD station was followed by a tow-yo survey in the early morning of July 13. In our trip, a tow-yo consists of repeateadly lifting and lowering the CTD within a range of 1,000 m above the sea floor to track the extent of the hydrothermal plume. Those measurements showed that the plume occurred between 3,600 and 3,100 m water depth and are consistent with the previous results from 2001. Between the July 14 and July 23, our measurements with the CTD- and OFOS-mounted chemical sensors (Fig. 1.2) indicated that the Aurora hydrothermal field is still active. In parallel with the work at 4 km water depth, we conducted ice-based seismological work as well as air-borne sea ice observations whenever the mist condition made helicopter flights possible. In the first week of station work, several seismometers were deployed on ice floes drifting at a safe distance around *Polarstern* in order to record earthquakes. The ice work mainly included investigations of optical parameters, snow thickness measurements, and the deployment of three ice-mass balance buoys. On July 15, we deployed an Ocean bottom seismometer (OBS) on the seafloor in this ice-covered region, with the hope that we can recover it from the ice before the end of the expedition.

The first evaluations of Hydrosweep records considerably improved the existing bathymetry of the Aurora vent field, and we could then clearly see a seamount of about 1x1.5 km dimensions with a summit at 400 m above the 4,200 m deep seafloor. From July 16 to July 18 the search for the active hydrothermal vent field concentrated on the summit and the flanks of the Aurora Seamount. The large hydrothermal plume was measured particularly pronounced towards the southwest of the Seamount, especially with the presence of methane and of high particle content. The OFOS dives to the foot, the sides and the top of the Seamount show partially sedimented pillow lava, densely overgrown with various Hexactinellid sponges (glass sponges) and sea anemones. However, the temperature lance measured a record heat flow north of the seamount. Nevertheless, heat flow measurements on the seamount were not possible due

to the low sediment cover. The sediments samples that were taken with the TV-MUC and the gravity corer showed a strong stratification and interesting colored deposits. Several meters of sediment were recovered in the ocean basin. Conversely, only one meter of sediments could be recovered from the seamount valley and flanks. The *in-situ* pumps showed a yellowish material with black deposits. All of these devices were continuously swapped in order to identify and locate the hydrothermal source.

The hybrid-ROV Nereid Under Ice (NUI) of WHOI was deployed on July 18 for the first time for a technical test dive. Nereid Under Ice (NUI) is the latest underwater robot "Deep Submergence Laboratory" at the Oceanographic Institute in Woods Hole (WHOI, USA). It was developed in collaboration with the John Hopkins University in the United States and its use on this *Polarstern* expedition was funded by NOAA together with other American foundations (Fig. 1.3). After the first successful tests, NUI was deployed every second day in order to perform various optical, hydrographic and biogeochemical measurements in the melt water directly below the multiyear ice. Simultaneously, the ice was photographed, measured and sampled from above.

Between July 19 and July 21, we visited two additional seamounts located on the ridge north of the Aurora field at about 83°00'N and 83°05'N. The two sites were surveyed with Hydrosweep and investigated with the CTD, the OFOS and the temperature lance. However, no evidence of active hydrothermal activity was found: unlike at the Aurora seamount, neither the physicochemical data from the CTD and the sensors nor the biological observations with OFOS revealed increased faunal densities on the rocks and sediments. The ice-based seismometers were regularly redeployed before they drift outside of the working area. Although the ice mostly drifted southwards at a speed of 0.2 to 0.3 knots, the ice drift direction and speed appeared to change almost every day.

Upon our return to the main working area on July 22, we focused on the area southwest of the Aurora seamount, where most water column and seafloor temperature anomalies were observed. By alternating water column and seafloor surveys, we tried to locate the origin of the plume, whose expression suggests a field of active black smokers. In July 24-25, OFOS dives directly under the steep southern slope of the seamount showed craters of the several meters in width and depth, which could be the result of gas eruptions from the sediment-covered seabed. On July 26 we transit to the sediment basin east of the Gakkel ridge to perform a reference stations for the temperature lance and the CTD water samplers that would not be affected by the ridge system. On July 26, on the first OFOS dive after returning to the Aurora seamount we found the first inactive but densely populated chimneys. They are located directly north of the crater area and are covered with different types of sponges. Besides the search for black smokers, the last week in the working area is also used to the conduct further ROV dives and to recover the OBS and the ice seismometers. Fortunately for us, the ice cover has further reduced and the weather conditions are favourable, which helped carrying out these tasks effectively. On July 27-29, after the end of the sediment sampling programme (gravity corer and TV-MUC), of the heat flow measurements (temperature lance), and of the *in-situ* pumping, the last stations concentrated on OFOS deployments and aimed at systematically investigating the southwest flank of the Aurora seamount in the area where craters and inactive chimneys were found. It is not until the very last dive in the night from July 29-30 that OFOS brought the long-expected images: an active vent field with sulfide chimneys and black smokers on the southern foothills of the Aurora seamount, north of the craters and canyons and south of the inactive chimneys. The station work stopped early on July 30 and the return journey through the Greenland polynya started. We crossed the Fram Strait on July 31 in order to allow for bird and marine mammal observations along the 500 m deep Norwegian continental margin all the way back to Tromsø. The very last station PS86/087 was dedicated to testing the Parasound

and Hydrosweep systems at a site of strong gas emission such as the Haakon Mosby mud volcano. Both systems clearly detected the 1,250 - 500 m deep gas-flares of the mud volcano.

The return voyage ended on August 3 at 6:00 am when *Polarstern* moored at the Breivik Pier in Tromsø. The expedition was a great success and, in the name of all participants we thank the captain and the crew of *Polarstern* for their outstanding support during the work at sea and the friendly cooperation during the expedition AURORA (PS86).

All participants in the *Polarstern* expedition PS86 (ARK-XXVIII/3) AURORA gratefully thank Captain Stefan Schwarze and his crew, as the success of our expedition was substantially supported by their excellent cooperation and efforts. This expedition was also supported by the Helmholtz Alliance ROBEX.

2. WEATHER CONDITIONS DURING PS86

Dipl. Met. Max Miller, Juliane Hempelt DWD

On Monday, July 7, 2014 (18:00 pm), *Polarstern* left Tromsø for the campaign PS86 (ARK-XXVIII/3) with northerly winds Bft 4, only few clouds and 25°C.

The high near Bear Island hardly moved. During the night to Tuesday (July 8) we entered an extensive area of fog which got thinner near Svalbard.

During the night to Thursday (July 10) *Polarstern* reached the sea ice at 78°N 3°W. Light southerly winds on the west side of the above mentioned high caused thickening of fog. Although reconnaissance flights were impossible we made good progress towards north within the polynya off Greenland.

On Friday (July 11) the weather conditions changed. A low located north of Greenland moved eastward and *Polarstern* got at its west side. Winds veered northwest, increased up to Bft 6 and caused a temporary improvement of visibility. However, snowfalls got heavier. On Saturday (July 12) we reached our research area at 82°53'N 6°15'W. The low moved away towards Franz Josef Land and weakened. On Sunday (July 13) the north-westerly winds abated but low stratus hampered helicopter flights.

From Monday (July 14) on, a high pressure area formed between the North Pole, Svalbard and the Barents Sea. The winds veered southwards and increased up to Bft 5 from Tuesday (July 15) on. Low stratus, mist or fog permitted only a few flight operations.

While the above mentioned high moved towards Russia, a new high formed over Greenland. On Thursday (July 17) this constellation caused a weak trough over the Fram Strait, which became stable for several days. Low stratus or fog continued with weak southerly winds and moist air.

On Monday (July 21) the trough moved away towards the east. A weak ridge followed and the sky cleared up under light and variable winds.

A low moved east from Bering Strait and built a new trough towards the Fram Strait. On Tuesday (July 22) the winds veered southwards and increased up to Bft 5. The trough moved slowly eastwards and, therefore, the winds abated and veered north-westwards on Thursday (July 24).

From Friday (July 25) on, we observed a weak pressure gradient combined with westerly winds at hardly Bft 4. Again fog and low stratus dominated.

At the beginning of the return journey (Wednesday, July 30) the synoptic situation changed. A low moved from Severnaya Zemlya towards Franz Josef Land and Svalbard. On Thursday north-westerly winds increased only temporarily up to Bft 6 and the swell did not exceed 1.5 m. At the weekend a ridge got the dominant feature over northern Norway and the winds abated.

On Sunday morning (August 3, 2014), *Polarstern* reached the harbour of Tromsø under light to moderate winds.

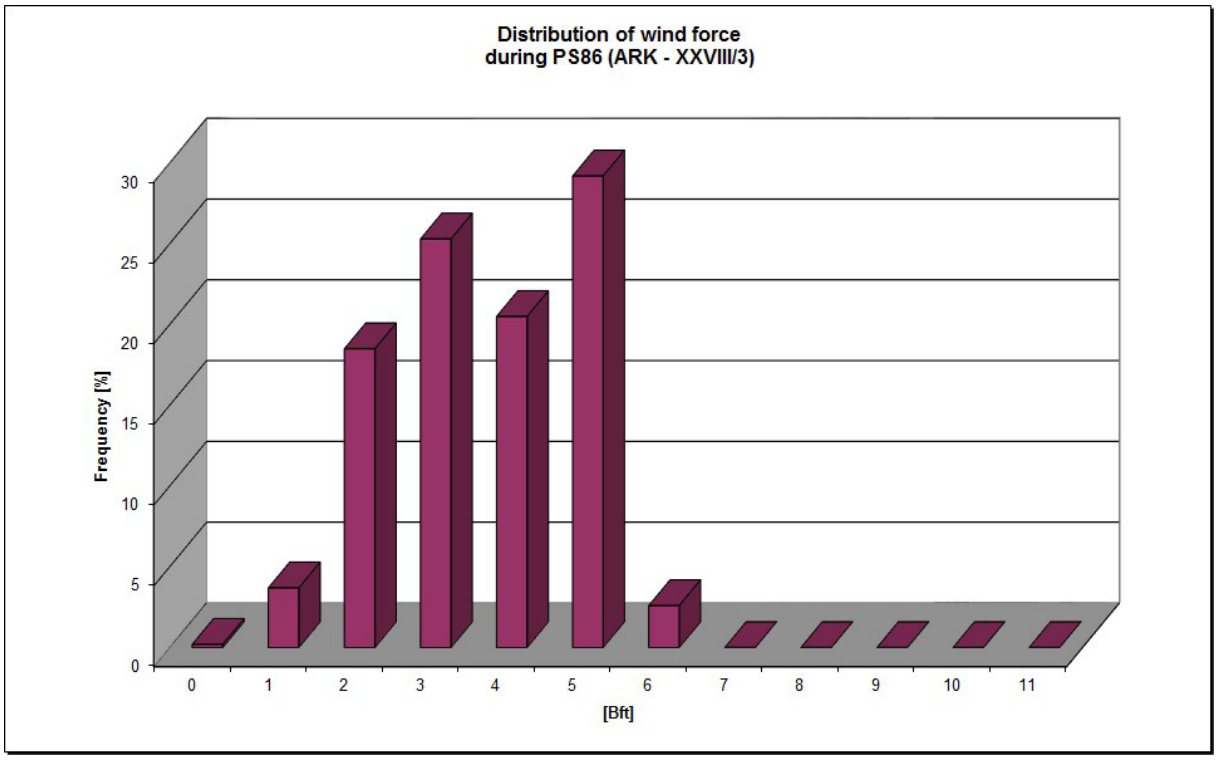

Fig. 2.1: Distribution of wind force

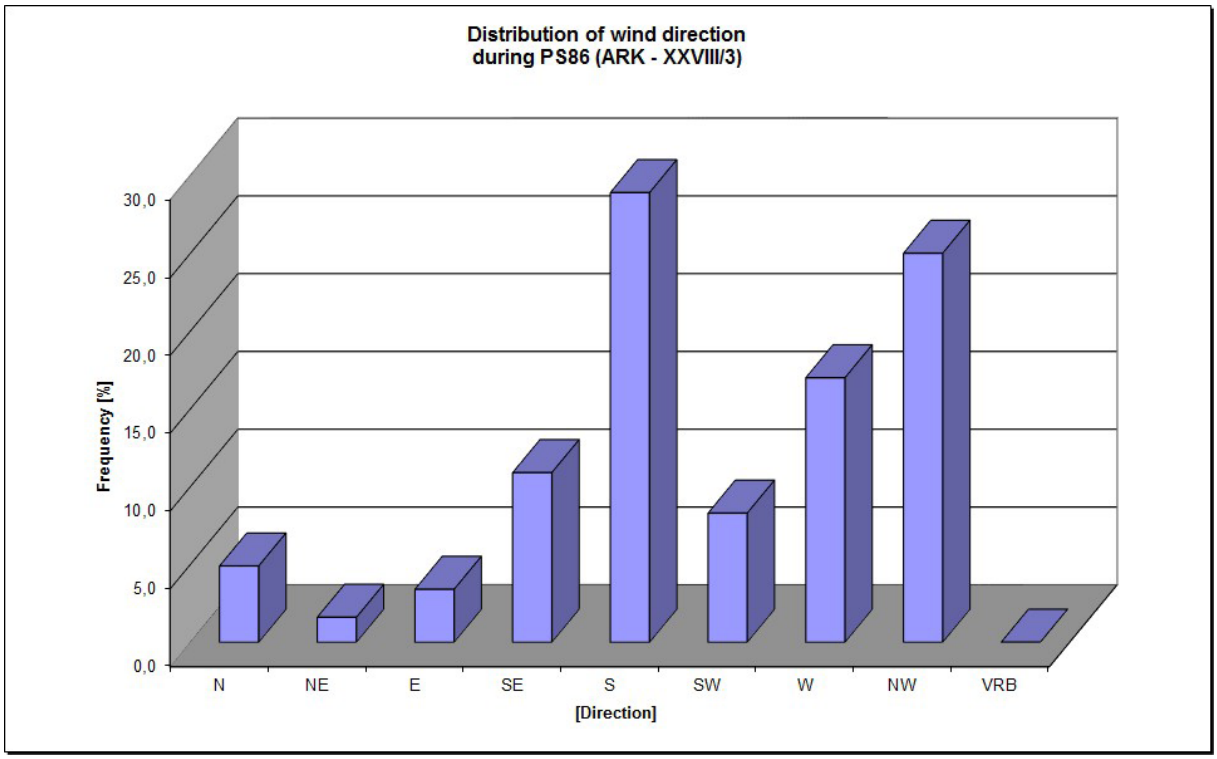

Fig. 2.2: Distribution of wind direction

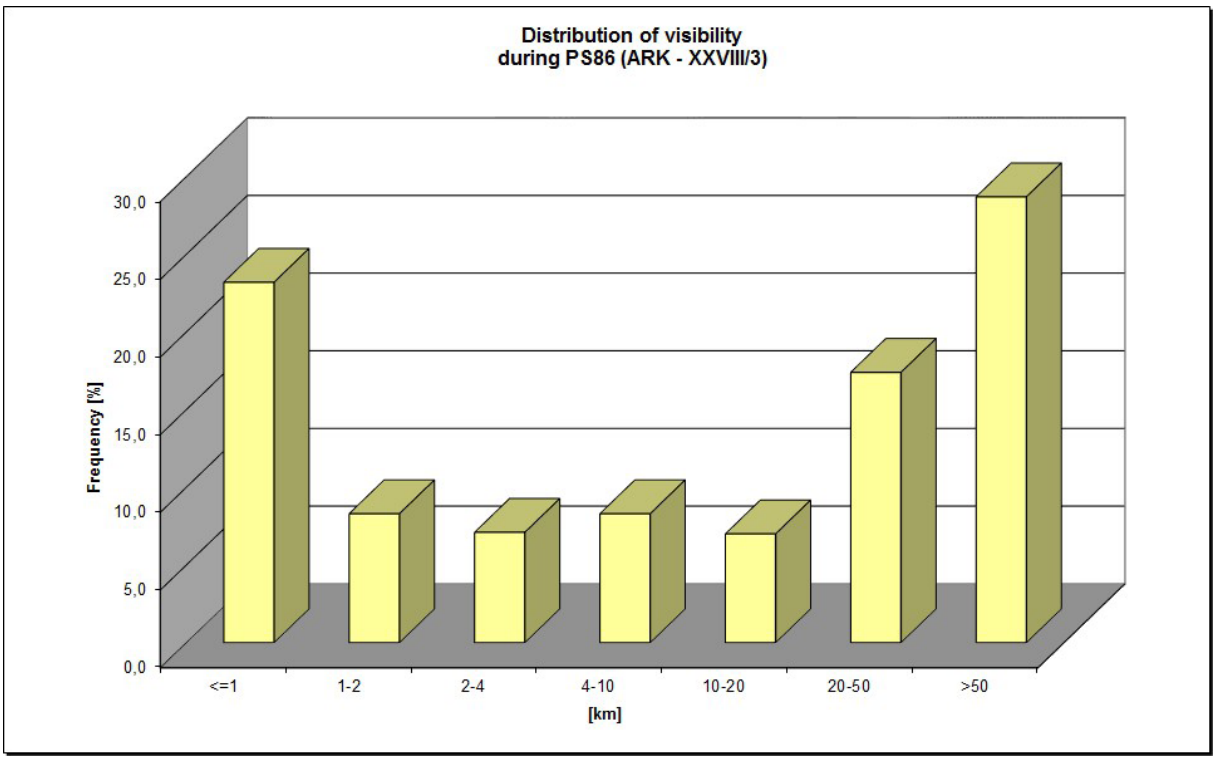

Fig. 2.3: Distribution of visibility

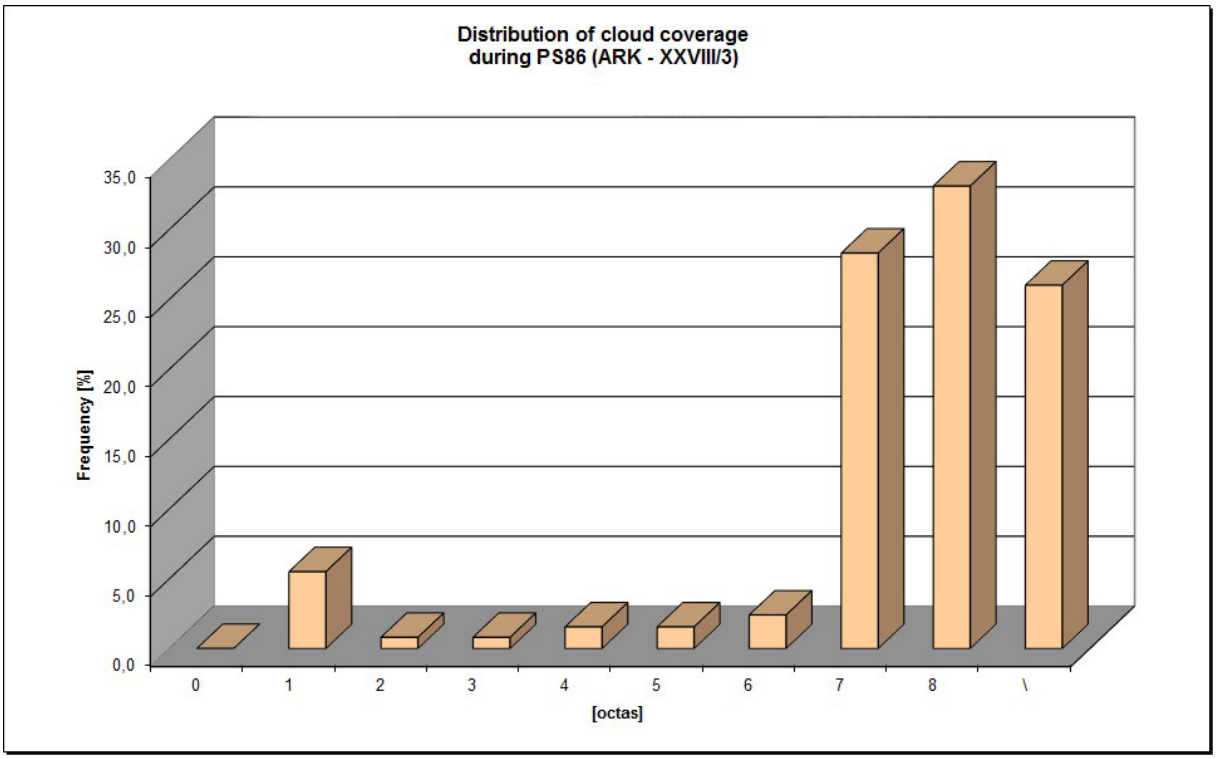

Fig. 2.4: Distribution of cloud coverage

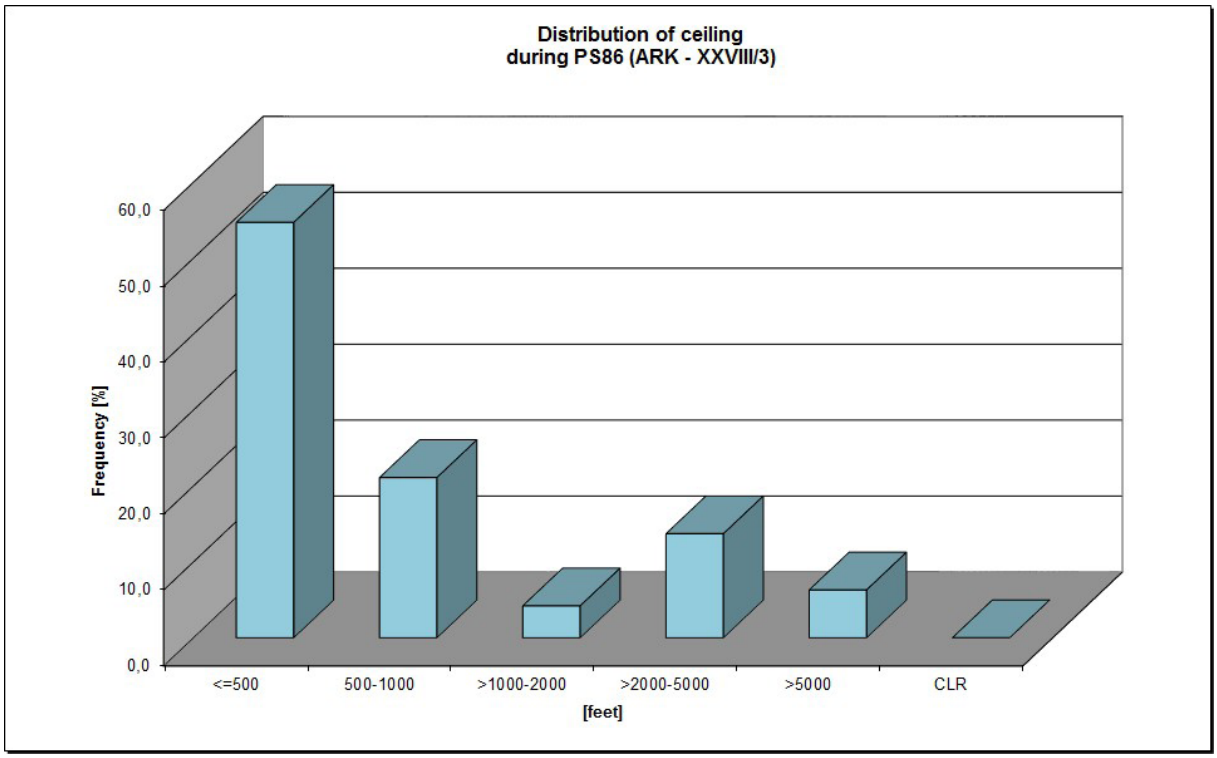

Fig. 2.5: Distribution of ceiling

3. HYDROACOUSTICS

3.1 Bathymetry - Hydrosweep

Sebastian Albrecht[1], Johannes Pliet[1] [1]FIELAX

Objectives

Most of the world's oceans' topography has still never been surveyed by echo sounders. Instead most of the existing chart data, such as those used in the IBCAO and GEBCO datasets, are derived from satellite altimetry and gravimetric data. Therefore, one objective of the mission is to acquire a full expedition track of multibeam bathymetry data that will contribute to the existing data sets.

The target research area, the Aurora vent field (82°54.1'N, 6°14.6'W), is a small mount located at 3,830 m water depth, about 200 m above the surrounding terrain. This area has already been surveyed by multibeam echosounders from the joined *Polarstern*/*Healy* expedition AMORE in 2001. During PS86 those existing data shall be enhanced by using a higher resolution multibeam echo sounding system. Also, the data are expected to be of higher quality and density due to the planned drift station work which will not be influenced by ice breaking.

Sensor description

The *Polarstern*-mounted deep sea multibeam echosounder is an Atlas Hydrosweep DS-3. Its transducer frequency ranges from 13.6 to 16.4 kHz. Each ping results in a depth profile of 141 preformed hard beams which are increased to up to 345 soft beams by algorithms. The individual beam width is approximately 2.3°, which gives a beam footprint of around 160 m at the general area depth of 4000 m. The swath width has been set to 120 % of the water depth throughout the whole mission. Peripheral sensors connected to the multibeam include a GPS receiver Trimble for position retrieving, an inertial navigation and heave sensor Raytheon Anschütz MINS2 (Marine Inertial Navigation System) for retrieving the ship's roll, pitch and heading angles and a sound velocity keel probe.

Work at sea

Hydrosweep was in operation 24 hours a day. System parameters were regularly adjusted depending on the sea and ice conditions. Beam profile and backscatter data was recorded and visualized with Hypack 2014. Water column data was not recorded as there were no relevant water column features visible. Vertical sound speed profiles from CTD or XCTD casts (kindly provided by the oceanographer's group) were regularly applied. The acquired data was processed on board using Hypack MBMAX 64bit Editor. The data was manually edited, filtered by applying matrix-based median filters and exported to grids and xyz soundings. Resulting grids were produced with GMT blockmedian and surface in a grid spacing of 50 m. These grids were regularly updated as background layers for the real time mapping tool GlobalMapper which was used for navigation display and tracking of the underwater instruments.

Preliminary results

The collected bathymetry and sub-bottom data covers a long transect (Fig. 3.1) that runs along the Norwegian shelf towards Svalbard, then, at about halfway, turns north-west through the Norwegian Basin, across the Knipovich Ridge, further north up on the Greenland shelf, through the northern part of the Lena Trough until the southern end of the Gakkel Ridge north-east of Greenland, where the Aurora vent field was discovered in 2001 by the AMORE cruise.

The transit back to Tromsø covers a long profile south along the 2,500 m contour line of the Greenland shelf, that turns south-east through Lena Trough along and partly across the Hovgaard Ridge towards the Svalbard shelf, following the 500 m depth contour line to Norway. The return track was shortly interrupted by a survey over the Håkon Mosby Mud Volcano.

The planning of both transects mainly depended on the current ice situation around Greenland in order to find the fastest way to and from the survey area. Following the 500 m depth contour line was a request from the Bird & Marine Mammals Observation group.

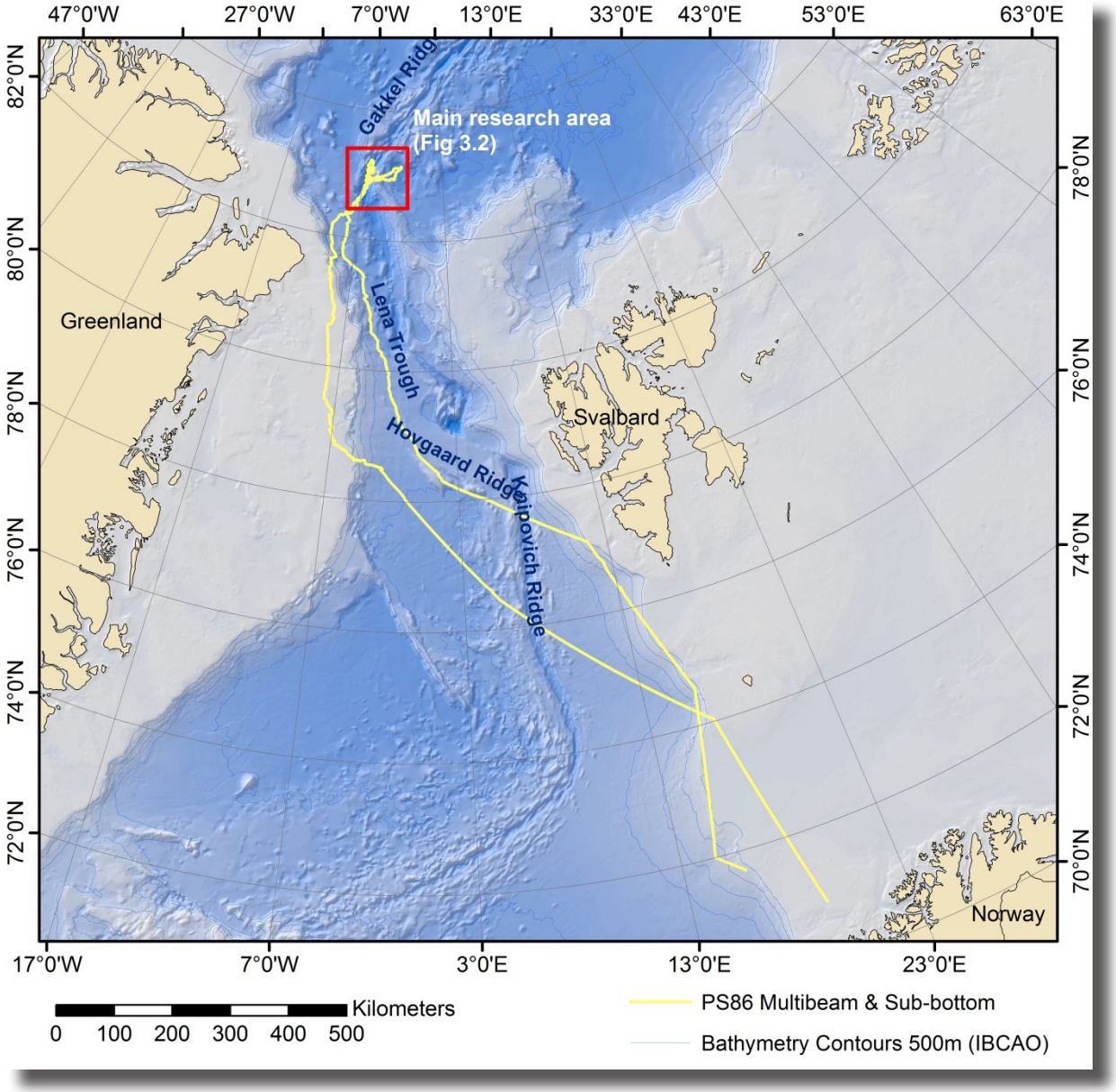

Fig. 3.1: Track (yellow) of collected Hydrosweep bathymetry and Parasound sub-bottom data collected during this mission; map projection UPS North (WGS84).

The Gakkel Ridge area around the Aurora vent field has already been charted during the AMORE cruise in 2001 with the former Hydrosweep DS-2 system of *Polarstern* (59 beams) and a Seabeam system of RV *Healy* (121 beams) (Thiede, 2001). The current Hydrosweep DS-3 provides 345 beams, which gives a higher spatial resolution and a higher density of measurements. Therefore, all data collected from the same regions further improve the local bathymetry grid (Fig. 3.2).

Additionally, three surveys of up to 12 hours each were conducted in order to fill the gaps of the AMORE bathymetry grid on the way to a reference site located outside of the existing grid. Thereby, the Johannsen Seamount and the Cagni Seamount (according to SCUFN database) were charted, which demonstrated a high deviation of more than 2,500 m between the IBCAO bathymetry grid and measured multibeam depths (Fig. 3.3).

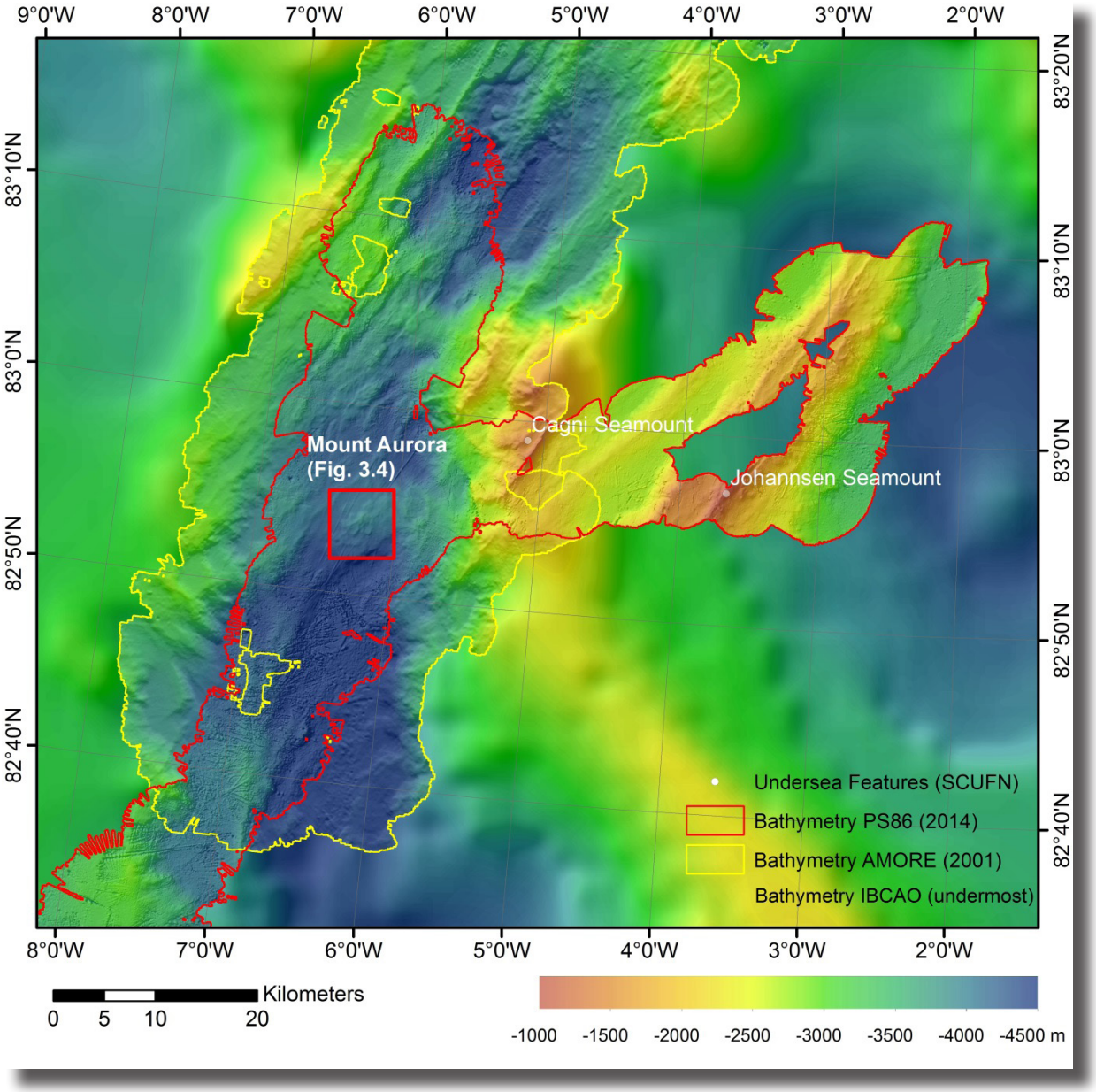

Fig. 3.2: Overlaying bathymetry grids from IBCAO charts (the under most layer), from AMORE cruise (yellow outline) and from the current cruise (red outline); projection UTM 30N; map projection UPS North (WGS84).

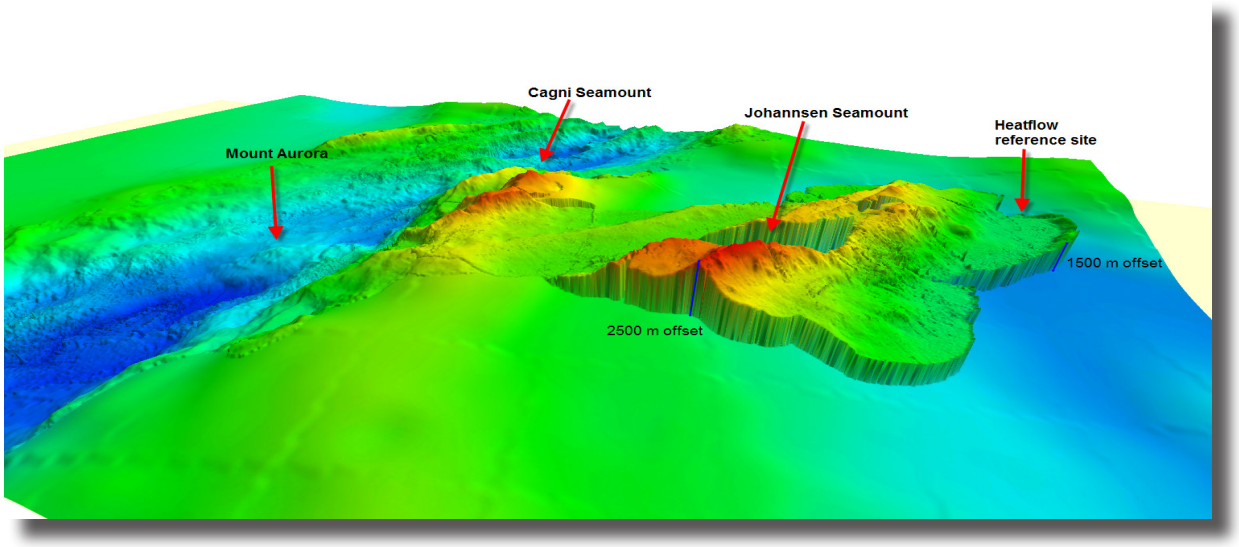

Fig. 3.3: Overlaying bathymetry grids from IBCAO charts (the under most layer), from AMORE cruise and from the current cruise (outstanding part on the right), which shows an offset of up to 2,500 m in water depth.

In the main research area at the Aurora vent field, a dense bathymetric dataset was collected during two weeks of station time (Fig. 3.4). Most of the stations were drift stations, during which the ship drifted slowly between ice floes at a maximum speed of 0.5 knot. The results include dense data of very good quality. Nevertheless the individual beam footprint of 160 m at a depth of 4,000 m physically restricts a higher spatial resolution of the bathymetric structures.

Data management

The data will be transferred to the AWI Geophysics / Bathymetry department and be made available in the scientific data warehouse PANGAEA. The available data formats are HSX (from Hypack), ASD PHF/PHS (from Atlas Hydromap Control) and a grid in GMT/NetCDF GRD, ESRI ASCII Grid and XYZ format, projected in UTM zone 30N (on ellipsoid WGS84), and in geographic coordinates (WGS84). Ship tracks are available at http://doi.pangaea.de/10.1594/PANGAEA.835512.

References

Thiede J (2002) *Polarstern* ARKTIS XVII/2 – Cruise Report: AMORE 2001, Alfred Wegener Institute for Polar and Marine Research, Berichte zur Polar- und Meeresforschung = Reports on polar and marine research 421, 397 pp.

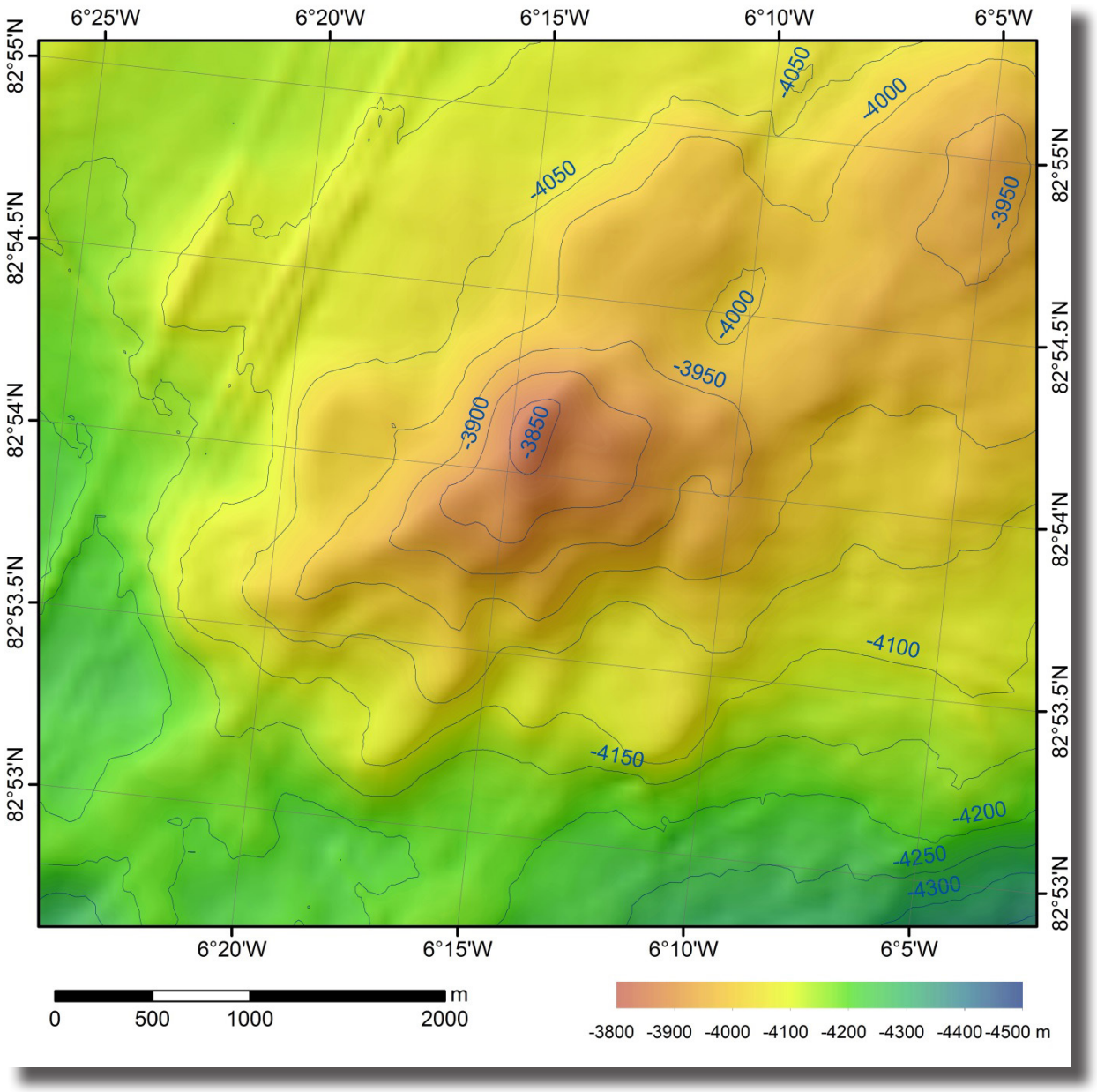

Fig. 3.4: Bathymetry grid of the main research area Aurora vent field (or Mount Aurora) retrieved from Polarstern's multibeam echosounder Hydrosweep during the PS86 expedition (50 m spatial resolution), map projection UPS North (WGS84).

3.2 Sub-bottom profiling - Parasound

Sebastian Albrecht[1], Johannes Pliet[1] [1]FIELAX

Objectives

The main objective of the sub-bottom profiling echosounder operations with the shipboard Atlas Parasound DS3 system was the detection of seafloor characteristics and sediment structures along the cruise track, which support geological analyses of the surveyed ridge system. During station work, sub-bottom data help to increase the success rate of sediment penetrating instruments (e.g. gravity corer, heat flow probe). The high frequency channel of the echosounder can be further used to detect gas flares in the water column. Such application has been successfully used with methane gas flares on previous cruises (e.g. MSM16-2). During this mission data shall be collected and analysed in order to find reflections of plumes in the water column.

Sensor description

The Atlas Parasound DS3 is a hull-mounted sub-bottom profiling echosounder on board *Polarstern*. It is used to detect the internal structures of sedimentary cover along the ship's track. To penetrate the sedimentary layers of the seafloor, a low frequency signal is required. Since a combination of a reasonably small transducer and a very narrow beam is desired the system takes advantage of the parametric effect, which results from the non-linear hydro-acoustic behaviour of water for high energy signals. The transmission of 2 high-energy wave-form signals of slightly different frequencies (20 kHz and 24 kHz) creates harmonics at the difference frequency (i. e. 4 kHz) and at the frequency sum (e. g. 44 kHz). With an opening angle of 4 x 4.5°, the system provides high resolution information of the sedimentary layers down to a depth of 200 m below sea floor. The system automatically compensates ship's movements by applying roll, pitch and heave values from the motion platform MINS. Navigation data is added by a Trimble GPS receiver (Gerchow, 2012).

Work at sea

The Parasound was in operation 24 hours a day. The echosounder parameters were set to 20.0 kHz desired primary high frequency (PHF) and 4 kHz secondary low frequency (SLF). The pulse length was adjusted between 0.5 to 1.0 ms. The system was not configured to synchronize pinging with the multibeam echosounder *Hydrosweep in order to receive a higher along-track coverage*. Interfering signals from both systems were observable but did not significantly affect the desired data information. During station time and drifting transects with towed instruments, the ship's bow thruster highly disturbed the low frequency signal. The system's pulse length was therefore set to values between 10 and 25 ms to ensure that the data would remain interpretable. However, this also resulted in a decrease of the vertical resolution and a blurring of the signal.

As for the plume-hunt, significant indications for hydro-acoustic anomalies due to plumes, active vents or gas flares were not found. Data files have been organised in daily subsets and data of both frequencies have been plotted as PNG image files.

Preliminary results

The collected Parasound data covers the same recording track than the Hydrosweep multibeam (Chapter 3.1). In the main research area the general data quality was low due to the steep slopes and cliffs of the ridge system, which resulted in a low reflection of the Parasound signals. Furthermore, during all station and drift station work the bow thrusters of the vessel were enabled, which led to a high noise level disturbing the Parasound pulses.

As for the plume-hunting, no reflections in the water column were found. To verify the echosounder gas flare detection settings, the Håkon Mosby mud volcano (HMMV) was surveyed on the transit back to Tromsø. Indeed, active gas emissions at the HMMV have been acoustically imaged during previous expeditions. There, clear signals of gas flares were detected on the 20 kHz high frequency channel (Fig. 3.5). In Fig 3.6 the corresponding sediment structure from the 4 kHz low frequency channel is shown.

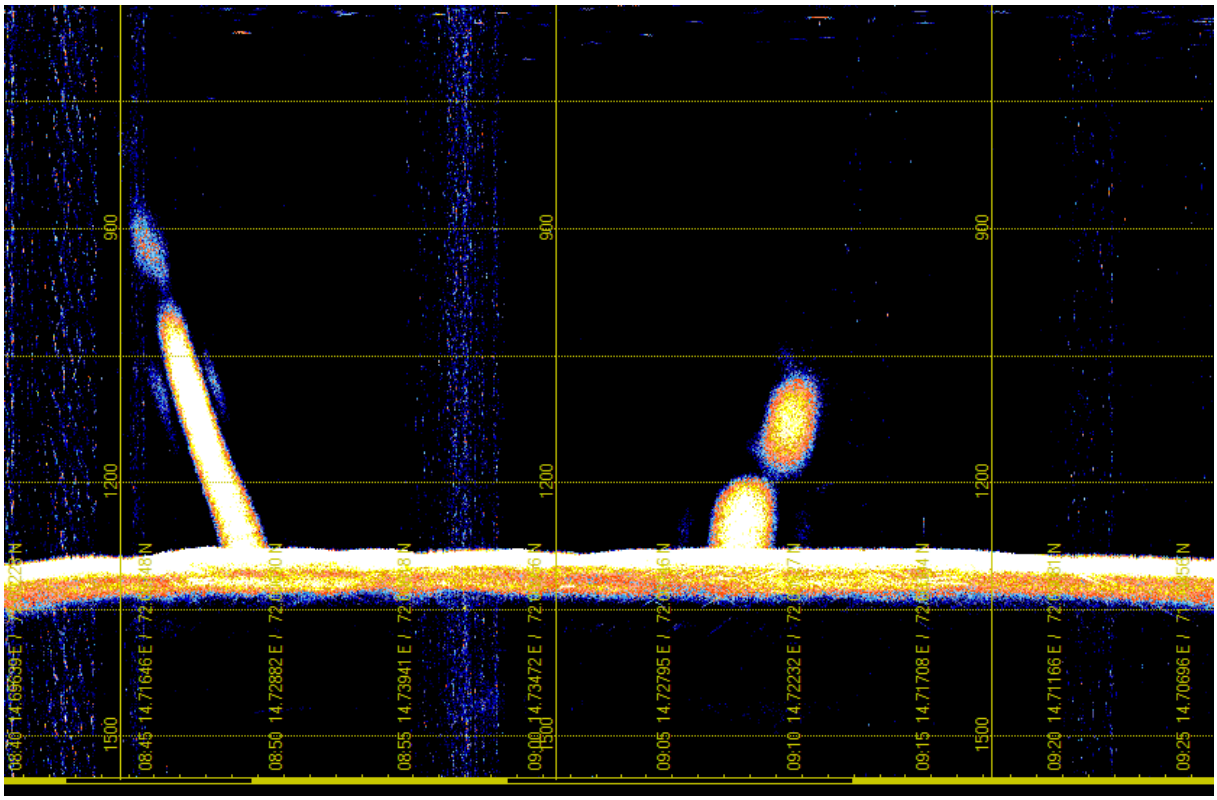

Fig. 3.5: A screenshot of the Parasound high frequency channel during the passage of the Håkon Mosby mud volcano on the way back for a successful verification of gas flare detection settings. One gas flare is visible rising up from the sea floor into the water column. The same flare was surveyed twice, from different directions.

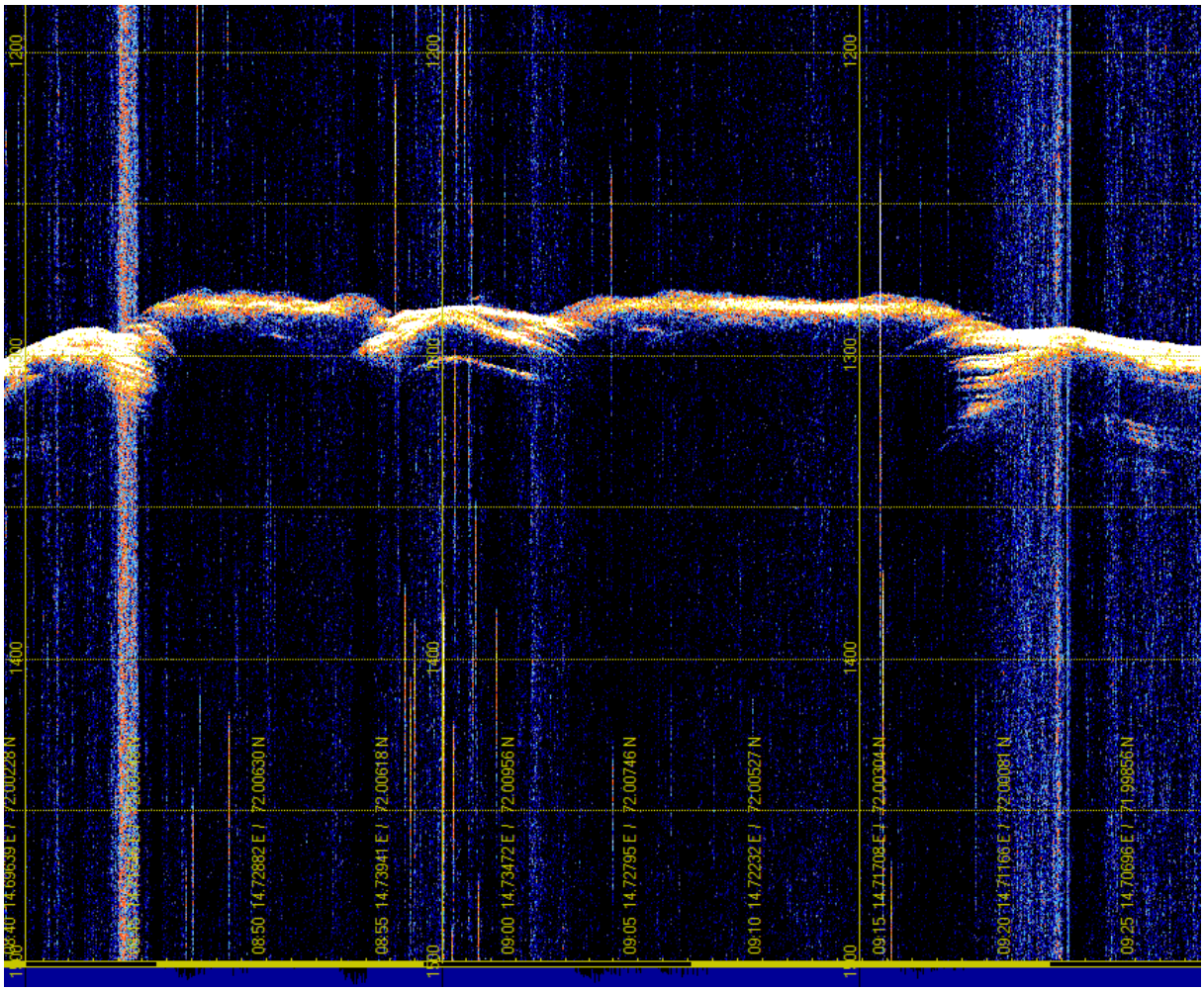

Fig. 3.6: A screenshot of the Parasound low frequency channel during the passage of the Håkon Mosby mud volcano on the way back. This corresponds spatially to Fig. 3.5 and shows the crater structure, passed two times from different directions.

Data management

The data will be transferred to the AWI Geology department and be made available in the scientific data warehouse PANGAEA. Ship tracks are available at http://doi.pangaea.de/10.1594/PANGAEA.835512.

References

Gerchow P (2012) FS *Polarstern* - Geräteakte: Sedimentecholot

3.3 Acoustic navigation - Posidonia

Sebastian Albrecht[1], Johannes Pliet[1], Yann Marcon[2]

[1]FIELAX
[2]AWI

Objectives

The shipboard acoustic navigation system IXSEA Posidonia was used to track underwater instruments during the station work. The main objective of the cruise is the plume-hunting whereby instruments like CTDs or video sleds are slowly towed by the ship. This results in an offset between the ship's and instrument's position of up to 1 km (at 4 km water depth). Also, towed instruments react very slowly to course changes of the ship. In case plume signals or interesting spots are found in CTD or imagery data, it is crucial to be able to relocate these positions for further sampling. Therefore, every towed instrument has to be equipped with a Posidonia transponder beacon.

Sensor description

The *IXSEA Posidonia* is an acoustic underwater positioning system that is used to determine and track the real-time position of underwater vehicles and instruments. The system is composed of two ultra-short baselines (USBL) consisting of four hydrophones and one main transducer. A *Posidonia* transponder beacon has to be mounted on the instrument that is to be tracked before the launch. Once the gear is lowered into the water the system's main transducer transmits an acoustic signal within a 60° wide cone at a frequency of 10.5 kHz to the water. The transponder mounted on the instrument receives this signal and replies with a 9.5 kHz acknowledge signal. This is being received by the four hydrophones of the vessel with small differences in travel time and phase from which a relative angle and distance to the transponder can be calculated. An absolute geographic transponder position and depth is calculated by applying the ship's current GPS position, the current motion state (roll, pitch and heading) and a sound velocity profile to compensate the refraction of the signal in the water column. The accuracy according to IXSEA is 0.3 % (IXSEA, 2006) of the water depth which gives a range of about 12 m at the general area depth of 4000 m. The data is continuously acquired and distributed to the ship's network for data visualization and mapping programmes.

Work at sea

The following instruments were equipped with transponders: CTD/Rosette water sampler, Ocean Floor Observation System (OFOS), TV-Multicorer, heat flow probe and gravity core. During this cruise, we used the mobile antenna array, which is mounted in the moon pool of the ship. This antenna had to be removed each time before ice-breaking and installed again for every station. Therefore, most of the datasets start when the instruments were already lowered to the water and end before the instruments reached the surface. The connected electronic processing unit was the IXBLUE USBL-BOX. The recurrence interval of the system has been set to 8 seconds. Sound velocity profiles were kindly provided by the oceanographer's CTD profiles and regularly updated. Acquired position data have been locally logged on a PC as raw NMEA telegram data. Positions of ship and transponder were both displayed in real-time with the mapping software GlobalMapper, as well as with the software PosiView (Ralf Krocker, AWI). Simultaneous tracking of several instruments with GlobalMapper is not straightforward and the raw NMEA data had to be converted into a different format. The conversion, as well as an outlier filtering, was performed in real-time using an online converter programme (Yann Marcon, AWI) that was running in the background during the entire cruise. GlobalMapper was used to display current positions and tracks from *Posidonia* together with further geographical datasets such as the bathymetry grid layers, station waypoints or points of interest (Fig. 8.5).

This highly contributed to the station work by allowing us to keep an overview of the instrument's track related to the local bathymetry and observed points at all times. Current bathymetry datasets were kindly provided by the bathymetry group on board.

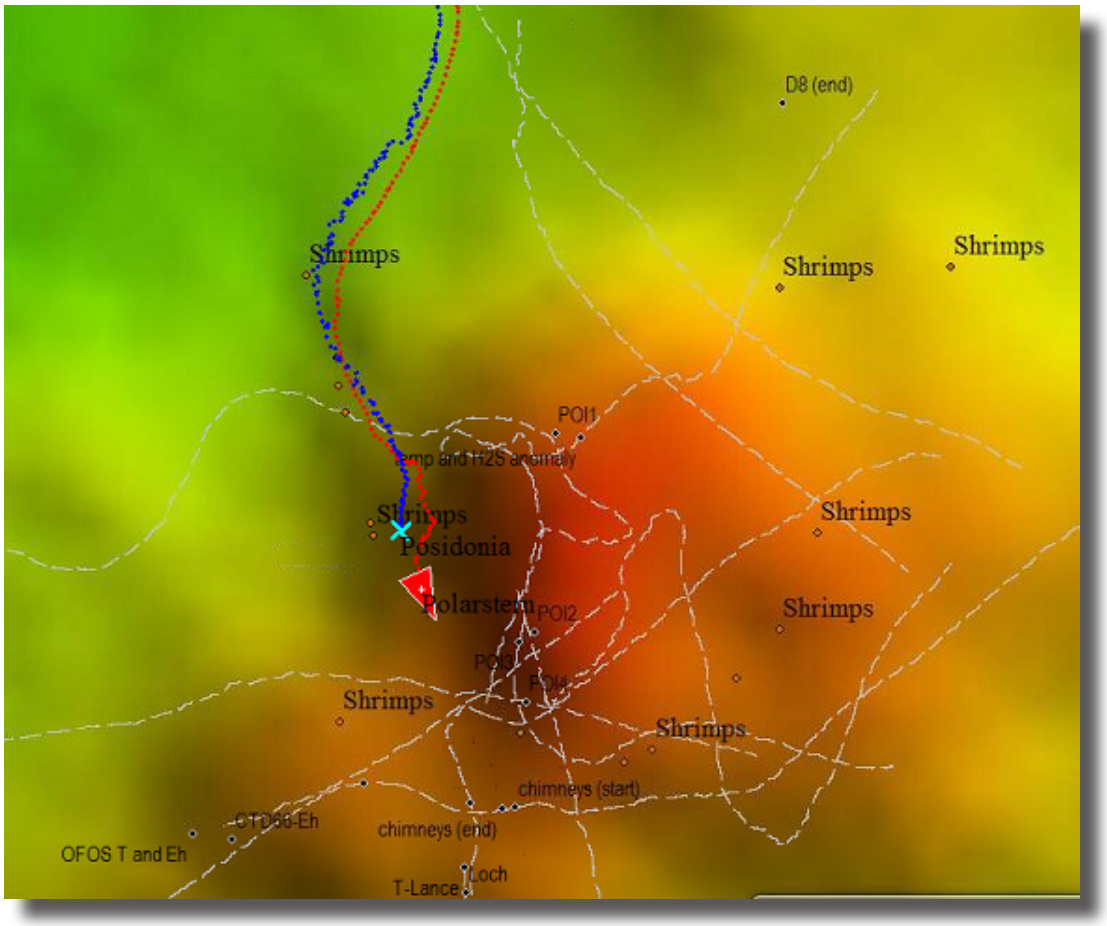

Fig. 3.7: A screenshot of the Global Mapper software used for real time plotting of an OFOS station PS86/084 showing the ship track (red) and the OFOS track (blue) together with the bathymetry, points of interest, and tracks of previous OFOS dives.

All positioning data have been post-processed on board by using a filtering/smoothing and interpolation tool by Yann Marcon (AWI). The programme filters outliers by applying a speed filter and reduces the high-frequency noise of the data with a moving average. Afterwards data are spline-interpolated to create a continuous dataset in 1-second intervals. The data can then be used to geo-reference other datasets such as photo imagery, MAPR, or micro-profiler data based on the time information.

The station positions of the final cruise station list have been modified accordingly so that for tracked instruments the much more accurate USBL position has been inserted instead of the default (ship) position.

Data management

The post-processed USBL navigation data for CTD-TOYO, OFOS and TV-MUC transects are available in the scientific data warehouse PANGAEA and can be accessed at this address: http://doi.pangaea.de/10.1594/PANGAEA.836641.

References

IXSEA User Manual (2006): Chapter 1.1 System General Description

4. SEISMOLOGY

Florian Schmid[1], Vera Schlindwein[1] (group leader), Henning Kirk[1]

[1]AWI, Bremerhaven

Objectives

As a part of the global Mid-Ocean Ridge system (MOR), the Gakkel Ridge represents an extreme of its kind in several ways. Firstly, it represents the northern-most ridge of all MORs and is constantly covered by a dense canopy of sea ice. Secondly the Gakkel Ridge exhibits the lowest spreading rates of all MORs. The Arctic Ridge System (ARS), (including Gakkel Ridge, Lena Trough and Knipovich Ridge) and the Southwest Indian Ridge (SWIR) comprise the class of so-called ultra-slow spreading ridges, which is characterized by full spreading rates of less than 20 mm/yr. Thermodynamic models of the oceanic crust predict that at spreading rates < 20 mm/yr, crustal cooling is mainly conductive and melt production is strongly reduced, producing only small amounts of melt at large depths (Bown & White, 1994). Therefore the observation of an exceptionally strong earthquake swarm in 1999 was most unexpected. It originated from a Gakkel Ridge segment around 85° E (Müller and Jokat, 2000), which was believed to be associated with a massive volcanic eruption at the sea floor (Edwards et al., 2001). The discovery of freshly erupted basalt pillows at the sea floor of the 85°E segment demonstrated that the processes of crustal accretion at ultra-slow ridges are more complex than previously assumed. Consecutive studies at the ARS and SWIR showed that at ultra-slow ridges magmatic segments are alternating with amagmatic segments where basaltic rocks are absent and mantle rocks are exposed at the sea floor (Michael et al., 2003; Sauter et al., 2004). To date, a detailed understanding of the spreading processes of ultra-slow spreading ridges is still lacking and a full explanation for the strong 1999 earthquake swarm at 85° E has not been found. Earthquake records from ultra-slow spreading ridges are sparse as their remote locations cause high teleseismic detection thresholds. The perennial sea ice cover above the Gakkel Ridge and the constantly unfavourable weather conditions at the SWIR have hindered the safe deployment of ocean bottom seismometer OBS until very recently.

Microearthquake activity at MOR settings is known to image active faults, magmatic diking (Dziak et al., 1995) and potentially clusters at sites where hydrothermal fluids are circulating (e.g. Tolstoy, 2008). The maximum hypocentral depth of earthquakes constrains the thermal state of the underlying lithosphere (Schlindwein et al., 2013). In the past, we have installed seismometers on drifting ice floes at multiple locations above the ARS for short-term experiments. The acquired datasets proved this method to be feasible and yielded first valuable insights into the local seismicity of ultra-slow spreading ridges. However, a profound understanding of the spreading processes and detailed studies of seismicity can only be achieved through long-term OBS deployments.

During the expedition PS86 (ARK XXVIII/3) we took a twofold approach to detect seismicity in the surroundings of the Aurora Mound area. The first part of our scientific operations comprised the installation of seismometer stations on ice floes drifting above the region of interest, serving at the same time as buoys for sea-ice drift observation. The second part of our scientific programme consisted of a 10-day deployment of an AWI Lobster OBS specially modified for recovery in sea-ice. This experiment was mainly intended as a feasibility study for future routine OBS deployments in densely ice-covered oceans.

Work at sea

4.1 Installation of seismometers on ice floes

8 seismometer stations were used for installation on ice floes for a total of 15 deployments within the period 12/07/2014 - 25/07/2014. Each station was equipped with a broadband seismometer type Güralp CMG-3ESP, 120s – 50Hz, a Reftek 130 data logger and a GPS antenna. The Reftek unit was set to lock GPS time and position every full hour. Six stations were equipped with an Argos transmitter to regularly obtain station positions and ice drift information on the ship via satellite. For every station two non-spillable batteries were used as power supply. One battery was connected to the breakout box of the seismometer. The second battery was connected to the Reftek, the Argos transmitter and to a solar panel via a charge control module.

A sampling rate of 100 Hz was chosen and the seismometer was set to auto centre every 24 hours. For the seismometer installation the snow cover was removed and a wooden plate was placed on the ice to achieve a good ground coupling. Seismic data was stored on Compact Flash memory cards and downloaded onto local hard drives after each deployment. All data were converted to the Mini Seed format and saved in a Seiscom archive format together with the OBS data.

Argos positions where downloaded several times a day via the Argos website. The Argos satellite recurrence over the survey area turned out to be more or less on an hourly basis. Thus, ice drift plots for the past hours could be achieved with relatively short delays. The drift information contributed to the scientific station planning and the nearly instant availability of Argos positions helped to minimize search perimeters for the station recovery.

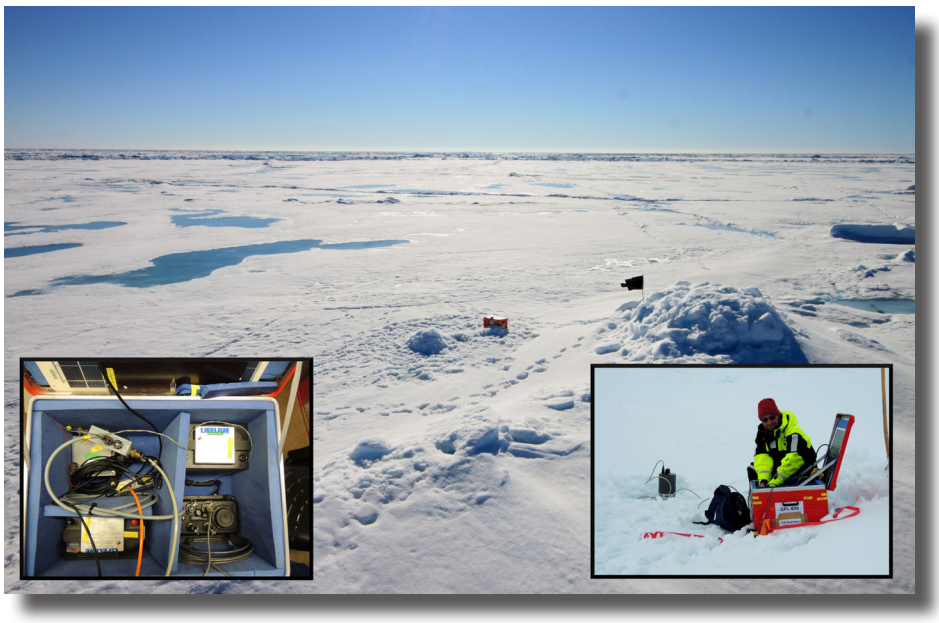

Fig. 4.1: Image of a seismometer station on an ice floe. Left inset shows the internal setup of the red Zarges box. Right inset depicts the station installation, with the seismometer placed on a white painted wooden plate in the background (large image F. Schmid, AWI, small images V. Schlindwein, AWI).

Initially we deployed a small array of 3 stations (approx. 0.5 nm distances between stations) on a single ice floe and placed the remaining stations on individual floes at a distance of approx. 4 nm around the array. A first scan of the data acquired during the first deployment indicated the local seismicity to be dominated by events identifiable at all stations. Based on these findings we decided to skip the central array of the network for the second deployment and just install 6 stations on individual ice floes as a network, keeping a distance of approximately 5 nm between adjacent stations.

The station tracks in Fig. 4.2 illustrate that ice drift direction and speed have changed dramatically during the course of the experiment. While a southward oriented drift component was predominant, changes of drift speed and eastward drift appeared very unpredictable. The resulting pattern of station tracks produced good station coverage for the area of the Aurora vent site and the rift flanks east and north east of the Aurora mound.

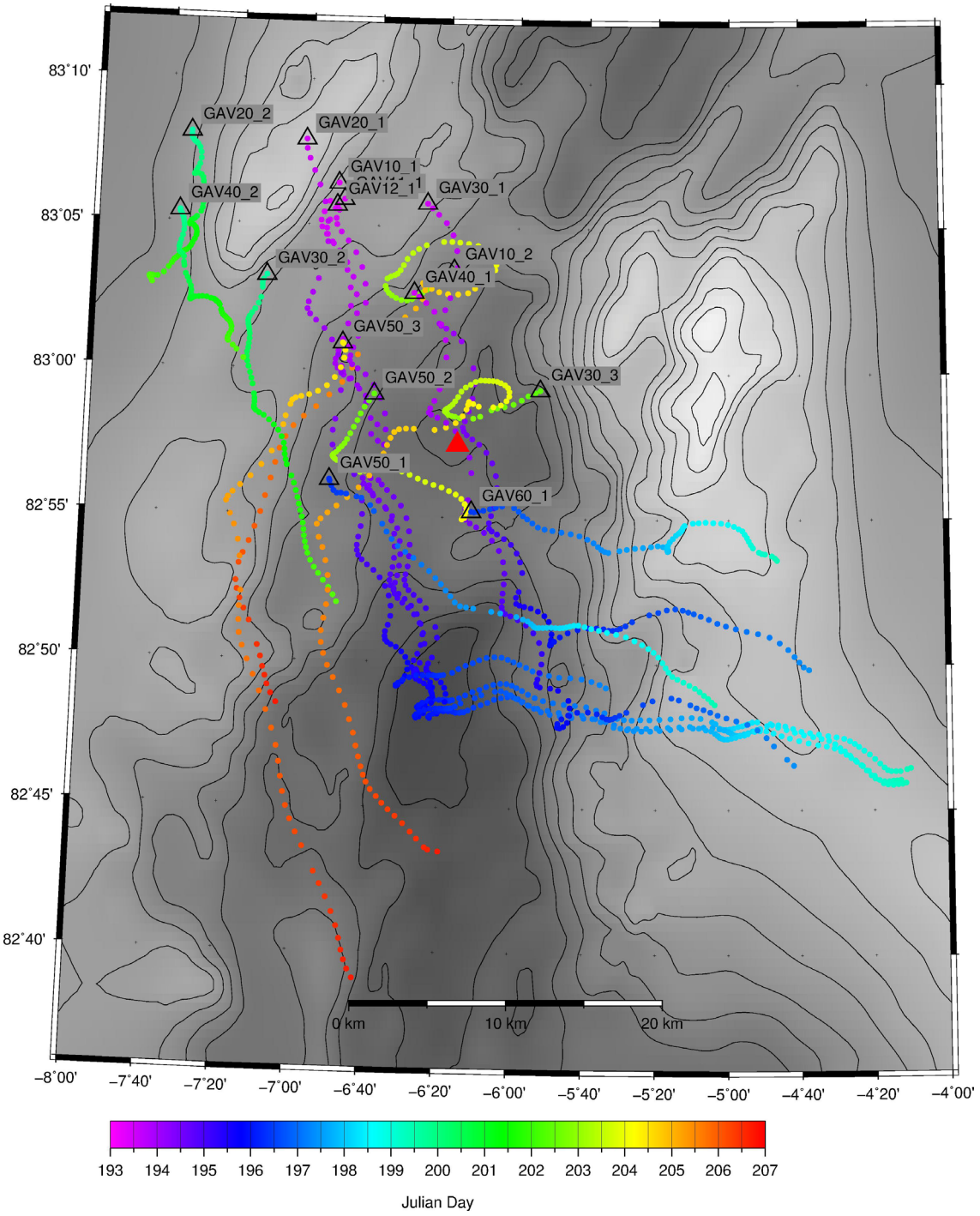

Fig. 4.2: Map displaying the drift paths of all seismometer stations installed on ice floes during ARK XXVIII/3 (PS 86). Triangles indicate deployment sites and dots (colour corresponding to Julian days) represent hourly retrieved GPS positions. Red triangle marks the OBS deployment site.

Tab. 4.1: Summary of seismometer station deployments (Positions correspond to first and last lock of GPS antenna)

Station	Action	Date	Time (UTC)	Longitude	Latitude
GAV10_1	deployment	12.07.2014	06:59	06° 51.678' W	83° 6.466' N
	recovery	18.07.2014	09:21	04° 12.766' W	82° 46.048' N
GAV10_2	deployment	21.07.2014	10:50	06° 18.156' W	83° 3.546' N
	recovery	25.07.2014	17:03	07° 4.772' W	82° 48.51' N
GAV11_1	deployment	12.07.2014	07:47	06° 49.96' W	83° 5.912' N
	recovery	18.07.2014	09:02	04° 10.077' W	82° 46.442' N
GAV12_1	deployment	12.07.2014	08:25	06° 52.006' W	83° 5.697' N
	recovery	18.07.2014	08:38	04° 11.361' W	82° 45.942' N
GAV20_1	deployment	12.07.2014	10:12	07° 1.38' W	83° 7.942' N
	recovery	18.07.2014	07:15	05° 33.847' W	82° 49.211' N
GAV20_2	deployment	18.07.2014	11:25	07° 34.525' W	83° 8.089' N
	recovery	21.07.2014	07:25	07° 44.172' W	83° 2.826' N
GAV30_1	deployment	12.07.2014	11:35	06° 26.176' W	83° 5.809' N
	recovery	16.07.2014	10:25	04° 37.796' W	82° 49.845' N
GAV30_2	deployment	18.07.2014	13:10	07° 11.477' W	83° 3.227' N
	recovery	21.07.2014	10:35	06° 48.948' W	82° 52.026' N
GAV30_3	deployment	21.07.2014	10:15	05° 53.124' W	82° 59.433' N
	recovery	25.07.2014	17:40	06° 19.271' W	82° 43.486' N
GAV40_1	deployment	12.07.2014	10:54	06° 29.408' W	83° 2.725' N
	recovery	16.07.2014	10:45	04° 42.042' W	82° 46.561' N
GAV40_2	deployment	18.07.2014	13:46	07° 37.038' W	83° 5.358' N
	recovery	21.07.2014	08:55	07° 17.343' W	83° 0.328' N
GAV50_1	deployment	15.07.2014	07:44	06° 51.965' W	82° 56.246' N
	recovery	18.07.2014	10:24	05° 3.857' W	82° 48.646' N
GAV50_2	deployment	21.07.2014	11:15	06° 40.002' W	82° 59.227' N
	recovery	23.07.2014	06:56	06° 13.833' W	82° 55.01' N
GAV50_3	deployment	23.07.2014	07:22	06° 49.302' W	83° 0.964' N
	recovery	25.07.2014	17:21	06° 41.741' W	82° 39.081' N
GAV60_1	deployment	15.07.2014	08:10	06° 11.961' W	82° 55.231' N
	recovery	18.07.2014	10:53	04° 46.563' W	82° 53.622' N

4.2 Deployment of an ocean bottom Seismometer under sea ice

For the feasibility study to operate AWI Lobster OBS instruments in ice covered regions, an external IXSEA Posidonia under water positioning transponder was attached with a 100 m, non-floating polypropylene rope to the instrument. The intention of the external Posidonia transponder was to track the instrument's path when rising from the sea floor to the surface. If the OBS should get stuck under an ice-floe, the Posidonia transponder hanging 100 m down would still be in the detection range of the ship-mounted Posidonia antenna.

The size of the head buoy was increased by additional packages of syntactic foam and the instrument's radio beacon was incorporated into the head buoy. In order to avoid entangling of the ropes of head buoy and Posidonia transponder, the head buoy and the rope were firmly

attached to the instrument's releaser hook and were given free upon release. Fig. 4.3 shows the instrument setup. As we intended to lower the instrument to the sea floor with the winch, a test of the instrument's sinking behaviour was conducted prior to the final deployment, in order to estimate the sink velocity.

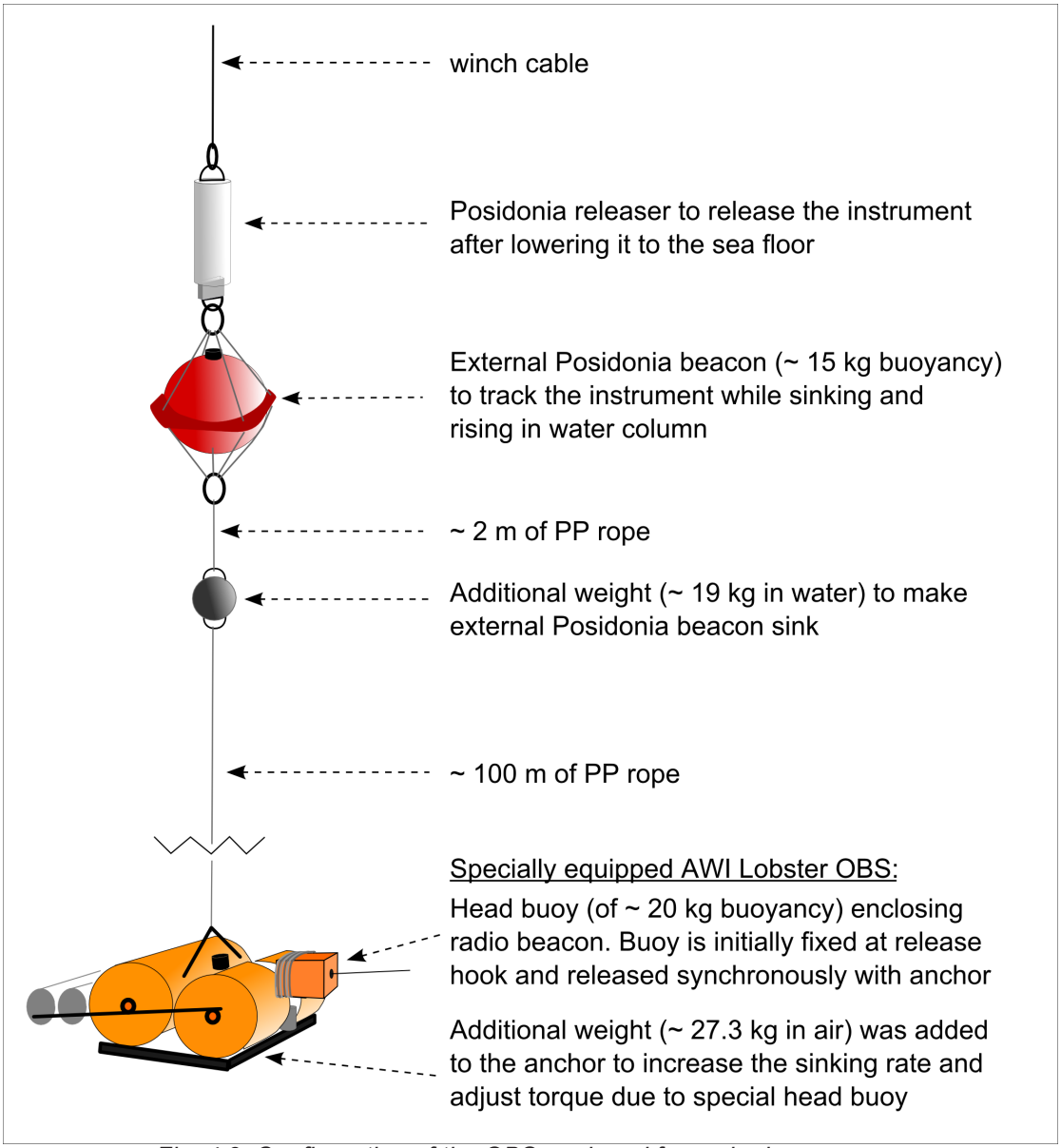

Fig. 4.3: Configuration of the OBS equipped for under ice recovery.

After the test of sinking behaviour the additional weight for the external Posidonia beacon was slightly increased and the instrument's sinking velocity was estimated to be about 0.8 m/s. For the deployment of the instrument, a suitable pond of open water was searched. For the lowering procedure a winch speed of 0.6 m/s was chosen. To separate the instrument from the ship's winch, an IXSEA Posidonia transponder-releaser unit was used.

While lowering the instrument to the sea floor, both Posidonia transponders could be tracked, as displayed in Fig. 4.5. Once the instrument was approximately 150 m above the sea floor, the ship advanced at full power a few hundred meters to horizontally separate OBS and transponder unit to avoid entangling of the rope. The instrument was then released. By tracking the external Posidonia transponder until the instrument hit the sea floor, we obtained an accurate position on the seafloor.

Fig. 4.4: Preparation on deck and deployment of the under ice OBS (images from F. Schmid, AWI)

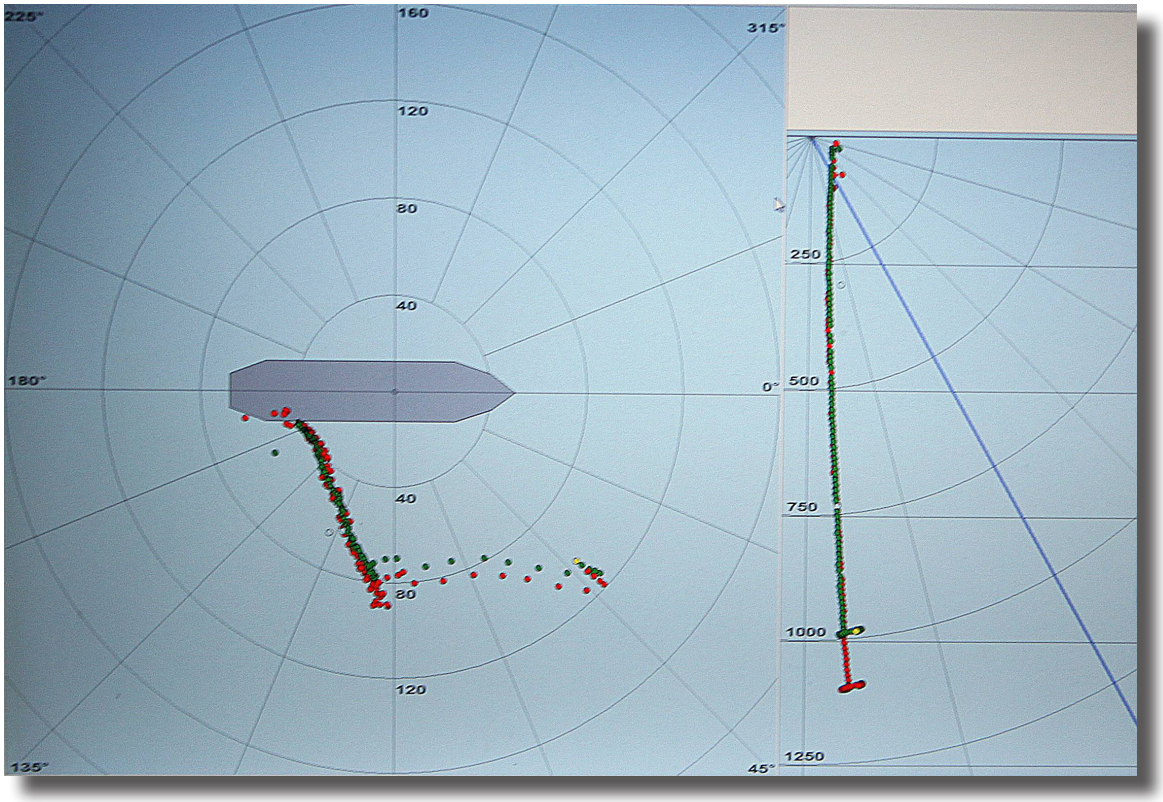

Fig. 4.5: PosiView screen grab displaying the track line and actual position of the OBS and the external Posidonia Beacon under the ship during the test of sinking behaviour (red dots: Posidonia transponder mounted on OBS, green dots: external Posidonia beacon). Screen grab was made when the ship had started reversing at slow speed. Horizontal and vertical distances are given in meters.

Prior to the recovery of the instrument, the ice drift was estimated by letting the ship drift with the ice for some time. When a large enough pond of open water was approaching the deployment site from upstream direction, the OBS was released from its anchor weight. Unfortunately, the external Posidonia beacon had imploded at that time, preventing us from tracking the instrument on the way up and slowing down the rising speed of the OBS to approximately 0.4

m/s. However, when *Polarstern*'s propellers had been stopped and most engines where shut off, we were able to acoustically range the OBS releaser via the deck unit hydrophone and confirm its low raising speed. Prior to surfacing of the OBS, we ranged it with the mobile acoustic unit from several ice floes reached by helicopter to determine its position by triangulation. The OBS finally surfaced in a pond of open water and its radio beacon could immediately be detected from the ship.

Tab. 4.2: OBS deployment and recovery positions

	Date	Time (UTC)	Latitude	Longitude	water depth (m)
deployment	15.07.2014	15:20	82° 57.517' N	6° 16.191' W	4265
recovery	24.07.2014	10:29	82° 57.376' N	6° 17.827' W	4265

Preliminary results

All loggers and sensors worked continuously during the deployments, apart from the intermittent failure of some horizontal components of ice stations, possibly caused by strong motions of colliding ice floes. After the data of all ice stations and the OBS were merged into a common archive, the whole dataset was visually scanned for quality control and for local earthquakes. As the OBS data exhibit a better signal to noise ratio, several events are only detected by the OBS. Altogether approximately 100 seismic events could be identified for the period 12/07/2014 – 25/07/2014, producing an average event rate of 7.6 events per day for the area of the Aurora mound. Additionally dozens of icequakes were recorded by the ice stations. The location of earthquakes and a detailed analysis and interpretation of the recorded signals will be performed at AWI Bremerhaven.

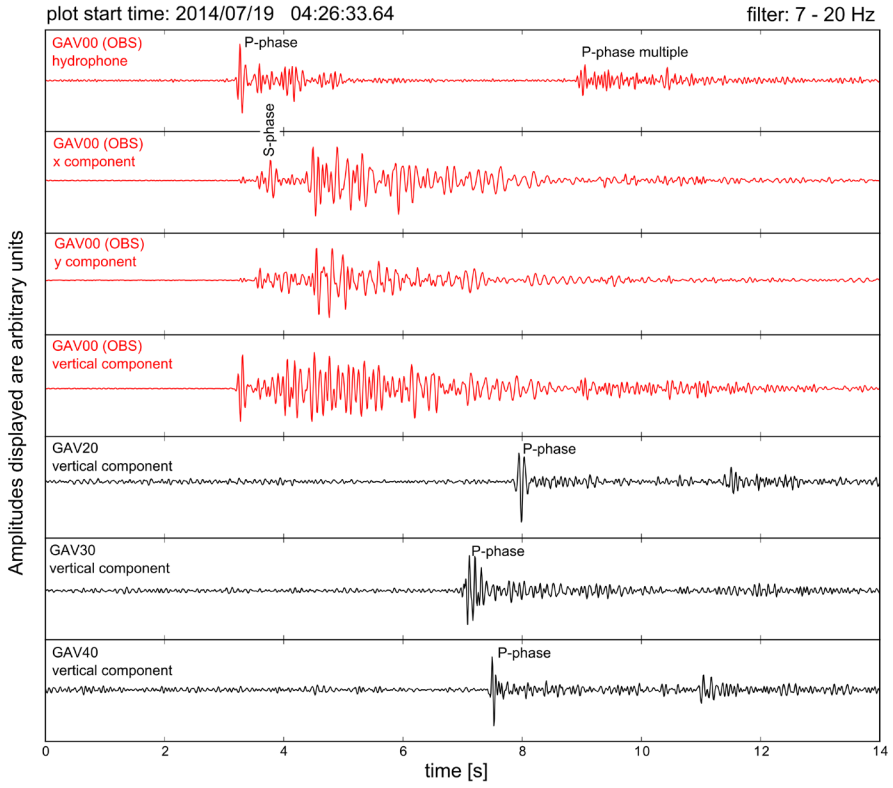

Fig. 4.6: Example of a local earthquake detected by the OBS and three seismometers on ice floes. Red lines represent components of the OBS. Black lines represent vertical components of ice stations.

Data management

Our seismic data will be archived in a common data repository for all data acquired with the ocean bottom seismometers of the DEPAS instrument pool. This archive is currently being developed and implemented at AWI. After 3 years of restricted access, the data will be made publicly available through the GEOFON seismic data request system.

References

Bown JW, White RS (1994) Variation with spreading rate of oceanic crustal thickness and geochemistry. Earth Planet. Sci. Lett., 121, 435-449.

Dziak RP, Fox CG, Schreiner AE (1995). The June-July 1993 seismo-acoustic event at CoAxial segment, Juan de Fuca Ridge: Evidence for a lateral dike injection. Geophys. Res. Lett., v. 22, no. 2, p. 135-138, doi: 10.1029/94GL01857

Läderach C, Schlindwein V (2011) Seismic Arrays on Drifting Ice Floes: Experiences from Four Deployments in the Arctic Ocean. Seismol. Res. Lett., 82(4), pp. 494-503, doi:10.1785/Gssrl.82.4.494.

Michael P.J. et al. (2003) Magmatic and amagmatic seafloor generation at the ultraslow-spreading Gakkel ridge, Arctic Ocean. Nature, 423, 956-961.

Müller C and Jokat W (2000) Seismic evidence for Volcanic Activity Discovered in Central Arctic, Eos, Transactions, American Geophys. Union, 81, 265–269.

Sauter D, Mendel V, Rommevaux-Jestin C, Parson L M, Fujimoto H, Mevel C, Cannat M, Tamaki K (2004) Focused magmatism versus amagmatic spreading along the ultra-slow spreading Southwest Indian Ridge: Evidence from TOBI side scan sonar imagery, Geochem. Geophys. Geosys., 5, 1–20.

Schlindwein V, Müller C, Jokat W (2007) Microseismicity of the ultraslow-spreading Gakkel ridge, Arctic Ocean: a pilot study. Geophys. J. Int., 169, pp. 100-112,doi:10.1111/j.1365-246X.2006.03308.x

Schlindwein V (2012) Teleseismic earthquake swarms at ultraslow spreading ridges: indicator for dyke intrusions? Geophys. J. Int., 190, pp. 442-456, doi: 10.1111/j.1365-246X.2012.05502.x.

Schlindwein V, Demuth A, Geissler WH, Jokat W (2013) Seismic gap beneath Logachev Seamount: Indicator for melt focusing at an ultraslow mid-ocean ridge? Geophys. Res. Lett., 40, pp. 1703-1707, doi:10.1002/grl.50329.

Tolstoy M, Waldhauser F, Bohnenstiel DR, Weekly RT, Kim WY (2008) Seismic identification of along-axis hydrothermal flow on the East Pacific Rise, v. 451, p. 181-184, doi: 10.1038/nature06424

5. HEAT FLOW

Norbert Kaul[1], Bernd Heesemann[1], Mechthild Doll[1]

[1]Universität Bremen, FB5

Objectives

Hydrothermalism can have different expressions. It can be as spectacular as black smokers, it can be visible as shimmering water or it can be below first hand evidence simply as enhanced geothermal heat flow. Even slow spreading ridge systems are known to have a vigorous hydrothermalism. However, ultraslow spreading ridges such as the Gakkel ridge are supposed to be “cold” ridges with minor amounts of melt. Observations of concentrated magmatic activity indicate that there must be a transport of magma and energy in direction of the magmatic centres (Bown and White, 1994, Michael et al., 2003, Standish et al., 2008).

The determination of geothermal heat flow is a valuable tool to characterize the pattern of thermal energy dissipation in the heterogeneous ridge environment. Fluid migration at fairly low rates is able to modify the “sea floor climate” in a sense that favours seafloor-bound fauna. Indeed, the global significance of spots with enhanced geothermal heat flow depends on the extent of the area that is affected by elevated heat flow.

Only few heat flow measurements exist on the Gakkel Ridge, most of them result from the AMORE expedition 2001 (Urlaub et al., 2009). With 26 successful heat flow determinations we are able to characterize the thermal structure of the Aurora mound. The first assumption that the top of the mound should be most active appears not to be correct. Indeed, we found higher heat flow values at the foot of the mound and in its vicinity. Elevated linear structures in the bathymetry might be expressions of fault zones. We find the highest values on these NNE-SSW trending structures.

Work at sea

The 6 m long Bremen heat probe (see Fig. 5.1) was used during the cruise to characterize the temperature field around the Aurora mound. Seven short heat flow profiles were attempted on and around the Aurora mound. Due to the ice coverage of 50 – 80 % and a significant ice drift in varying directions, we could only aim at one target per profile and proceed further according to the actual ice drift.

Eight short transects were carried out within a distance of 4 km of the Aurora mound. One aimed at the top of the mound. Visual inspections of the mound by OFOS showed steep flanks and sparsely sedimented rocky areas, which we needed to avoid in order not to damage the heat flow probe. Therefore most of the positions are located at the foot of the steep flanks (see Fig. 5.2). The direction of transects is dictated by the ice drift.

A reference site is situated some 30 km ENE of the rift axis on approximately 6 Ma old crust. On each site several penetrations were carried out in a local spread. One station consists of two to five single penetrations, positioned 150-200 m apart, depending on the speed of the ice drift. The transit is done in pogo style with the instrument approximately 200 m above ground. One station takes about 5 to 6 hours altogether.

Fig. 5.1: The 6 m Bremen heat flow probe immediately before deployment on Polarstern

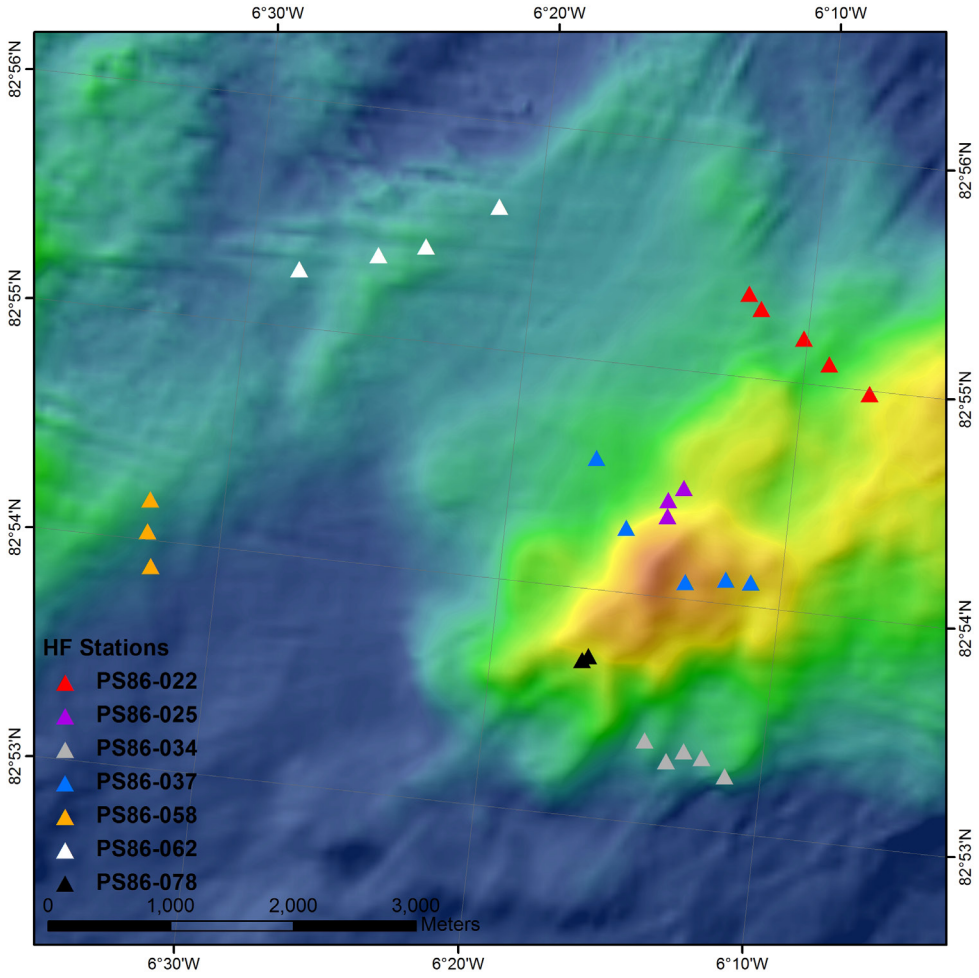

Fig. 5.2a: Location map of heat flow sites on Aurora vent field

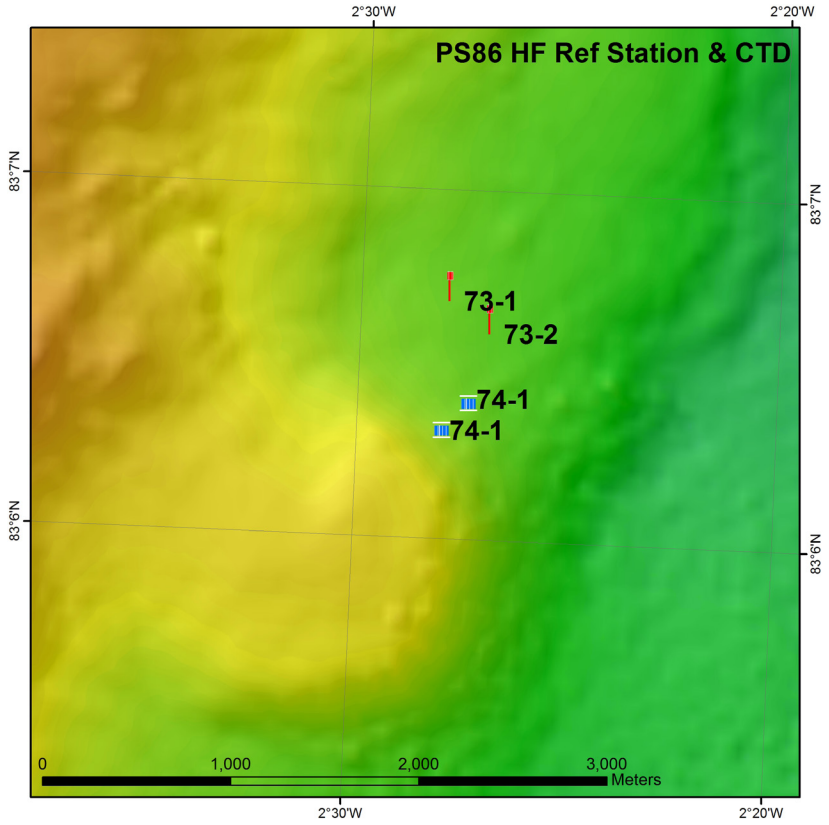

Fig. 5.2b: Location map of reference site for heat flow and CTD approximately 30 km NE of Aurora vent field. The measured bathymetry in this unexplored area differs from IBCAO data by 1,500 m. Annotation refers to stations PS86-0XX.

Furthermore, miniaturized temperature loggers (MTLs, Pfender et al., 2002) were used for monitoring variations in bottom water temperature in time and space (Fig. 5.3).

On this cruise, those loggers were mounted onto the frames of the Ocean Bottom Observatory System (OFOS) and of the Multicorer (TVMUC) during surveys to monitor the temperature at the dive height, nominally 4 m above ground.

Fig. 5.3: Miniaturized Temperature Logger (MTL), produced by Antares, Stuhr. They operated reliable short term deployments besides some battery issues in cold water (-0.7°C) environment. They are rated at 6,000 m water depth, 1 second time resolution and 64,000 samples.

Preliminary (expected) results

A number of 32 heat flow sites were attempted on 9 different stations. 26 of them (81 %) yielded temperature gradients of good or very good quality. The list of stations is summarized in table 5.1. In those cases where the penetration failed, hard ground was the reason for poor penetration. Data reduction and processing of measured time series was done using the programme MHFRED according to an algorithm of Villinger and Davis (Villinger et al., 1987). *In-situ* thermal conductivity could be measured on 12 sites resulting in very good and representative regional estimates. Values between 1.04 and 1.32 W/m*K are fairly high for deep sea sediments. We attribute this to a high content of volcanogenic material e.g. volcanic glass, fragments of basalts and sulfide. Those particles were found in gravity corer PS 86/27 in abundance.

Almost all measured thermal gradients are of good quality. Nevertheless the scatter spreads from values below 0.006 K/m up to 1.578 K/m. A vigorous hydrothermal circulation is supposed to be one reason for that, especially because strong signs of fluid venting were found in the water column. Rough terrain with significant topography might be a second one due to thermal refraction. This needs further investigation.

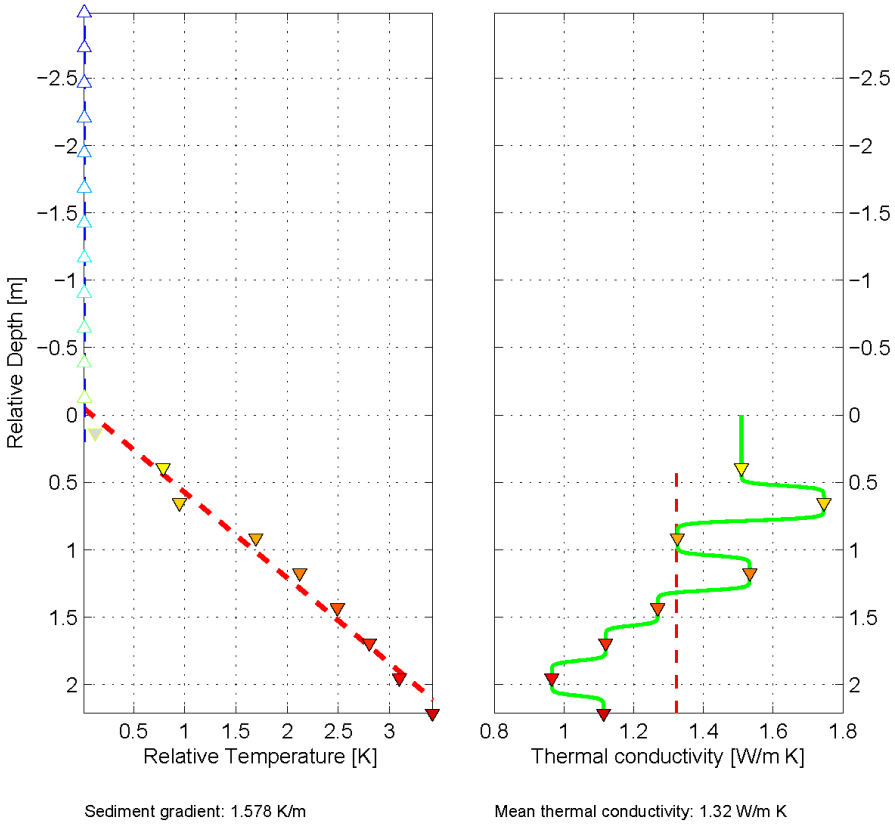

*Fig. 5.4: Temperature gradient of position PS 86/22-1. Despite the partial penetration the gradient of 1,578 mK/m is the highest observed during this survey. The horizontal axis is relative temperature, the vertical axis depth relative to the instrument. The panel on the right side shows thermal conductivity. The mean value of 1.32 W/m*K at this position is as well one of the highest observed during the survey.*

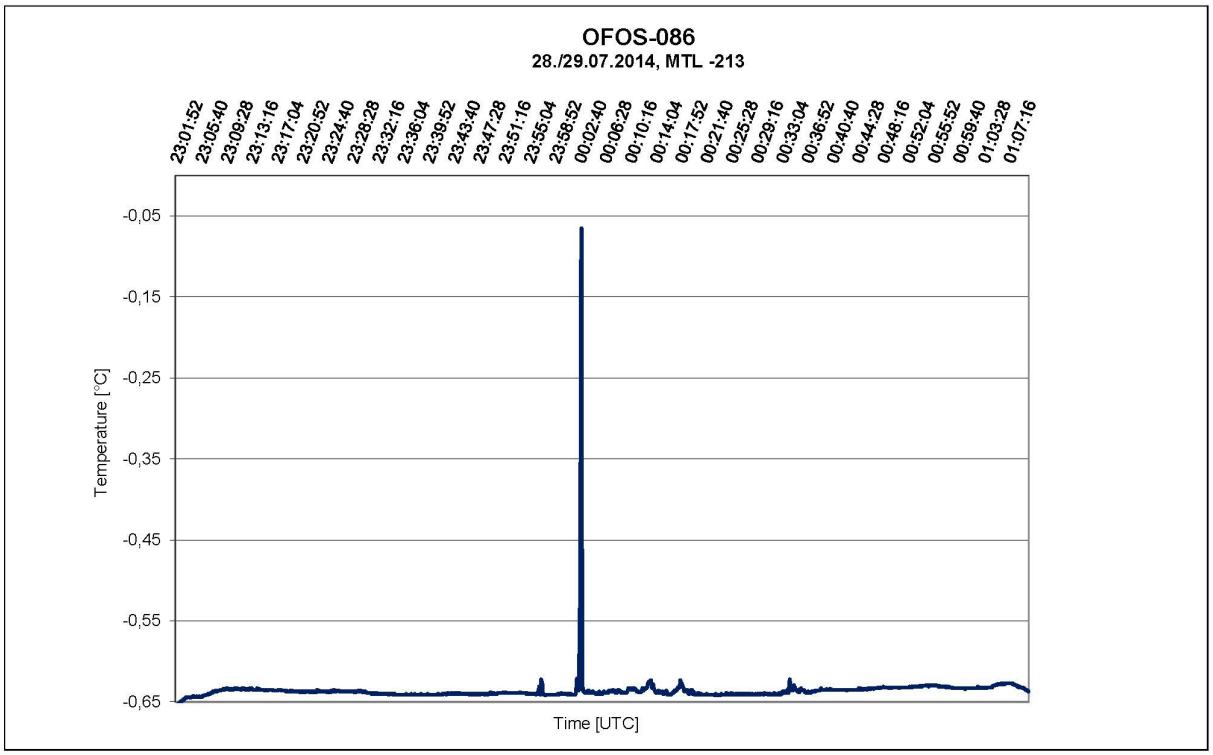

Fig. 5.5: Data example of MTL temperature data of OFOS station PS86-86. The horizontal axis is time UTC, the vertical axis temperature in mK resolution, calibrated against the CTD. The peak in the temperature data of +0.6°C indicates the vicinity of a hot vent.

Evaluating the temperature data of the MTLs deployment on the OFOS and TVMUC brought additional information, regarding plume detection in the water body. On two dives a temperature anomaly of +15 mK could be detected.

Data management

All data produced by the heat flow probe are available on the PANGAEA database at the following address: http://doi.pangaea.de/10.1594/PANGAEA.837142.

References

Bown, J., White, R., 1994. Variation with spreading rate of oceanic crustal thickness and geochemistry, Earth Planet. Sci. Lett., v. 121, no. 3-4, p. 435-449, doi: 10.1016/9912-821X(94)90082-5.

Michael, P.J. et al. (2003). Magmatic and amagmatic seafloor generation at the ultraslow-spreading Gakkel ridge, Arctic Ocean, Nature, v. 423, p. 956-961, doi: 10.1038/nature01704.Pfender, M., and H. Villinger (2002) Miniaturized data loggers for deep sea sediment temperature gradient measurements, Marine Geology, 186, 557 – 570.

Pfender, M., and H. Villinger (2002) Miniaturized data loggers for deep sea sediment temperature gradient measurements, Marine Geology, 186, 557 – 570.

Standish, J.J., Dick, H.J.B., Michael, P.J., Melson, W.G., O'Hearn, T. (2008). MORB generation beneath the ultraslow spreading Southwest Indian Ridge (9–25°E): Major element chemistry and the importance of process versus source. Geochem. Geophys. Geosyst., v. 9, Q05004, doi: 10.1029/2008gc001959.

Urlaub, M., et al. (2009) Gravity crustal models and heat flow measurements for the Eurasia Basin, Arctic Ocean, Mar. Geophys. Res., 30:277-292, doi: 10.1007/s11001-0100-9093-x

Villinger, H., Davis, E. E. (1987) A new reduction algorithm for marine heat flow measurements, Journal of Geophysical Research, 92 (B12), 846-856.

Tab. 5.1: List of heat flow stations on PS86 (ARK XXVIII/3). Thermal conductivities with an asterisk (*) are interpolated.

PS-name	Station	Latitude	Longitude	Water depth	Temp. Grad. [mK/m]	k [W/m K]	Heat flow [mW/m²]
PS86-22-1	H1401P01	82 55.367	-6 12.296	4085	1578	1.32	2058
PS86-22-2	H1401P02	82 55.314	-6 11.756	4084	651	1*	651
PS86-22-3	H1401P03	82 55.167	-6 10.007	4075	32	1*	32
PS86-22-4	H1401P04	82 55.108	-6 09.065	4046	743	1.14	846
PS86-22-5	H1401P05	82 54.992	-6 07.527	4002	NAN	NAN	NAN
PS86-25-1	H1402P01	82 54.500	-6 13.752	3978	188	1.06	198
PS86-25-2	H1402P02	82 54.434	-6 14.336	3979	177	1*	177
PS86-25-3	H1402P03	82 54.358	-6 14.177	3951	147	1*	147
PS86-34-1	H1403P01	82 53.366	-6 13.310	4097	8	1.04	8
PS86-34-2	H1403P02	82 53.289	-6 13.444	4112	66	1*	66
PS86-34-3	H1403P03	82 53.335	-6 12.836	4096	10	1*	10
PS86-34-4	H1403P04	82 53.317	-6 12.132	4089	4	1*	4
PS86-34-5	H1403P05	82 53.253	-6 11.268	4096	14	1.09	15
PS86-34-1	H1404P01	82 54.365	-6 16.050	4066	129	1.06	137
PS86-37-2	H1404P02	82 54.083	-6 13.907	3884	130	1.09	140
PS86-37-3	H1404P03	82 54.083	-6 12.510	3901	47	1*	47
PS86-37-4	H1404P04	82 54.126	-6 11.577	3930	19	1*	19
PS86-51-1	H1405P01	83 06.565	-5 45.812	4266	202	1.16	225
PS86-51-2	H1405P02	83 06.300	-5 46.190	4244	7	1.16*	8
PS86-51-3	H1405P03	83 06.141	-5 46.318	4188	NAN	NAN	NAN
PS86-51-4	H1405P04	83 06.097	-5 46.190	4177	NAN	NAN	NAN
PS86-58-1	H1406P01	82 54.219	-6 32.593	4101	335	1.12	376
PS86-58-2	H1406P02	82 54.078	-6 32.570	4113	469	1.16	523

PS-name	Station	Latitude	Longitude	Water depth	Temp. Grad. [mK/m]	k [W/m K]	Heat flow [mW/m²]
PS86-58-3	H1406P03	82 53.919	-6 32.347	4171	376	1.05	398
PS86-62-1	H1407P01	82 55.653	-6 21.385	4096	109	1.18	128
PS86-62-2	H1407P02	82 55.429	-6 23.850	4099	193	1.16*	224
PS86-62-3	H1407P03	82 55.358	-6 25.531	4101	254	1.16*	295
PS86-62-4	H1407P04	82 55.255	-6 28.267	4132	388	1.16*	451
PS86-73-1	H1408P01	83 06.687	-2 27.938	3041	7	1.30	9
PS86-73-2	H1408P02	83 06.597	-2 26.944	3066	-6	1.33	-8
PS86-78-1	H1409P01	82 53.735	-6 15.965	3947	NAN	NAN	NAN
PS86-78-2	H1409P02	82 53.710	-6 16.338	3973	NAN	NAN	NAN

6. MARINE GEOLOGY

Andreas Türke[1], Denise Bachmann[1], Alexander Diehl[1], Luise Wagner[1]

[1]Uni Bremen, MARUM

6.1 Sediments

Objectives

Sediments were sampled by gravity corer in the sedimented areas of the 'Aurora' vent field to determine the lithostratigraphy and type of sediments. The presence and distribution of ash layers and layers of metalliferous sediments is indicative of volcanic and/or hydrothermal events. Hence, gravity core sampling was conducted specifically in regions where heat flow anomalies were detected and where hydrothermal vents were suspected to occur in order to look for hydrothermal precipitates and to learn about the type of vent system. Furthermore sediments were sampled to learn about biogeochemical cycling of elements, in particular carbon (*cf*. Chapter 8).

Work at sea

A 5.75 m long gravity corer with a 2,000 kg weight stack was lowered to the seafloor at a speed of 0.8 – 1.2 m/s, depending on penetration depths of the heat flow lance at previous nearby stations (*cf*. Chapter 5). After hoisting on board, the plastic liner holding the core material was cut into 1 m long sections. Section ends were capped and immediately stored at 4°C and sampled for pore waters by rhizone-extraction (*cf*. Chapter 8). Eight to twelve hours after retrieval the cores were split lengthwise into an archive and a working half. The working half was sampled immediately for microbiological, biogeochemical and mineralogical analyses. Archive halves were photographed and described, before both halves were put into D-tubes and stored at 4°C for the remainder of the cruise.

Preliminary results

Five gravity cores were recovered at the 'Aurora' vent field. PS86/038-1GC, PS86/044-1GC, PS86/045-1GC, PS86/067-1GC, and PS86/079-1GC directly targeted sedimented sites at or in close proximity to the seamount, whereas PS86/027-1GC, PS86/059-1GC and PS86/064-1GC targeted deeper sites towards N and NW, where strong heat anomalies were detected (cf. Chapter 5). PS86/038-1GC, PS86/044-1GC and PS86/067-1GC failed to sample any sediment, but hit hard rocks, of which some fragments were recovered (*cf*. Chapter 6.2).

Station PS86/027-1GC (82° 55.39' N, 6° 11.91' W; 4097 m water depth) likely overshot, as mud was pushed into the weight stack of the gravity corer. The core revealed 5.43 m of soft and muddy clay sediments with high porosity ranging from light-grey to dark grey (Fig. 6.1.1). The uppermost 40 cm show even higher porosities and are composed of dark brown muddy clay. Some small black grains (basalt?) are spread over the entire core, but are very prominent in the uppermost 40 cm. The greyish sediment is intersected by numerous thin yellowish and reddish layers, which could indicate to hydrothermal precipitates or volcanic ash layers (Sohn et al., 2008). At 388 cm depth a 1 cm thick layer of 1-3 mm sized fresh basalt glass fragments were present, which could either indicate a magmatic event or have accumulated by breaking off of pillow basalts.

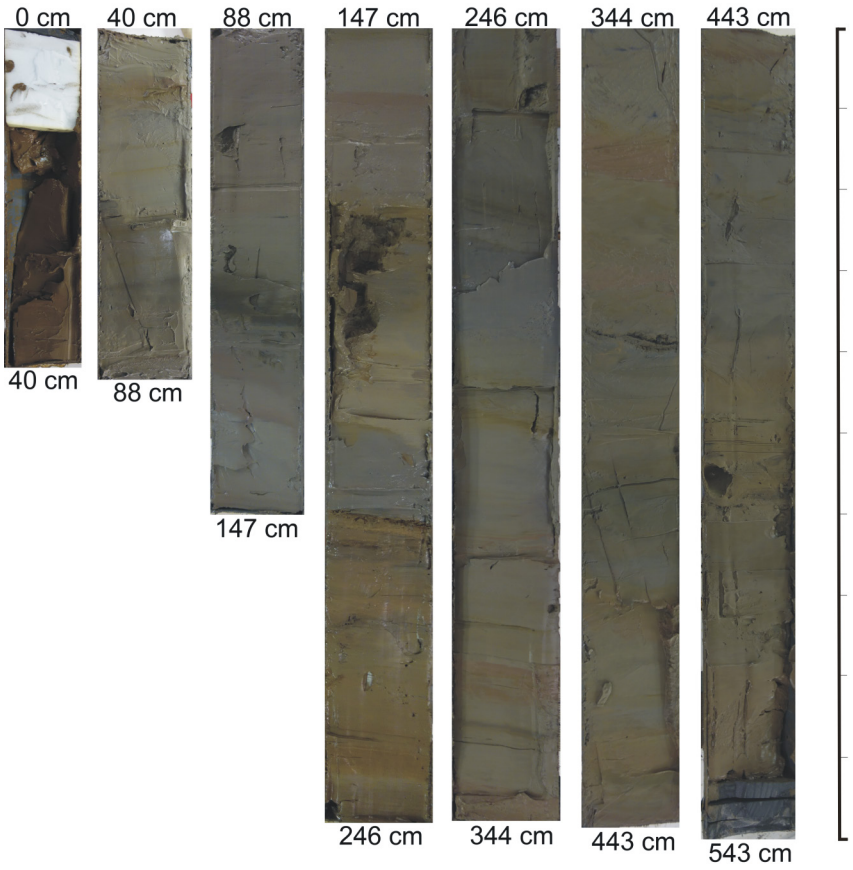

Fig. 6.1.1: Photograph of core PS86/027

Station PS86/059-1GC (82° 54.45' N, 6° 25.94' W; 4,163 m water depth) recovered 4.80 m of greyish soft and muddy clay sediments (Fig. 6.1.2) off the western flank of the seamount. They resemble those of PS86-027-1GC, but the upper brown muddy clay layer has a thickness of 80 cm. There were no indications of overshooting as the gravity corer only penetrated approximately 5 m. Reddish or yellowish layers were less common with only two reddish layers at 3.62-3.65 m and 4.60-4.66 m, pointing to less volcanic or hydrothermal activity in the NW area.

Fig. 6.1.2: Photograph of core PS86/059

Station PS86/064-1GC (82° 55.33' N, 6° 19.67' W; 4163 m water depth) targeted the NW site off the 'Aurora' seamount. 3.78 m of greyish muddy clay sediment (Fig. 6.1.3) were recovered and there were no signs of overshooting. The uppermost 68 cm are composed of brown muddy clay with some very thin light brownish and yellowish interlayers. Small reddish and yellowish interlayers are common within the entire core.

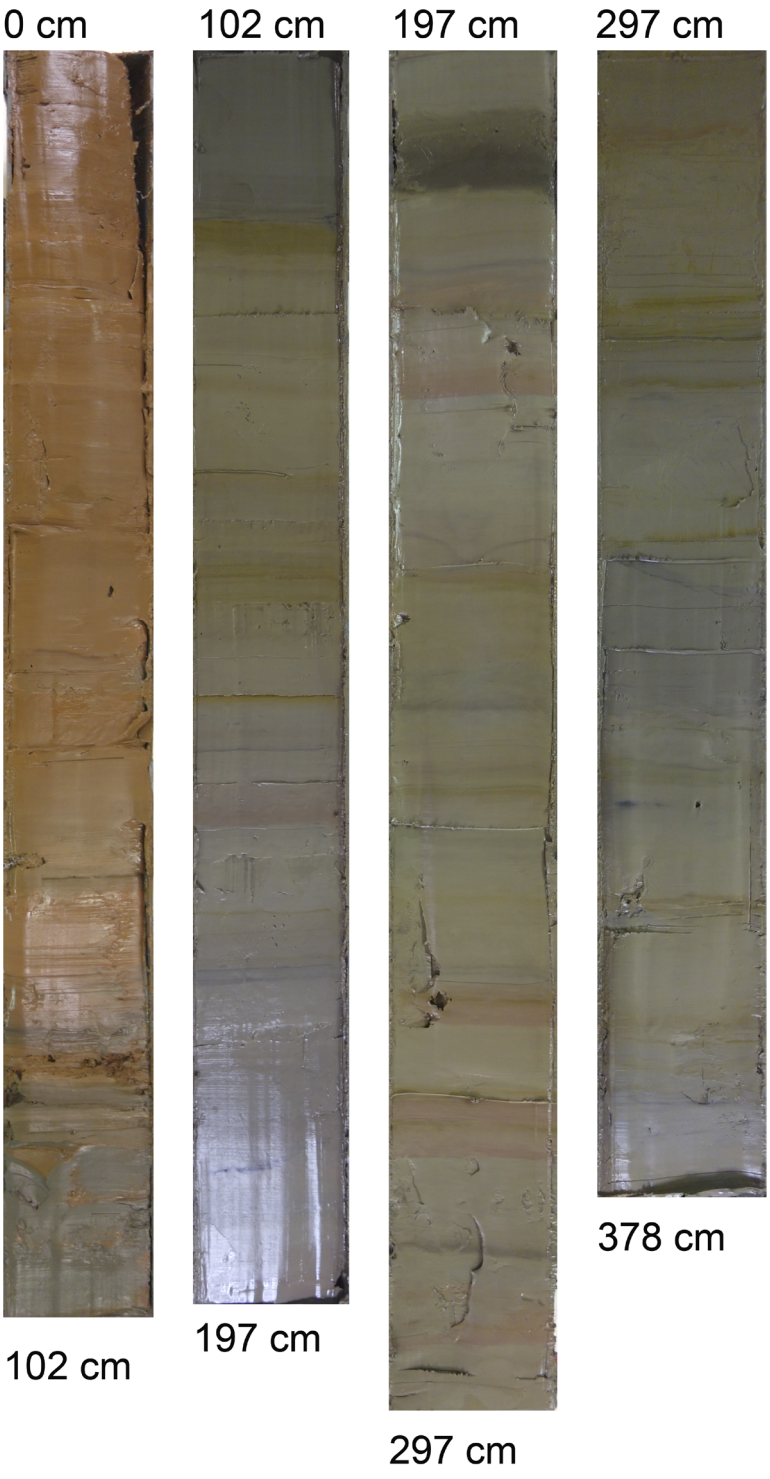

Fig. 6.1 3: Photograph of core PS86/064

Station PS86/045-1GC (82° 54.02' N, 6° 13.61' W; 3874 m water depth) succeeded in recovering 3.86 m of muddy clay sediment (Fig. 6.1.4) from very close to the top of the mount,

without any signs of overshooting. Layering in the core is not horizontal, but in an angle of about 15°, indicating sedimentation at a slope. The uppermost 62 cm consist of highly porous brown muddy clay and are separated by a very sharp grey-brown boundary layer from the remaining brownish grey muddy sediment. Yellowish and reddish (inter)layers are common over the entire core.

Fig. 6.1.4: Photograph of core PS86/045

Station PS86/079-1GC (82° 53.73’ N, 6° 13.41’W; 3986 m water depth) targeted the southern part of the mount. Only 94 cm of muddy clay sediment (Fig. 6.1.5) with high porosity were recovered. Three yellowish/reddish layers of possible hydrothermal provenance of approximately 3 cm are found in the lower half of the core.

Fig. 6.1.5: Photograph of core PS86/079

All core descriptions can be found in the appendix.

Data management

X-Ray fluorescence scanning (XRF) will be conducted onshore to look for enrichments in Ti, Al and Mn that would point to a volcanic or hydrothermal provenance of some of the layers. The glassy basalt fragments will be analyzed for their chemical composition by electron microprobe and LA-ICP-MS. All data produced will be submitted to the PANGAEA Data Publisher for Earth & Environmental Sciences.

6.2. Hard rocks

Objectives

The study area in the transition zone between the ultraslow spreading Gakkel Ridge and the Lena Trough is of considerable petrological interest, because of the large variety of rocks exposed in these settings. Previous work has shown chemical and isotopic heterogeneities of the mantle in the area that were explained by differing extents of partial melting and the presence of continental lithospheric material in the melting zone. The Western Volcanic Zone (WVZ) of the Gakkel Ridge from 6°W to 6°E (Michael et al., 2003) is particularly interesting in this regard because of its peculiar lead isotope composition that is elsewhere found only in the South Atlantic and Indian Ocean (e.g. Goldstein et al., 2008). While the WVZ, despite half-spreading rates <13 km/Myrs, is volcanically robust, the Lena Trough is volcanically starved south of 82.4°N (Snow et al., 2011). Rock dredging and multibeam surveys in the area suggest that predominantly magmatically accreted seafloor north of 82.6°S transitions sharply to the south into a seabed made of mantle peridotite. The peridotite exposed along steeply dipping normal faults bounding both sides of the rift valley (Michael et al., 2003; Snow et al., 2011). Rock sampling through this transition has been spotty, and one perspective of the rock sampling programme is to recover more basement sample to help better constrain this intriguing geodynamic boundary. Specific questions we hope to address include: how much did the mantle melt? How deep did melting take place? How deep were crustal magma reservoirs? What were the tectonic-hydrothermal interactions during exhumation (pressure-temperature-mass transfer)? What are the relations to active venting?

Work at sea

Since hydrothermal vents were discovered very late during the cruise no dedicated rock sampling took place. However, OFOS dive 019 accidentally brought up rock samples. These were photographed and are described below.

Preliminary results

None of the recovered samples show any evidence for hydrothermal alteration, only minor replacement of basalt by nontronite/smectite was observed, which occurs at low temperatures (< 40 °C).

PS86/019-RO1:

Rock sample PS86/019-RO1 (Fig. 6.2.1) was retrieved during OFOS dive 019. It is a very fine grained slightly weathered basalt of ca. 6x9x5 cm. The glassy rim is particularly altered and some of these glassy pieces broke off when examining the rock on board.

Fig. 6.2.1: Photograph of rock sample PS86/019-RO1

PS86/019-RO2:

Rock sample PS86/019-RO2 (Fig. 6.2.2) is a large piece of pillow basalt of approximately 30x12x10 cm. It is moderately weathered and most of the glassy rim had already fallen off. Several sponges were attached to the surface of the rock, which were sampled by the biologists (cf. Chapter 8).

Fig. 6.2.2: Photograph of rock sample PS86/019-RO2

PS86/019-RO3:

Rock sample PS86/019-RO3 (Fig. 6.2.3) is a large piece of pillow basalt of approximately 35x30x20 cm. The exterior is thoroughly weathered with only little glass left. Along fractures, replacement of basalt by nontronite/smectite is evident.

Fig. 6.2.3: Photograph of rock sample PS86/019-RO3

References

Goldstein, S.L., Soffer, G., Langmuir, C.H., Lehnert, K.A., Graham, D.W., Michael, P.J. (2008). Origin of a 'Southern Hemisphere' geochemical signature in the Arctic upper mantle. Nature, v. 453, p. 89-93, doi: 10.1038/nature06919.

Michael, P.J., Langmuir, C.H., Dick, H.J.B., Snow, J.E., Goldstein, S.L., Graham, D.W., Lehnert, K., Kurras, G., Jokat, W., Muehe, R., Edmonds, H.N. (2003). Magmatic and amagmatic seafloor generation at the ultraslow-spreading Gakkel ridge, Arctic Ocean. Nature, v. 423, p. 956-961, doi: 10.1038/nature01704.

Snow, J.E., Hellebrand, E., von der Handt, A., Nauret, F., Gao, Y., Schenke, H.-W. (2011). Oblique nonvolcanic seafloor spreading in Lena Trough, Arctic Ocean. Geochemistry, Geophysics, Geosystems, v. 12, no. 10, Q10009, doi: 10.1029/2011GC003768.

Sohn, R.A., Willis, C., Humphris, S., Shank, T.M., Singh, H., Edmonds, H.N., Kunz, C., Hedman, U., Helmke, E., Jakuba, M., Liljebladh, B., Linder, J., Murphy, C., Nakamura, K., Sato, T., Schlindwein, V., Stranne, C., Tausenfreund, M., Upchurch, L., Winsor, P., Jakobsson, M., Soule, A. (2008). Explosive volcanism on the ultraslow-spreading Gakkel ridge, Arctic Ocean. Nature, v. 453 p. 1236-1238, doi:10.1038/nature07075.

7. OCEANOGRAPHY

Christian Mertens[1], Janna Köhler[1], Martin Vogt[1,2], Tammy Lee[1], Christopher Nowak[1], Maren Walter[1] (not on board), François Fripiat[3] (not on board)

[1]UHB-IUP
[2]MPI-Bremen
[3]Friye Universiteit Brüssel

Objectives

The global distribution of hydrothermal venting along mid-ocean ridges controls heat and mass fluxes from the Earth's crust and mantle to the ocean and is supposed to be related to their spreading rate. This relation predicts a low incidence of hydrothermal venting at the ultraslow-spreading Gakkel Ridge (spreading rate about 1 cm per year). In contrast, Edmonds et al. (2003) found evidence for abundant venting along the Gakkel Ridge based on water column profiles of light scattering, temperature and manganese concentrations during the AMORE cruise in 2001. In addition to the water column data, fresh sulfide chimneys were recovered in one dredge haul and a subsequent camera tow indicated shimmering water and abundant macrofauna in an area that was then named Aurora.

The main objective of the oceanography group was to identify plume signals in the water column and to study mixing and spreading of plume material from the Aurora field. High-temperature water emanating from the seafloor ascends through the water column. It loses buoyancy by entraining ambient seawater until a level of neutral buoyancy is reached. Subsequent lateral spreading of the plume signals in temperature, suspended particles and chemical tracers allows to identify areas where hydrothermal vents can be located. Water in hydrothermal plumes is highly enriched in Helium (Isotopes: 3He and 4He); comparisons of the He/Ne ratios with that of water outside the plume and with air show 5-8 times higher ratios within the plume. The primordial components of helium isotopes are ideal tracers for the distribution of vent fluids in the water column, since they are non-reactive and detectable over long distances away from the source.

During the cruise measurements of temperature, salinity, turbidity, Eh, and velocity were made to study the plume dispersal at the Aurora site. A map with the CTD casts carried out at the Aurora field is shown in Fig. 7.1. Water samples with high vertical resolution were taken to be analyzed for helium and neon isotopes later in the noble gas lab (University of Bremen). Direct current measurements parallel to the CTD casts were made to interpret the dispersal of plume signals above the vent site. In cooperation with the University of Brussels (François Fripiat) samples of $\delta^{18}O$ and $\delta^{15}N$ were taken to study the nitrogen biogeochemical cycles in the area.

Work at sea

CTD

Conductivity-temperature-depth (CTD) casts were carried out using a Sea-Bird Electronics, Inc. SBE 911plus system (AWI Bremerhaven) that was equipped with double temperature and conductivity sensors. Additionally a custom build Seapoint Turbidity Meter (5x normal gain), a transmissometer and two redox potential (Eh) sensors were used to identify hydrothermal plume signals in the water column. The first Eh-sensor was built by Koichi Nakamura (AIST, Japan) and the second one was a CTD version of the MAPR Eh sensor build at NOAA PMEL.

A comparison of the two sensors is shown in Fig. 7.2, indication that the MAPR Eh sensor (although less dynamic) is able to detect the same signals as the Koichi Nakamuras sensor.

The underwater unit was attached to a SBE 32 carousel water sampler for 24 Niskin bottles. Two bottles were left out for a lowered acoustic Doppler current profiler system (LADCP) and, hence, a maximum of 22 bottles was used. The complete system worked properly throughout the cruise, except for missing turbidity data on station 52. After that station the turbidity sensor was replaced. The CTD work consisted mainly of tow-yo stations where the instrument package is lowered and heaved repeatedly in between the seafloor and the upper boundary of the non-buoyant plume layer, while the ship is drifting slowly with the ice. Typical ship velocities during the drift were between 0.2 and 0.6 kn. In total 17 CTD casts were carried out, 12 of them close to the Aurora vent field (Fig. 7.1).

LADCP

Velocity data were collected during all CTD stations by two RD Instruments 300 kHz Workhorse Monitor ADCPs (AWI Bremerhaven) that were attached to the water sampler. The ADCPs were operated in a synchronized configuration in which the downward looking instrument (S/N 1368) triggers the upward looking instrument (S/N 0951). Both ADCPs were used with a ping rate of 1 Hz. As the abundance of scatterers at depth was extremely sparse, the configuration was changed from broad- to narrowband and the bin size was increased from 10 m to 12 m after the first CTD station. However, typically at depths below 1,500 m only two bins per instrument contained usable data, resulting in a range of less than 50 m (Fig. 7.3). This is about half of the minimum range that is needed to obtain reliable velocity estimates. Both instruments worked well during all stations, except for the last 20 minutes of station 33, where the upward looking instrument did not record any data due to low battery power.

MAPR

Miniature Autonomous Plume Recorders (MAPRs, E. Baker and S. Walker, NOAA, PMEL) were deployed on CTD, OFOS, TVMUC and heat-flow stations. MAPRs are self-contained instruments, that record data at pre-set time intervals (5 seconds) from temperature (thermistor mounted in a titanium probe, resolution 0.001°C), pressure (0-6000 psi gauge sensor, resolution 0.2 psi), nephelometer (Sea Tech Light Backscatter Sensor), and redox potential (Eh) sensors (Baker and Milburn, 1997). The instruments were either directly attached to the instrument (OFOS, TVMUC) or 100 m above (Heat-flow lance). During CTD-tow-yo stations four MAPRs were used 300, 600, 900, and 1,200 m above the instrument.

Water Sampling

During the cruise a total of 206 water and blank samples for noble gas analysis were taken. For 158 of these the method of Roether et al. (2013) was used, where previously evacuated glass ampoules are filled half with the sample. Another 48 noble gas samples were taken with the standard method, where a copper tube is flushed with the sample and the ends are closed gas-tight with clamps. For comparison 13 Niskin Bottles were sampled with both methods. Since the background signals for ^{3}He in this area are completely unknown, 40 samples for the analysis of CFC/Freon and Tritium were taken around the plume signal. These samples as well as the noble gas samples will be analyzed after the cruise in the Bremen Trace Gas Laboratory. Further we collected 135 samples that will be shipped to François Fripiat for analysis of $\delta^{15}N$ and $\delta^{18}O$ at the Friye Universiteit Brüssel after the cruise. To calibrate the conductivity sensors at the CTD, 85 salinity samples were analyzed directly on board. A summary of water samples taken on the cruise is given in Tab. 7.1.

Preliminary (expected) results

The hydrothermal plume at the Aurora vent site was identified by its Eh signal in 10 of the CTD casts (Tab. 7.1). The depth range where plume signals were observed was between 2,680 and 3,850 m. Plume rise height and thickness varied considerably along the tow-yo tracks and in between stations. An example of the horizontal Eh distribution along a north-south track above the small mound at the Aurora vent site is shown in Fig. 7.3. At the beginning the plume had a thickness of about 700 m and a rise height of 3,100 m. It gradually became thinner toward the south and its rise height decreased. Near the end of the track the rise height increased and a second maximum of Eh signals was found, now higher in the water column. The first CTD casts up to station number 48 showed a non-buoyant plume mainly above the northwestern part of the explored area. The later stations 57, 66, and 69 showed signals of the buoyant plume with temperature anomalies of about 1-2 mK and large Eh changes of up 88 mV. CTD within the buoyant plume at about 3350 m depth are shown in Fig. 7.5. The corresponding density and salinity anomalies in the buoyant plume are small but above the noise level of the CTD sensors.

With the combination of turbidity, Eh, and helium measurements we expect to characterize the plume properties and to estimate the vent fluxes. Further we will study the vertical exchange of plume material between rift valley and the Arctic Ocean.

Data management

CTD and MAPR data were available for all cruise participants on board and are now available through the PANGAEA database. The CTD and MAPR data can be accessed at http://doi.pangaea.de/10.1594/PANGAEA.836219 and at http://www.pangaea.de/search?count=100&q=PS86+MARP respectively. The trace-gas data will be made public through the PANGAEA data base approximately one year after the cruise.

References

Baker ET, Milburn H (1997) MAPR: a new instrument for hydrothermal plume mapping. Ridge Events 8(1), 23–25.

Edmonds HN, Michael PJ, Baker ET, et al. (2003) Discovery of abundant hydrothermal venting on the ultraslow-spreading Gakkel ridge in the Arctic Ocean. Nature 421, 252–256.

Roether W, Vogt M, Vogel S, and Sültenfuß J (2013) Combined sample collection and gas extraction for the measurement of helium isotopes and neon in natural waters. Deep-Sea Research I, 76(6), 27–34.

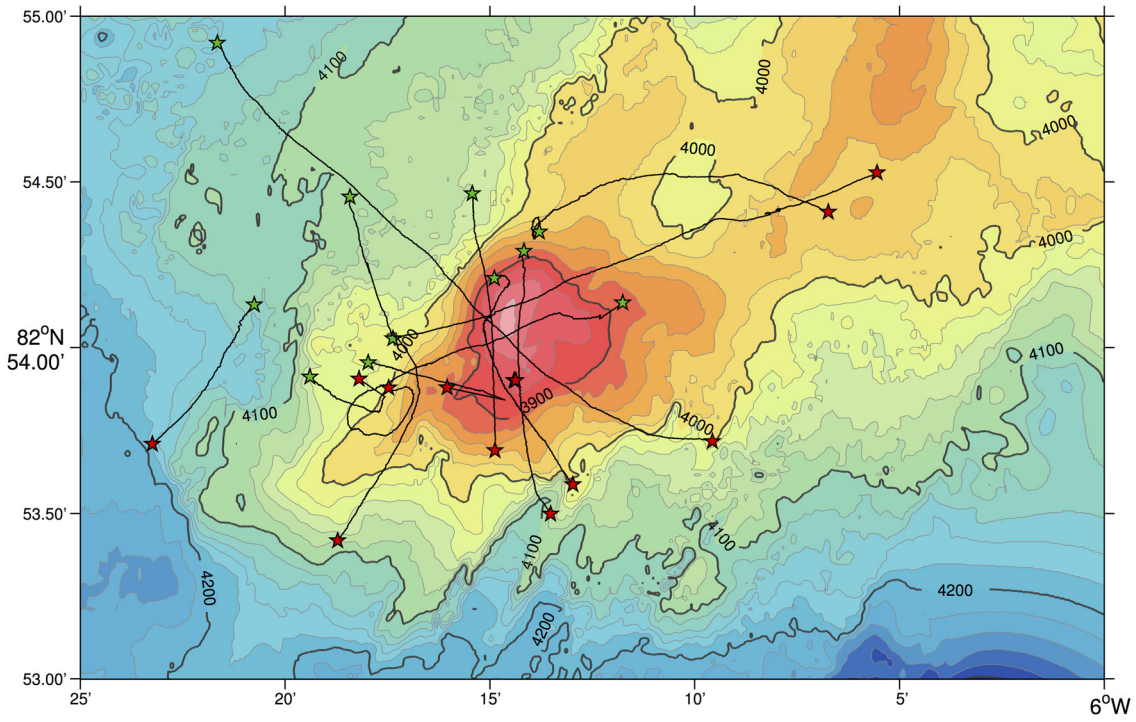

Fig. 7.1: Map of CTD casts at the Aurora vent site. Green stars show the instrument location at the start and red start show the location at the end.

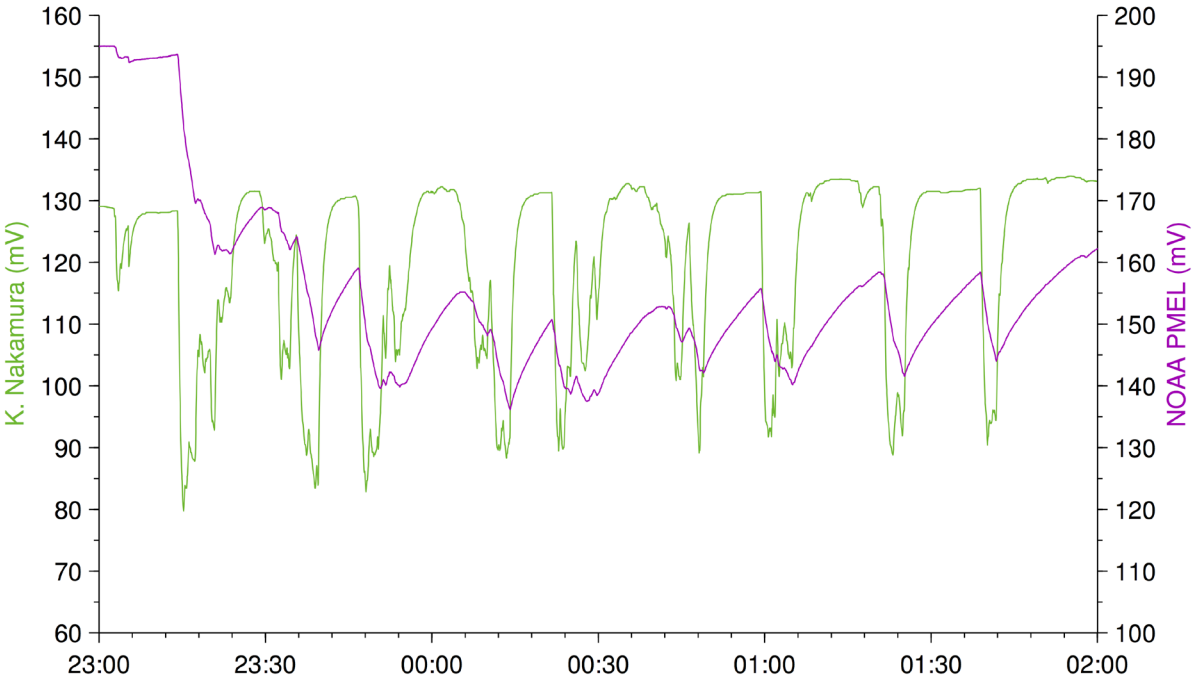

Fig. 7.2: Eh measurements during CTD station 36 with the sensor build by Koichi Nakamura (green) and the CTD version of the PMEL MAPR Eh sensor (magenta).

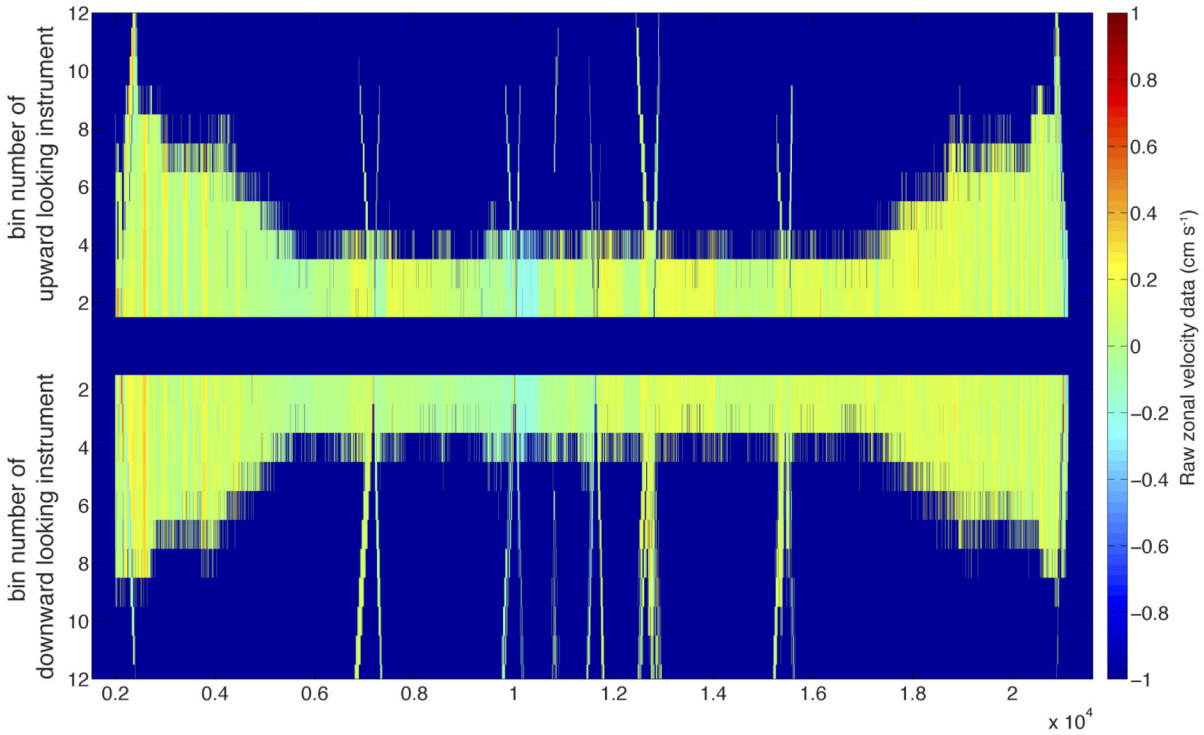

Fig. 7.3: Raw data of east-west velocity from lowered ADCP measurements at station 66. The axis are ensemble number and bin (depth cell) number. Dark blue indicates missing data. During most of the cast (ensembles 6000 to 15000), each instrument recorded valid data only in bins 2 and 3 which is only half the number of measurements necessary to acquire reliable estimates of the current velocity.

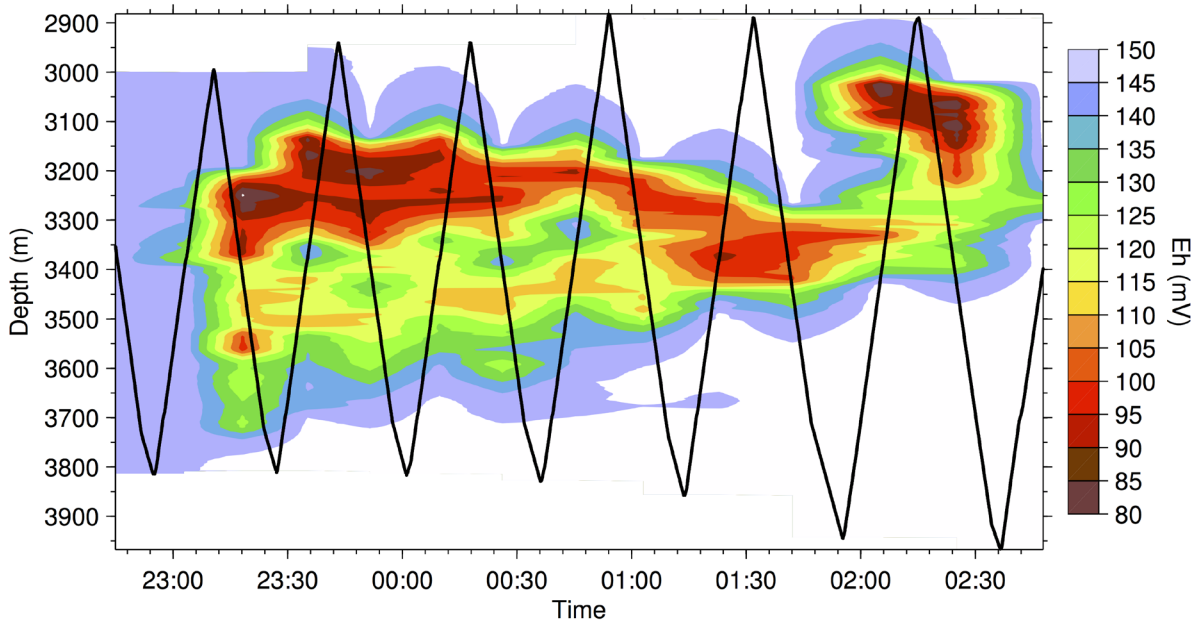

Fig. 7.4: Horizontal distribution of redox potential (Eh) along the track of CTD tow-yo station 36. The track started north of the Aurora vent site and went southward.

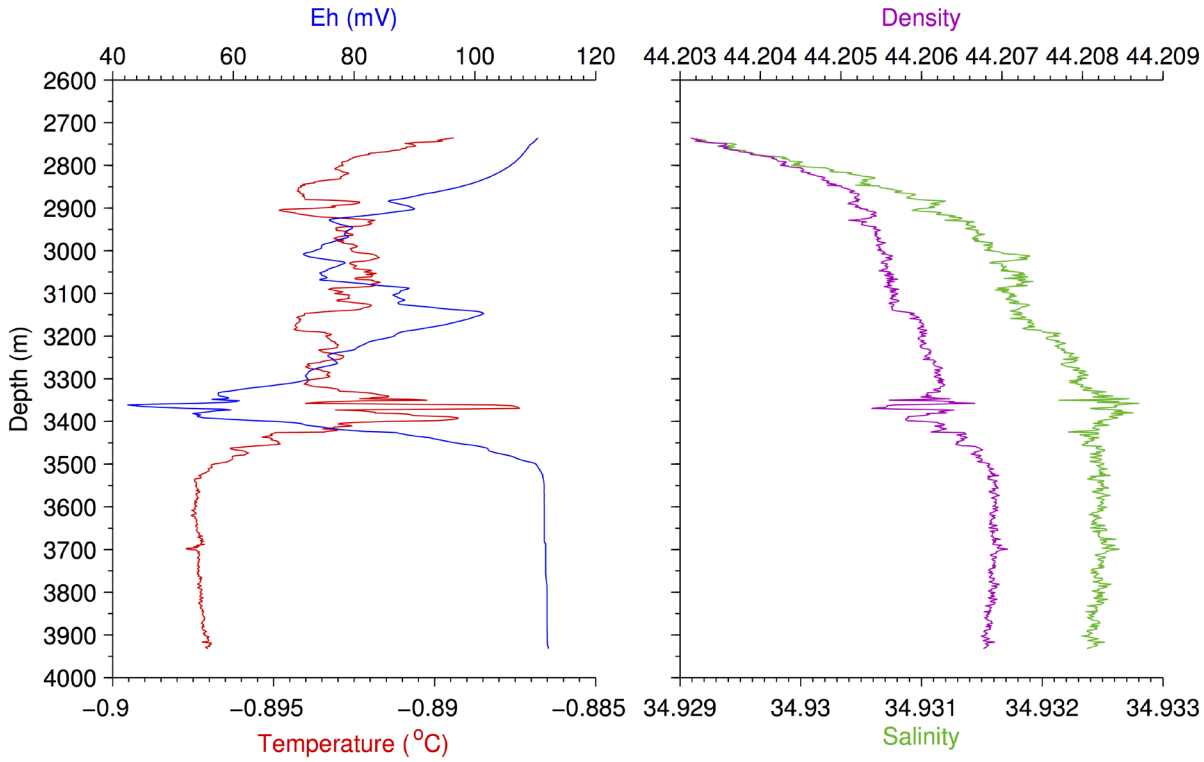

Fig. 7.5: Temperature and Eh (left) at CTD station 57 showing a buoyant plume at a depth of 3350 m below the non-buoyant plume centered at 3000 m. Salinity and density anomalies at 3350 m (right) are extremely small but consistent with a rising buoyant plume.

Tab. 7.1: Overview of water samples collected from CTD casts. Also listed is the depth range where Eh signals were observed during the cast as well as the maximum Eh change observed which is a good indicator for the distance to the hydrothermal vent.

Station	Tow-yo	Pump Station	Plume Range (m)	ΔEh (mV)	Samples
PS86/0018			-	-	CFC, ^{4}He, O_2, ^{3}H, δ^{18}O
PS86/0021	x		3000 - 3350	10	CFC, ^{4}He, CH_4, O_2, ^{3}H, δ^{18}O, FISH, C-FIX, DOC, M_DNA (Symb), Sal
PS86/0023	x		2970 - 3740	66	CFC, ^{4}He, O_2, ^{3}H, FISH, C-FIX, DOC, Metal, PART, M_DNA (Symb)
PS86/0029	x		-	-	CFC, ^{4}He, ^{3}H, δ^{18}O
PS86/0033		x	3130 - 3700 (before pumping)	37	^{4}He, ^{18}O, M_DNA (DSET), Metal, M_DNA (Symb)
PS86/0036	x		3100 - 3730	50	CFC, ^{4}He, CH_4, FISH, M_DNA (DSET), C-FIX, Metal, Sal
PS86/0040		x	unknown (shortly after pumps started)	38	^{4}He, CH_4, δ^{18}O, Metal, Sal

Station	Tow-yo	Pump Station	Plume Range (m)	ΔEh (mV)	Samples
PS86/0043		x	3020 - 3540 (before and while pumping)	60	^{4}He, CH_4, $\delta^{18}O$, M_DNA (DSET), Metal, M_DNA (Symb), Sal
PS86/0048			-		^{4}He, CH_4, $\delta^{18}O$, Sal
PS86/0049			-		^{4}He, CH_4, $\delta^{18}O$, Part, Sal
PS86/0052			-		^{4}He, CH_4, $\delta^{18}O$, M_DNA (DSET), Metal, M_DNA (Symb), Sal
PS86/0055		x	2710 - 3300	48	CH_4, M_DNA (DSET), Metal, M_DNA (Symb), Salt, Part
PS86/0057	x		2680 - 3380	68	^{4}He, CH_4,Fish, M_DNA (DSET), C-Fix, Metal, Part, M_DNA (Symb), Sal
PS86/0066	x		2980 - 3850	66	CFC, ^{4}He, CH_4, ^{3}H, M_DNA (DSET), Metal, Part, M_DNA (Symb), Sal
PS86/0069	x		2780 - 3780	88	CFC, ^{4}He, CH_4, M_DNA (DSET), C-Fix, Metal, Part, M_DNA (Symb)
PS86/0074			reference	-	^{4}He, CH_4, O_2, $\delta^{18}O$, Fish, C-Fix, Metal, Part, M_DNA (Symb), Sal
PS86/0083		x	-	-	CH_4, M_DNA (Symb), Sal

8. BIOGEOCHEMISTRY AND BIOLOGY

8.1. Plume chemistry and microbiology

Gunter Wegener[1,3], Rafael Stiens[1], Mirja Meiners[1], Christian Borowski[1], Antje Boetius[1,2,3], Luise Wagner[3], Denise Bachmann[3], Alexander Diehl[3], Andreas Türke[3]

[1]MPI Bremen
[2]AWI
[3]Uni Bremen, MARUM

Objectives

Hydrothermal fields are characterized by temperature-driven sub-seafloor fluid circulation and emissions. The fluids are enriched in reduced species such as methane, hydrogen, helium and they are depleted in oxygen. They carry high loads of sulfur minerals and metal oxides that precipitate to particles forming the typical black smoke when the fluids are emitted into the cold ambient seawater. Fluid emissions rise as buoyant hydrothermal plumes in the near-bottom water column until cooling and mixing with seawater leads to density equilibrium and to horizontal dispersal of the neutrally buoyant plume. The reduced species in the plume provide potential energy sources for specialized microorganisms which can lead to specific compositions of the microbial plume community and to increased microbiological activity and carbon fixation.

Our main objective in this cruise was to characterize the composition of the microbial plume community, to identify and quantify the special energy sources for microbial activity and to evaluate the consumption of these energy sources in the plume in comparison to hydrothermally uninfluenced arctic deep water. Therefore, we sampled hydrothermal plume and seawater from reference sites for analyses of the contents of methane, mineral and particles and to compare the metabolic activity of the communities in the different microbial habitats, in particular with respect to methane oxidation and carbon fixation.

Work at sea

We used 17 CTD casts to sample hydrothermal plume from AURORA vents and surrounding water bodies. The depth of the neutrally buoyant plume was located between 2900 and 3600 m water depth by sensor measurements of turbidity, oxidation redox potential and temperature. In two casts, very strong temperature anomalies indicated that we had met the rising hydrothermal plume. Water samples were collected in the plume, below and above it and also at reference stations that did not reveal hydrothermal influence. The sampling was closely coordinated with the oceanography group to ensure maximum information on the various geochemical and oceanographic parameters from the selected water layers. Methane concentrations measured aboard ship from all collected samples indicated whether the location of the plume source could be assumed close or far from the sampling sites. Selected stations were sampled for analyses of dissolved trace metal concentrations, precipitated mineral phases and isotopic signatures of methane carbon. These samples will be analyzed in the home laboratories of MARUM (W. Bach) and at AWI Bremerhaven (E. Damm).

The microbial carbon fixation in the different water layers was measured using a ^{14}C-radiotracer assay on sample material incubated under ambient temperatures. Stimulation of carbon

fixation was tested using methane, hydrogen, thiosulfate and organic carbon phases. Rates of methane oxidation were determined using an isotope labeling assay. The composition of microbial communities was analyzed from seawater collected with the CTD that was purged through 0.22 µl membrane filters (~50 different samples). Microorganisms were also collected for metagenomic and deep community sequencing. We used McLane *in-situ* pumps attached to the CTD wire at selected plume (3) and reference stations (2) to concentrate sufficient microbial cell material on microfilters with 0.22 µm pore size. The plume depth was determined by measurements of the oxygen redox potential (sensors provided by K. Nakamura (Tsukuba, Japan) and S. Walker (PMEL Seattle, USA), see oceanographic section). We positioned the pumps next to the CTD and at 500 m distance above to ensure the sampling of plume and non-plume water at the same site. To determine the abundances of total microbes and specific microbial groups at the *in-situ* filtered depths, we blotted water collected with the rosette water sampler on 0.22 µm filters.

Preliminary results

We analyzed all CTD stations for methane concentrations. Methane concentrations in plume layers were up to 50-fold increased towards oceanic background (Fig. 8.1.1), while samples from reference locations and from non-plume layers at plume stations resembled oceanic background (approximately 0.5 nM) and were even under-saturated in relation to the atmosphere. Highest methane concentrations correlated with the most pronounced Eh minima in water depths of 2,900 to 3,600 m (cf. Section 7). In these water layers the particle loads were significantly increased as it was indicated by the different coloration of *in-situ* pump filters that had collected at plume and non-plume depths (Fig. 8.1.2). First analyses suggested that the particle loads collected within plumes represented mixtures of mineral and organic particles. Further analyses in the home laboratories (acidic dissolution, microscopic analyses) will reveal the exact nature of the particles. Our incubation experiments indicated significantly increased carbon fixation in plume layers (Fig. 8.1.3) suggesting that at least parts of the plume material consists of reduced compounds that are used by microbes for autotrophic metabolism. Test with different substrates revealed that hydrogen and methane are potentially important substrates for the plume microbiota.

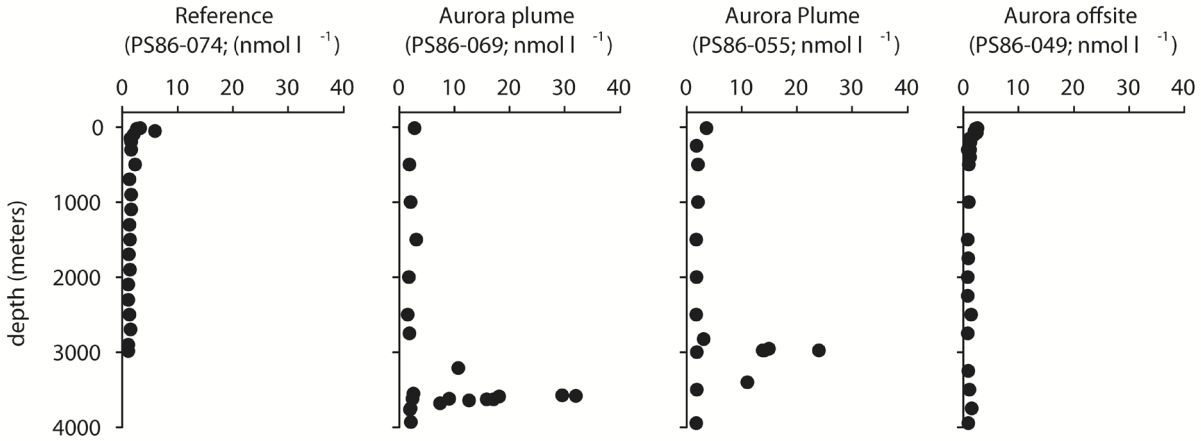

Fig. 8.1.1: Methane concentration profiles of a reference site, the Aurora field and on lee site of the plumes. Surface waters were in equilibrium with atmospheric methane concentrations. Highest methane concentrations (up to 32 nM) were measured in approx. 3,600 m. They were associated with heat anomalies and low Eh values.

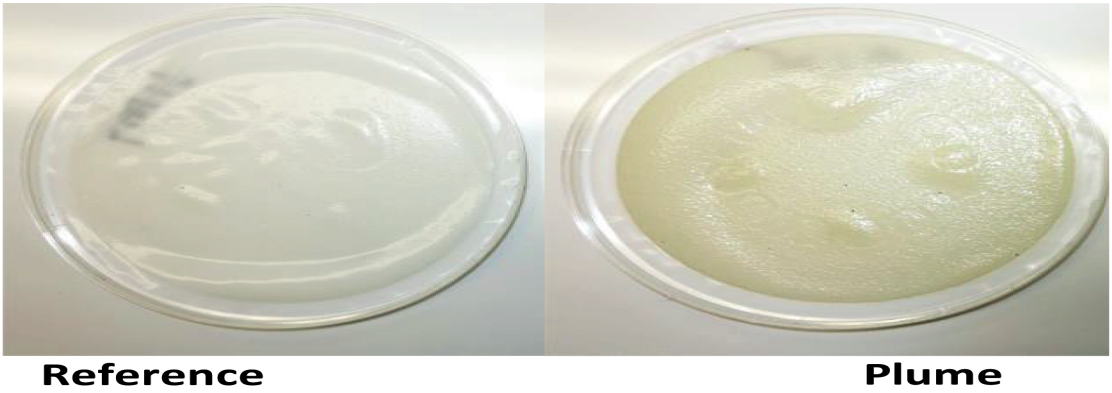

Fig. 8.1.2: Particles filtered in situ on 0.22µm membrane filters from approx. 250 liters each in reference and plume water layers. Plume layers were characterized by strongly increased density of particle that consisted most likely of inorganic matrix and microbial cells. Plume particles retrieved by in situ pumping and from CTD/rosette water samples will be analyzed in the home laboratories (i.e. massive gene / metagenome sequencing, fluorescence in situ hybridization).

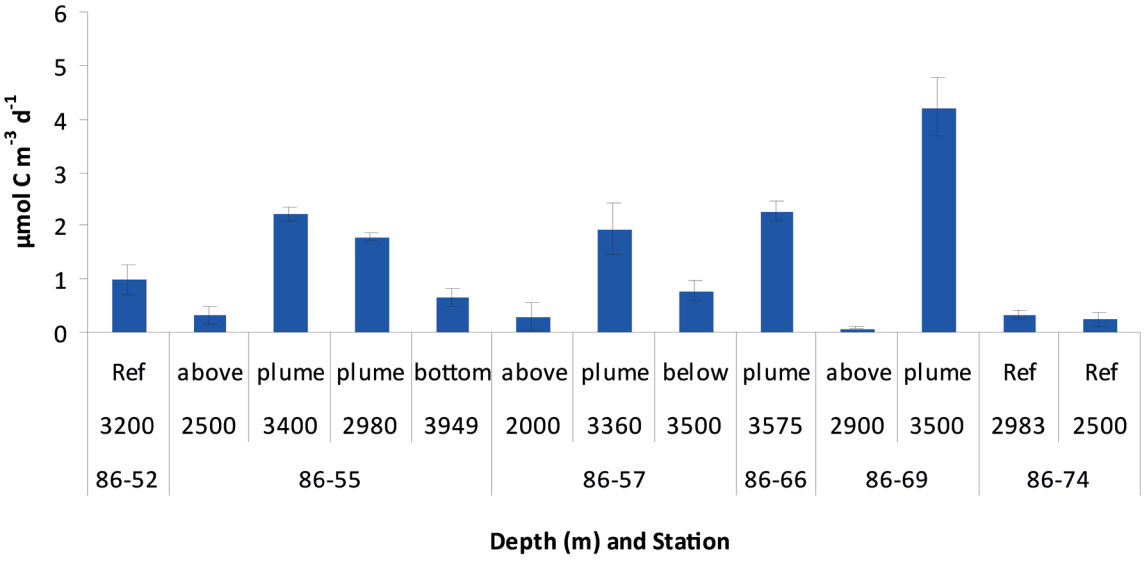

Fig. 8.1.3: Results from inorganic carbon fixation experiments using ^{14}C-labeled dissolved inorganic carbon tracer; preliminary results, awaiting correction by true DIC concentrations which are determined in the home laboratories.

Data management

Geochemical data will be quality-checked, stored and be available after publication in peer-reviewed journals through PANGAEA Data Publisher for Earth & Environmental Science. Gene sequence data of plume microbiota will be publicly available via GenBank after publication latest in two years.

8.2. OFOS Mapping

Yann Marcon[1], Christian Borowski[3], Norbert Rieper[2], Axel Nordhausen[3], Fabian Schramm[3], Alexandra Sorgenicht[4], Antje Boetius[1]

[1]AWI
[2]Isitec
[3]MPI-Bremen
[4]144film

Objectives

The existence of active hydrothermal venting on the Western segment of the Gakkel Ridge has been strongly suggested by previous exploration work in the area (Edmonds et al., 2003). The main objective of the Ocean Floor Observation System (OFOS) mapping work was to localise and confirm the occurrence of such hydrothermal vent sites on the Gakkel Ridge, as well as to investigate if they support rich chemosynthetic communities similar vents in other oceans and to investigate the composition of such communities .

Another objective of the OFOS surveys was to investigate the composition of deep sea fauna in the area and to evaluate the biogeographic role of the Gakkel Ridge in relation to the oceanography and geology of the area. The exploration of the Gakkel Ridge will indeed provide valuable data for studying the dispersal and colonization pathways for chemosynthetic and non-chemosynthetic organisms between ocean basins. Such data are rare to date because perennial ice cover makes the Gakkel Ridge hardly accessible for scientific research expeditions and thus better knowledge is urgently required. Therefore, the OFOS observations were used (1) to document the benthic macro- and megafauna populating the Gakkel Ridge, (2) to search for signs of hydrothermal activity (occurrence of fluid venting, hydrothermal precipitates and chemosynthetic organisms), and (3) to find targets for geological, geochemical, geophysical and biological exploration with other research instruments used during this cruise such as the TV-guided multicorer (TV-MUC), the TV-Grab, the gravity corer and the heatflow lance.

Furthermore, we aimed at linking observations on biological diversity and density to seawater chemistry and to assess how biology is controlled by fluid flow from hydrothermal venting. To that end, a set of sensor packages were mounted on the OFOS in order to measure several physicochemical parameters of the water column. In particular, a micro-sensor package unit provided live readings of several parameters that are directly or indirectly linked to fluid venting: temperature, redox potential, pH, as well as hydrogen sulphide (H_2S) and O_2 concentrations (Kühl and Revsbech, 2000).

Work at sea

The OFOS is a towed underwater camera system equipped with both a high-resolution photo-camera (iSiTEC, CANON EOS 5D Mark III) and a high-definition video-camera (iSiTEC, Sony FCB-H11). The cameras are mounted on a steel frame (140L x 92W x 135H cm), together with two strobe lights (iSiTEC UW-Blitz 250, TTL driven), three laser pointers at a distance of 50 cm from each other that were used to estimate the size of seafloor structures, four LED lights, a Tritech Altimeter, and a USBL positioning system (Posidonia) to track the position of the OFOS during deployments. A set of micro-sensors was mounted on the OFOS in order to provide live readings of several parameters: temperature, redox potential, pH, and H_2S and O_2 concentrations. Real-time readings permitted a rapid identification of the areas of fluid venting during the dives. This ability was rendered possible by the fast response of micro-sensors in comparison to traditional macro-sensors, which is essential as venting fluids may occur locally and be passed over rapidly by the OFOS. Additional sensors, such as the miniaturized temperature loggers (MTL) and the Miniaturized Autonomous Plume Recorders (MAPR, Baker and Milburn, 1997) were systematically mounted on the system's frame to record and monitor various physical and chemical parameters (temperature, pressure, turbidity, redox potential). Those sensors did not provide real-time feedback but their higher robustness over the micro-

sensor package ensured that most parameters were recorded.

The TV-MUC is a video-guided multi-corer system, which is able to sample up to eight 1-m long cores. It is equipped with a high-definition video-camera, two strobes, and a USBL positioning system (Posidonia) in order to visualize the sampling area and to precisely select the sampling site and record the sampling.

The OFOS and the TV-MUC were deployed from the side of *Polarstern* and towed at speeds of less than 1 knot (depending on the drift speed of the ice) and at distances of about 1.5 to 2.5 m above the seafloor. For safety reasons *Polarstern* could not break ice during deployments. Therefore, the survey paths were highly dependent on the ice drift direction, apart from a few stations where large water holes permitted slight repositioning of the vessel during the dives.

In total, 16 OFOS and 5 TV-MUC deployments were carried out during the cruise (Table 8.2.1). Deployments were mostly focused around the main Aurora mount, where previous work had identified intense hydrothermal plumes. During the cruise, further temperature or redox anomalies measured during CTD casts or with the OFOS-borne sensor packages allowed to fine-tune the search area.

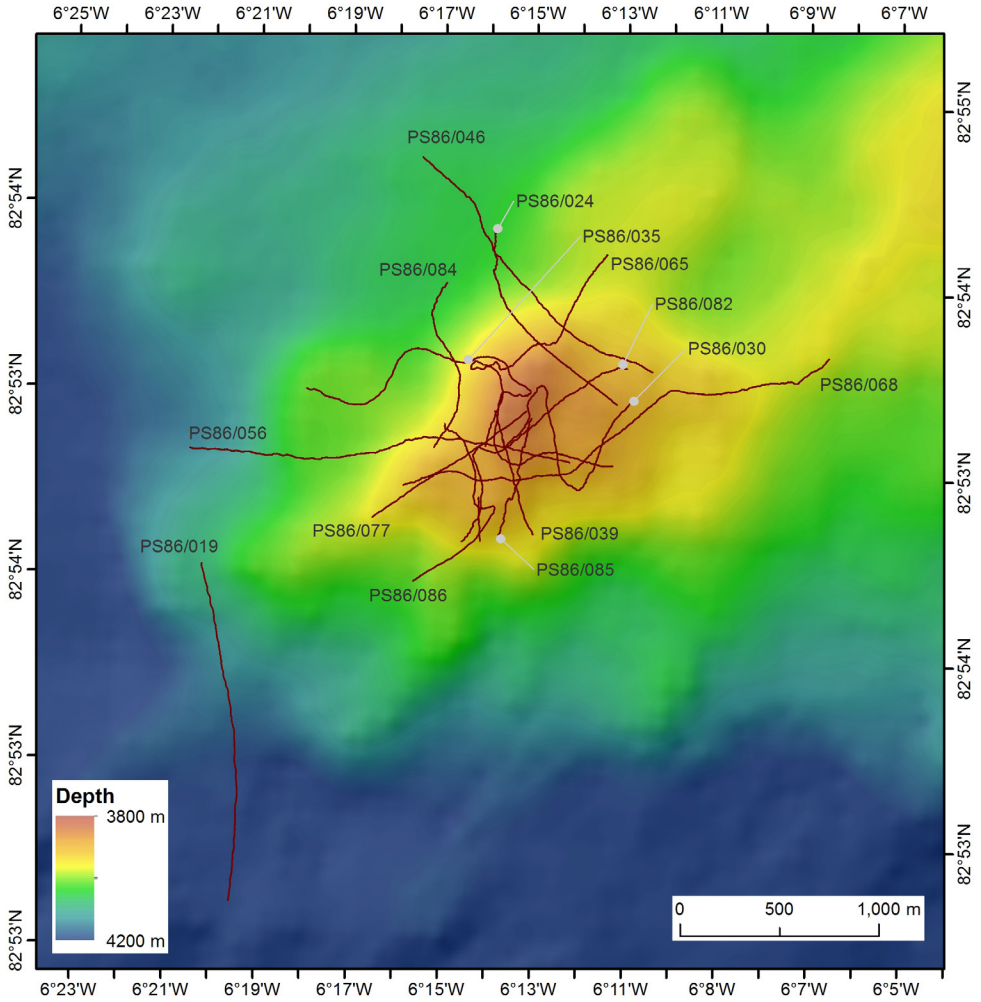

Fig. 8.2.1: Overview of the OFOS deployments at the Aurora mount

Tab. 8.2.1: Summary of OFOS and TV-MUC deployments during PS86

Device	Station No	Date	Start					End					Mounted sensors	Comments
			Off deck	At bottom	Latitude	Longitude	Depth	From bottom	On deck	Latitude	Longitude	Depth		
OFOS	PS86/019	12.07.2014	15:15:00	16:33:03	82°53.565'	-6°21.097'	4046	18:15:48	19:52:00	82°52.688'	-6°19.706'	4127	Microsensors MTL MAPR	
TV-MUC	PS86/020	12.07.2014	20:09:00	21:35:48	82°51.06'	-6°23.738'	4580	21:51:39	23:30:00	82°51.009'	-6°24.149'	4602		
OFOS	PS86/024	13.07.2014	21:03:23	22:21:03	82°54.546'	-6°15.454'	4046	01:40:04	02:55:00	82°54.116'	-6°12.401'	3895	Microsensors MTL MAPR	
TV-MUC	PS86/028	14.07.2014	19:11:10	20:34:17	82°55.191'	-6°16.467'	4119	20:40:43	22:12:06	82°55.179'	-6°16.65'	4125		
OFOS	PS86/030	15.07.2014	07:37:47	08:47:36	82°53.987'	-6°14.783'	3826	12:26:15	13:44:00	82°54.122'	-6°12.178'	3878	Microsensors MTL MAPR	
OFOS	PS86/035	16.07.2014	12:56:00	14:16:00	82°54.069'	-6°19.211'	4023	19:35:09	20:51:00	82°53.949'	-6°12.351'	3906	Microsensors MTL MAPR	
OFOS	PS86/039	17.07.2014	17:19:00	18:42:55	82°54.062'	-6°15.059'	3816	19:56:51	21:57:00	82°53.741'	-6°13.942'	3965	Microsensors MTL MAPR	
TV-MUC	PS86/041	18.07.2014	07:27:00	08:48:37	82°54.76'	-6°21.063'	4113	11:32:37	12:50:00	82°53.938'	-6°14.488'	3822		
OFOS	PS86/046	19.07.2014	15:57:20	13:13:09	82°54.728'	-6°17.245'	4060	15:56:28	17:14:00	82°54.214'	-6°11.695'	3941	Microsensors MTL MAPR	No video camera Microsensors data useless (caps still on)
OFOS	PS86/050	20.07.2014	16:10:00	17:18:36	83°4.721'	-6°5.893'	3526	20:46:20	22:06:00	83°4.17'	-6°4.407'	3641	Microsensors MTL MAPR	No video camera
OFOS	PS86/054	21.07.2014	19:11:11	20:29:50	83°1.209'	-6°17.173'	3986	22:02:41	23:32:00	83°1.086'	-6°17.495'	3928	Microsensors MTL MAPR	No video camera
OFOS	PS86/056	22.07.2014	12:54:00	14:14:19	82°53.876'	-6°21.612'	4141	17:09:01	19:36:00	82°53.941'	-6°13.084'	3684	Microsensors MTL MAPR	No video camera
TV-MUC	PS86/061	23.07.2014	18:40:06	19:54:09	82°54.027'	-6°16.051'	3952	21:19:20	22:50:00	82°53.849'	-6°15.811'	3902	MTL	one light only
OFOS	PS86/065	24.07.2014	15:03:41	16:21:38	82°54.519'	-6°12.967'	3975	20:48:00	22:16:00	82°53.709'	-6°15.071'	3944	Microsensors MTL MAPR	No video camera
OFOS	PS86/068	25.07.2014	10:57:00	12:12:44	82°54.301'	-6°7.877'	3949	17:33:37	18:57:00	82°53.838'	-6°16.878'	3894	Microsensors MTL MAPR	No video camera
TV-MUC	PS86/076	27.07.2014	17:41:40	18:55:05	82°53.781'	-6°14.79'	3901	18:56:02	21:30:42	-6°14.816'	-6°14.816'	3899		
OFOS	PS86/077	27.07.2014	22:24:31	23:28:11	82°54.072'	-6°14.368'	3814	01:08:23	02:20:00	82°53.742'	-6°17.475'	3961	Microsensors MTL MAPR	No video camera
OFOS	PS86/082	28.07.2014	21:16:17	22:22:17	82°54.216'	-6°12.264'	3905	01:54:52	02:20:00	82°53.703'	-6°15.474'	3946	Microsensors MTL MAPR	No video camera
OFOS	PS86/084	29.07.2014	10:34:28	11:53:30	82°54.396'	-6°16.403'	4052	14:13:25	15:25:00	82°53.949'	-6°16.296'	3876	Microsensors MTL MAPR	No video camera
OFOS	PS86/085	29.07.2014	17:20:01	18:18:35	82°54.055'	-6°14.232'	3858	20:15:24	21:26:00	82°53.728'	-6°14.697'	3944	Microsensors MTL MAPR	No video camera
OFOS	PS86/086	29.07.2014	22:05:51	23:09:17	82°54.015'	-6°16.115'	3955	01:07:36	02:22:00	82°53.582'	-6°16.434'	4025	Microsensors MTL MAPR	No video camera

Preliminary results

OFOS and TV-MUC dives were all conducted within the ridge axis, and all but one OFOS and one TV-MUC deployments targeted the Aurora mount (Fig. 8.2.1). The remaining dives targeted a northerly mount, which served as a reference site.

The main result is that the suggested existence of focused hydrothermal fluid discharge at the Aurora mount (Edmonds et al., 2003) was confirmed by visual observations during OFOS dive PS86/086. The dive video showed black smoke outlets as well as shimmering water and chimneys covered by bright orange material, likely iron-rich precipitates. These observations were complemented by data from the OFOS-mounted micro-sensors, which recorded increases in temperature (+0.95°C) and H_2S concentration (+600 nM) while passing above the shimmering water near the chimneys. Bacterial mats and small white organisms, possibly limpets, occurred on and around the chimneys. However, typical chemosynthetic megafauna such as tube worms, mussels, clams or symbiotic shrimp similar to those known from the Mid-Atlantic Ridge were not observed.. The hydrothermal vent field lies on a sulphide mount that is located to the southwest of the main Aurora mount. Several dives (PS86/065, PS86/068, PS86/082 and PS86/085) around this area revealed small inactive chimneys as well as deep canyons and holes in the sediment cover, most of which were associated with strong temperature anomalies (up to +0.04°C above background temperature). In a few cases, anomalies in H_2S concentrations were also recorded. Although the water column data and the spatial proximity to the active vent fields suggest a close link between these features, the mechanisms involved in the formation of these holes and canyons are not yet fully understood.

More generally, the seafloor topography appeared a lot rougher than previously suggested by the hydroacoustic data. In particular, the Aurora mount is bordered on every side by 10 to 30 m-high vertical basaltic rocky cliffs and it is topped with a mostly flat cover of sediments. The rocky cliffs were either populated by abundant filter feeders or they were covered by thin layers of sediments and devoid of organisms. Positive temperature anomalies up to 0.02°C were consistently measured near the top of the western cliffs (PS86/035, PS86/039, PS86/056 and PS86/077), indicating release of geothermal energy in the area. Those cliffs were abundantly populated by sessile organisms. Finally, numerous holes (mostly below 1 m in diameter) in the sediment cover were observed in the vicinity of the rocky slopes, some of which were likely caused by sediment collapse between pillows.

The seafloor observations from the remaining dives revealed a variety of terrain types, which mostly included flat areas covered with soft sediments occasionally rippled and whitish, steep cliffs of basaltic pillows and talus material, as well as high-dissected terrains of hardened and layered sediments including canyons and holes of various sizes. An overview of the terrains and features of interest that were encountered is provided in Fig. 8.2.2.

Overall, the most striking discoveries are located on the southwestern side of the Aurora mount (Table 8.2.2) and include the following:

- Dive PS86/065 and PS86/086: huge circular holes in the sediment cover (4 - 5 m wide, 4 m deep); the layering of the surrounding sediments indicates that the depressions were created after the sediment deposition, probably from an explosive event. The walls of the different depressions revealed similar layers of white sediment as well as one dark layer (likely ashes). The occurrence of those depressions coincided perfectly with localized peaks in temperature (up to 0.02°C above background temperature) and H_2S concentrations (up to 100 nM above background value). Hardened or rocky layers near the bottom of the deepest depressions were populated by sponges, indicating locally enhanced energy supply.

- Dives PS86/082 and PS86/086: Deep canyons in the sediment cover, oriented in an NW-SE direction. Anemones and sponges occurred on the hard layers in the lower part of the gullies. The micro-sensors recorded temperature anomalies up to 0.04°C.
- Dives PS86/068 and PS86/085: Chimney structures at the bottom of the Aurora southwestern flank. While the chimneys looked hydrothermally inactive, they were densely populated by filtering organisms, such as sponges. According to the laser pointers, the chimneys may be between 0.5 and 2 m wide, and up to 2 m high. The micro-sensors did not indicate any anomaly.
- Dives PS86/086: Discovery of an active hydrothermal venting site, with black smoke, shimmering water, chimneys and iron precipitates. The micro-sensors recorded temperature anomalies close to 1°C, and H_2S and O_2 anomalies up to +600 nM and -3.4 µM, respectively.

Tab. 8.2.2: Location of the main features observed during the OFOS surveys

OFOS dive	Feature	USBL Latitude	USBL Longitude	USBL Depth
PS86/065 PS65/086	Main hole area (see text)	82° 53.81' N	6°15.2' W	3890 m
PS86/068	Chimney structures (inactive)	82° 53.88' N	6°14.90' W	3878 m
PS86/068	Chimney structures (inactive)	82° 53.87' N	6°15.17' W	3893 m
PS86/082	Canyon area	82° 53.80' N	6°15.14' W	3893 m
PS86/085	Chimney structures (inactive)	82° 53.81' N	6°14.59' W	3906 m
PS86/086	Canyon area	82° 53.80' N	6°15.06' W	3944 m
PS86/086	Vent field	82° 53.83' N	6°15.32' W	3883 m

Faunal observations included many sightings of two shrimp species on sediment- and rock-covered areas that were easy to distinguish by their different morphology and colour. However, these shrimp live solitary and swarms were not observed. Sessile filtering organisms (e.g. sponges, anemones) populated most rocky areas with often surprising abundances that were highest on the basaltic cliffs marking the western slopes of the Aurora mount. They included two or more species of anemones and a variety of at least five different sponge spiecies. These animals were also abundant on the hard substrata near the bottom of the canyons and holes. Large patches of dead sponges as well as numerous holes resembling animal burrows were commonly encountered on sediment-covered areas, however, we were not able to discover the origin of these structures. Holothurians were extremely rare and this was striking because this taxon is usually very common in sedimented deep-sea habitats including other investigated Arctic regions. Other animals which were encountered regularly, although not in large abundances, were brittle stars, very actively swimming ribbon-shaped worms that resembled nemertines and slender crustations of approximately 10 cm body length which we preliminarily determined as isopods.

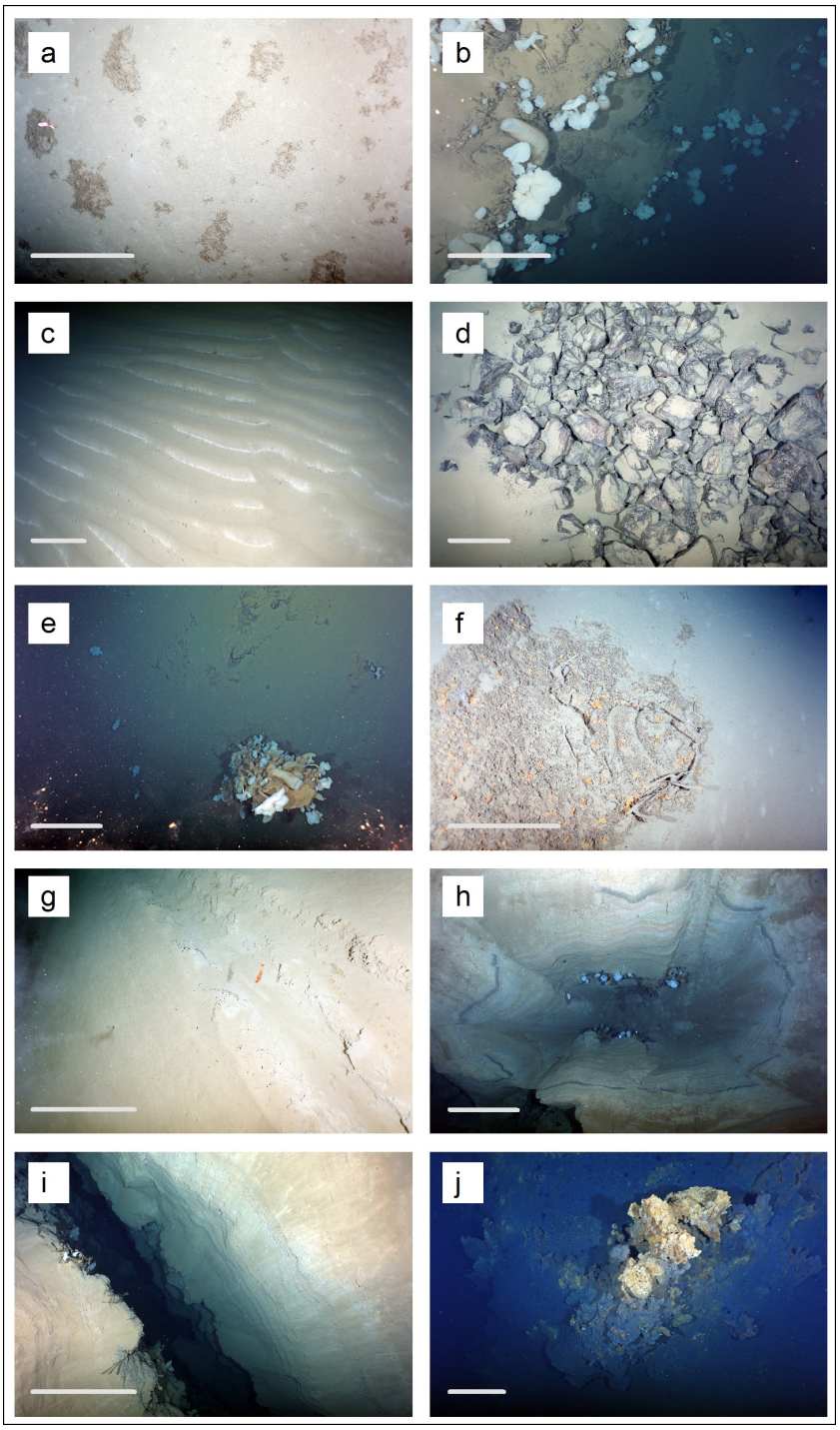

Fig. 8.2.2: Photos taken with the OFOS. On all photos, the scale bar represents 50 cm. (a) Dead sponges on soft sediments; (b) Abrupt cliff of sediment-covered pillows populated by sponges; (c) Sediment ripples; whitish sediments occur within the ripples; (d) Broken pillows; (e) Inactive chimney covered by sponges; (f) Unidentified orange material retained by the texture of the dead sponges; the orange material seems to originate from the venting activity; (g) Red shrimp in soft sediments; the mark on the seafloor is that of former dredge D8 from the 2001 AMORE cruise (Edmonds et al., 2003); (h) Deep hole (4-5 m deep) showing the layering of the sediments; the dark layer near the top may be ashes; sponges populate the hard layers near the bottom; (i) Canyon/rift crossing the sediment layers as in (h); sponges populate the hard layers near the bottom; (j) Vent site with active sulphide chimney.

A comparison of the two studied areas (the Aurora mount and the northern reference site) indicates that the faunal abundance varies greatly between the two sites. Indeed, the reference stations on the northern mount (PS86/50 and PS86/54) showed much less faunal abundances than the Aurora mount. This indicates that energy supply at the Aurora mount is higher than in the northern reference site and it is likely that this is related to the venting activity at Aurora.

Indeed, our sensor measurement suggest that Aurora hydrothermal vent fluids are rich in reduced substances, such as reduced metals, hydrogen and sulphide. The micro-sensors unit that was deployed with all OFOS dives is convenient to identify the presence of venting fluids. The most sensitive sensors for anomalies indicative of fluid venting were redox, temperature and sulphide. Redox anomalies were almost exclusively observed in the water column during the descent and ascent of the OFOS (Table 8.2.3), while anomalies in temperature and hydrogen sulphide (Table 8.2.4) were generally measured close to the bottom (< 2 m altitude). Furthermore, anomalies in H_2S always coincided with positive temperature anomalies (Fig. 8.2.3). Oxygen concentrations and pH did not show consistent trends with anomalies in redox or sulphide.

Tab. 8.2.3: Water column anomalies detected with the micro-sensor package during OFOS dives.

OFOS dive	Water column anomalies	From	To
PS86/024	Redox (OFOS descent) (50-70 mV decrease)	Lat.: 82°54.62' N Lon.: 6°15.23' W Depth: 2900 m	Lat.: 82°54.55' N Lon.: 6°15.46' W Depth: 4000 m
PS86/039	Redox (OFOS descent) (25-40 mV decrease)	Lat.: 82°54.12' N Lon.: 6°15.31' W Depth: 3000 m	Lat.: 82°54.06' N Lon.: 6°15.05' W Depth: 3800 m
	Redox (OFOS ascent) (30-50 mV decrease)	Lat.: 82°53.71' N Lon.: 6°13.85' W Depth: 3500 m	Lat.: 82°53.67' N Lon.: 6°13.83' W Depth: 2750 m
PS86/068	Redox (40-130 mV decrease) and temperature variations (OFOS ascent)	Lat.: 82°53.83' N Lon.: 6°17.07' W Depth: 3600 m	Lat.: 82°53.81' N Lon.: 6°17.29' W Depth: 3200 m
PS86/077	Redox (OFOS descent) (80 mV decrease)	Lat.: 82°54.14' N Lon.: 6°13.89' W Depth: 2950 m	Lat.: 82°54.11' N Lon.: 6°14.10' W Depth: 3600 m
PS86/086	Redox (OFOS descent) (50 mV decrease)	Lat.: 82°54.1' N Lon.: 6°15.98' W Depth: 3100 m	Lat.: 82°54.03' N Lon.: 6°16.10' W Depth: 3900 m

Tab. 8.2.4: Location of the bottom anomalies in temperature and hydrogen sulphide that were detected with the micro-sensor package during OFOS dives.

OFOS dive	Bottom anomalies	USBL Latitude	USBL Longitude	USBL Depth
PS86/035	Temperature (+0.015°C)	82° 55' N	6°15' W	3855 m
	Temperature (+0.02°C)	82° 54.03' N	6°14.99' W	3824 m
PS86/039	Temperature (+0.005°C) and H_2S (+150 nM)	82° 54.03' N	6°14.93' W	3819 m
PS86/056	Temperature (+0.01°C)	82° 53.97' N	6°14.98' W	3835 m
	H_2S (+200 nM)	82° 53.97' N	6°14.99' W	3840 m

OFOS dive	Bottom anomalies	USBL Latitude	USBL Longitude	USBL Depth
PS86/065	Temperature (+0.02°C)	82° 54.15' N	6°15' W	3826 m
	H_2S (+150 nM)	82° 54.18' N	6°15.16' W	3865 m
	Temperature (+0.02°C)	82° 53.80' N	6°15.19' W	3892 m
	H_2S (+100 nM)	82° 54.15' N	6°15' W	3825 m
	Temperature (+0.02°C)	82° 53.76' N	6°15.15' W	3904 m
	H_2S (+100 nM)	82° 53.75' N	6°15.11' W	3912 m
PS86/068	Temperature (+0.005°C)	82° 54.28' N	6°08.01' W	3953 m
PS86/077	Temperature (+0.01°C)	82° 54.01' N	6°14.9' W	3828 m
PS86/082	Temperature (+0.05)	82° 53.79' N	6°15.14' W	3890 m
	Temperature (+0.05°C)	82° 53.77' N	6°15.17' W	3902 m
PS86/086	Temperature (+0.95°C) and H_2S (+600 nM) and O_2 (-3.4 µM)	82° 53.83' N	6°15.32' W	3883 m

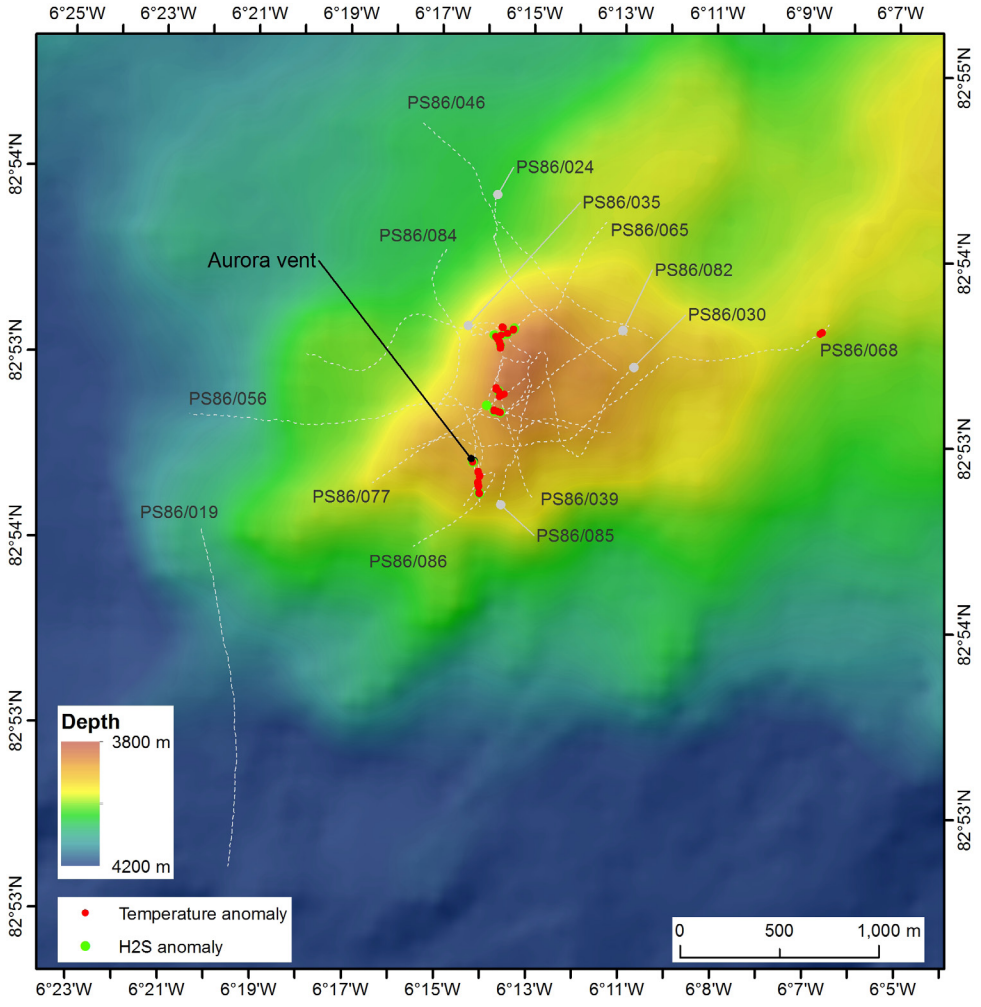

Fig. 8.2.3: Locations of all temperature and H_2S anomalies recorded during the OFOS deployments at the Aurora mount

Data management

Tracks of video and photography surveys will be stored in PANGAEA Data Publisher for Earth & Environmental Science archive. The photographic material will be made available to taxonomists and further image analysis via BIIGLE, while the video material will be made available on the MARUM Deep-Sea Video Database (marum.vidlib.de).

References

Baker E, Milburn H (1997) MAPR: a new instrument for hydrothermal plume mapping. Ridge Events, 8 (1), 23-25.

Edmonds HN, et al. (2003) Discovery of abundant hydrothermal venting on the ultraslow-spreading Gakkel ridge in the Arctic Ocean, Nature, 421, 252-256.

Kühl M, Revsbech NP (2000) Biogeochemical microsensors for boundary layer studies., in: Boudreau, B., Jørgensen, B.B. (Eds.), The benthic boundary layer. Oxford University Press, 180-210.

8.3. Sediment biogeochemistry

Gunter Wegener[1,3], Rafael Stiens[1], Mirja Meiners[1], Luise Wagner[2], Denise Bachmann[2], Alexander Diehl[2], Andreas. Türke[2]

[1]MPI Bremen
[2]Uni Bremen, MARUM

Objectives

The main objective here was to investigate sediments, sedimentary porewater and sediment microbial communities for patterns derived from volcanism and hydrothermal activity. The sediments would archive signs of volcanic activity such as ash or basalt glasses, or their diagenesis products. Hydrothermal activity may cause specific sulfate profiles, elevated concentrations of methane, dissolved iron or other reduced compounds or rapid pH changes. Furthermore, hydrothermal activity may lead to enhanced microbial metabolic activity, changes in cell abundances and distinct microbial community compositions. To search for these patterns we sampled and compared sedimented areas in the Aurora field with background sediments by gravity coring and TV-guided multicoring. Furthermore we investigate dark CO_2-fixation in the Aurora vent area.

Work at sea

Sediment samples for microbiological and biogeochemical analyses were retrieved by TV-guided multicoring (MUC) and gravity coring (GC). High resolution bathymetry and video-guided observation (OFOS) identified sampling spots, which were confirmed by the telemetry of the TV-MUC.

Sampling with TV-MUC was only possible in flat, sedimented areas, which excluded deep troughs, cliffs or rocks. The retrieved sediment cores were stored in the refrigerated container at 0°C. The porewater was sampled from intact cores (every cm from the top to 10 cm, in deeper depth every 2 cm) using Rhizons (19.21.21F, mean pore size 0.15 µm; Rhizosphere Research Products, Wageningen, Netherlands). The porewater was split and fixed for later determination of dissolved inorganic carbon, alkalinity, nutrient content (silicate, phosphate, ammonium, nitrate, nitrite), sulfate and sulfide in the home laboratory. Replicate multicorer cores were subsampled in three depth layers (0-1 cm, 1-5 cm, 5-10 cm) for the determination of total cell numbers (acridine orange direct counts; AODC), and for the determination of phylogenetic groups by 16SrDNA specific fluorescence *in-situ* hybridization; CARDFISH).

Measurements of the activity of extracellular enzyme activities (EEA; β-glucosidase, chitobiase, aminopeptidase and esterase) were performed directly on board using a fluorescence-labelled assay. The microbial inorganic carbon fixation in the sediments was tested with in 14C-DIC tracer incubations of surface sediments and deeper sediments. To analyze microbial community compositions and functioning (DNA and RNA analysis), sediment subsamples are collected and stored at -80°C. Furthermore, samples for the determination of chlorophyll-a (Chl-a) and sediment porosity were also taken.

Gravity cores were stored in the 0°C room. First, pore water was sampled using Rhizons. Our sampling included parameters such as DIC, alkalinity, sulfide/ sulfate content and nutrients as well as metal contents. After that, gravity cores were cut into working and archive halves. The sedimentology in these cores was documented (for documentation and systematic core description, see Chapter 6). Immediately samples were collected to analyze methane content (directly on board). Furthermore, sediments samples were collected for acridine orange direct cell counts (AODC; fixation in formamide solution). Frozen samples were stored for microbial DNA analyses in the home laboratory.

Preliminary results

On board, MUC sample analysis was limited to the enzyme assay, which tests the potential of the sedimentary community to degrade specific compound classes, such as sugars (via β-glucosidase), esters (via esterases), chitin (via chitobiases) and aminoacids (via aminopedidases). The activity of glucosidase and chitobiase were clearly concentrated in the upper horizon, whereas aminopeptidase and esterase are similarly high in all three horizons (Fig. 8.3.1). The inorganic carbon fixation was tested and fully analyzed for several surface sediments recovered by multicoring (Fig. 8.3.2). Experiments on the subsurface inorganic carbon fixation (material from gravity cores) will be processed in the home laboratory. The measured activities reflect those of arctic background sediments, and confirm the low hydrothermal imprint on the MUC sampling sites. In combination with geochemical data, obtained enzyme activities and microbial carbon fixation rates will be used to explain patterns in microbial community structures within the Aurora area.

Sediments sampled by gravity coring have low methane concentrations, reflecting arctic background sediments (Fig. 8.3.3). Methane concentrations remained low throughout the core. In the home laboratory the sampled waters will be analyzed for signs of advective porewater flow.

Data management

Geochemical data and AODC cell counts will be quality-checked, stored and be available after publication in peer-reviewed journals through PANGAEA Data Publisher for Earth & Environmental Science. Gene sequences of processes sediment microbiota will be publicly available via GenBank after publication aimed within the next two years.

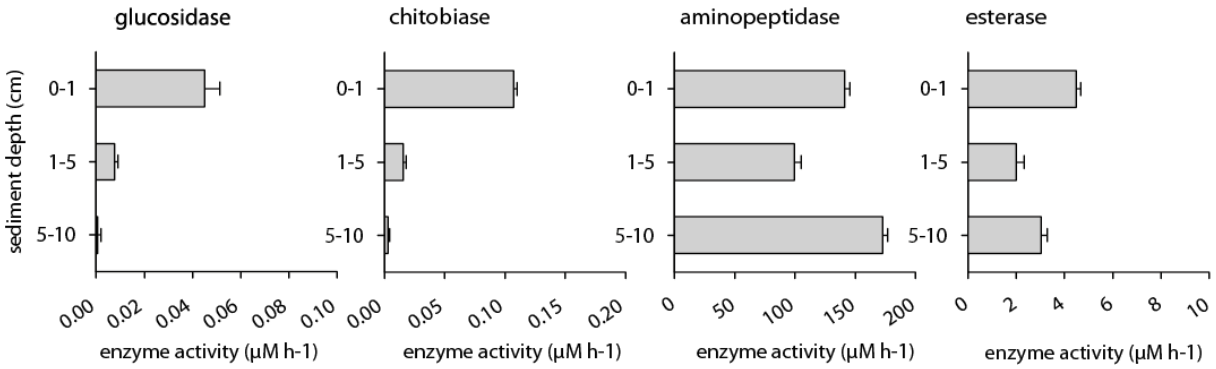

Fig. 8.3.1: Example for enzyme activity measurements in surface sediments of the TV-MUC sediments core PS86/020

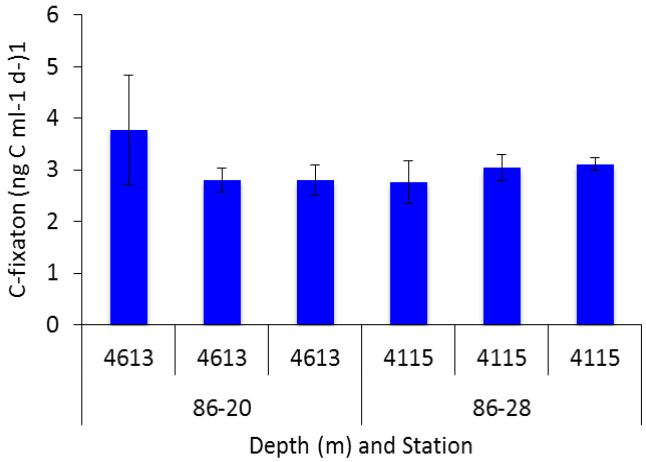

Fig. 8.3.2: Dark CO_2 fixation in surface sediments (0-1 cm layer) of sediments from the wider Autora area. Sediments were recovered by TV-guided multicoring. Carbon fixation is evenly distributed in the vent area. Samples for carbon fixation in subsurface sediments are processed in the home laboratories.

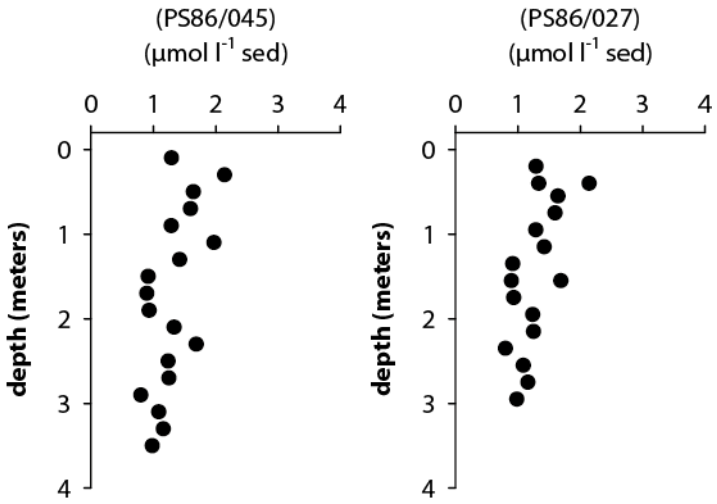

Fig. 8.3.3: Example for methane concentration profiles in the vicinity of the Aurora vent field. Sediments are recovered by TV-guided gravity coring.

9. SEA ICE OBSERVATIONS

Christian Katlein[1], Stefanie Arndt[1], Mikko Lensu[2,] [1]AWI
Marcel Nicolaus[1] (not on board) [2]FMI

Objectives

The observed shift from thicker multi-year to thinner first-year sea ice in the Arctic has consequences for various physical and biological processes within the sea ice and the upper ocean layer. For example, thin ponded sea ice transmits a significantly higher portion of the incoming solar radiation than snow covered thick ice (Nicolaus et al., 2012). Hence, the optical properties of sea ice determine the amount of light (energy) that is transmitted into the ice and further into the upper ocean, contributing to warming and melting of sea ice. In addition, the amount of solar radiation dominates primary production and other biological processes in and below the ice layer. Following up observations during earlier cruises (ARK XXVI/3 and ARK XXVII/3), which took place during August / September 2011/2012, we tried to quantify the amount of light transmitted through sea ice during early summer. The availability and the variability of light in and under different types of sea ice differ compared to later phases in the seasonal cycle. These data will lead to a better understanding of the seasonal evolution of Arctic sea ice, in particular during July, when the solar surface energy fluxes are large, such that small changes in ice properties have large impacts on the energy budget. In that respect, the thickness and properties of the snow cover are known to be most critical for energy budget estimates. Hence, it is necessary to obtain snow measurements along with the optical measurements.

An additional source of information regarding the state of the Arctic sea ice and its snow cover is visual classification of key sea ice variables by sea ice observers. Though quite subjective, visual observations have the promise of creating large datasets due to the numbers of vessels in the summer Arctic. Such datasets are of high value to record the ice conditions during various observations during the cruise and for validation of remote sensing products.

The geometry of sea ice exhibits large variation in all scales which is mirrored by the variation of energy fluxes. The geometric variation can be described in terms of distributions for key variables: ice thickness, floe size, leads, and ice ridges. These are needed especially in sub grid scale, the length scale shorter than the resolution of Arctic ice drift models. The geometric variation is inherently related to local scale ice kinematics related to opening, closing and deformation. The local kinematics has strong stochastic features contrasting to the continuous larger scale fields of ice drift models. We seek to quantify the local geometry around the ship in high temporal and spatial resolution. Such data can also be compared with the visual observations so that rules for estimating errors and correcting systematic biases in the observational data can be formulated.

Work at sea

Spectral light transmission through snow and sea ice was measured during dives with the WHOI ROV (see chapter 10). In close collaboration with the WHOI group, three scientific dives under sea ice were performed, revealing spatial variability of under-ice radiation as a function of sea ice and surface types and vertical profiles for the determination of optical properties of the underlying water column.

Transects of snow depth on sea ice were obtained on a total of 8 ice floes accessed via gangway or helicopter.

The basic physical properties of different sea ice types such as thickness and snow cover were assessed during one ice station conducted in concert with the last ROV dive.

Fig. 9.1: Snow thickness measurements during a helicopter ice-station using the Magna Probe

Continuous observations of the sea ice conditions were made during hourly observations of sea ice conditions by trained observers from the bridge.

During the cruise we deployed three SAMS type ice mass balance buoys, and sea ice drift was monitored using the ARGOS position of the drifting seismometer array (see chapter 4). We assisted station and navigation planning by providing several remote sensing and forecast products:

- OSSI near real time maps of sea-ice concentration updated every 3 hours from passive microwave sensors obtained via Drift&Noise,
- daily MODIS image of the target area in the visible channel,
- daily 8 day forecast of sea-ice conditions and drift as provided from the TOPAZ forecast system via myocean.org.

Both the OSSI ice concentration maps and the MODIS images were shown as background map in the software GlobalMapper to assist navigation on the bridge.

The local geometry of ice cover was monitored from radar imagery and by field observations. Radar images (polar files) stored by the continuously operating WaMoS wave radar were retrieved and processed on board. The generated plan position indicator images, displaying also location and ship data, were stored during all ice going. Their range is 2.1 km and resolution

7.5 m. Radar mosaics along selected route sections were generated. Aerial photographs taken from helicopter were used to identify ice signatures and surface types in time matching radar images. Control points were identified between the two and the aerial photographs were rectified and co-registered with respect to the radar image. Additional validation data was provided by the surface elevation profiles measured during field stations.

Preliminary results

Spectral light transmission was measured during three dives of the NUI ROV using two RAMSES ARC/ACC spectrophotometers (TriOS Gmbh, Rastede, Germany) connected via the glass-fibre network to a recording computer at the topside similar as shown by Nicolaus et al. (2013). Both, lateral transects, as well as vertical profiles were recorded. All under-ice measurements were evaluated as relative to the incoming light field registered with a third sensor mounted in the ships crow's nest.

As expected, light transmittance of the thick snow covered multi-year sea ice was very low and the spatial variability mostly related to the melt stage of the surface. Light absorption in the water column was clearly depth dependent, with higher values of the extinction coefficient (1.8 m^{-1}) above 10 m and lower values (0.9 m^{-1}) below 15 m.

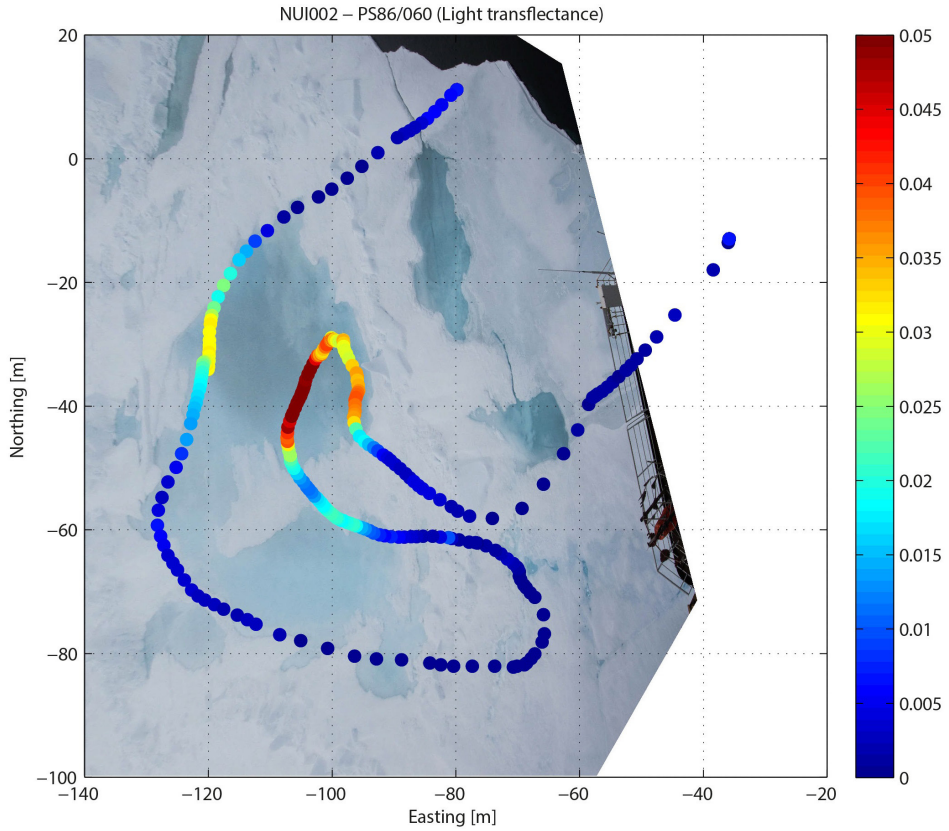

Fig. 9.2: Lateral transect of light transflectance during PS86/060 (NUI-dive 002) plotted on top of an image taken from the ships crow's nest.

Transects of snow depth measurements with 2,617 data points acquired with the Magna Probe (Snow Hydro, Fairbanks, USA) were taken on a total of 8 ice floes. We observed a mean snow thickness of 14 cm and a modal maximum around 5-6 cm. Frequently, parts of the snow surface were flooded with footsteps leaving behind little puddles.

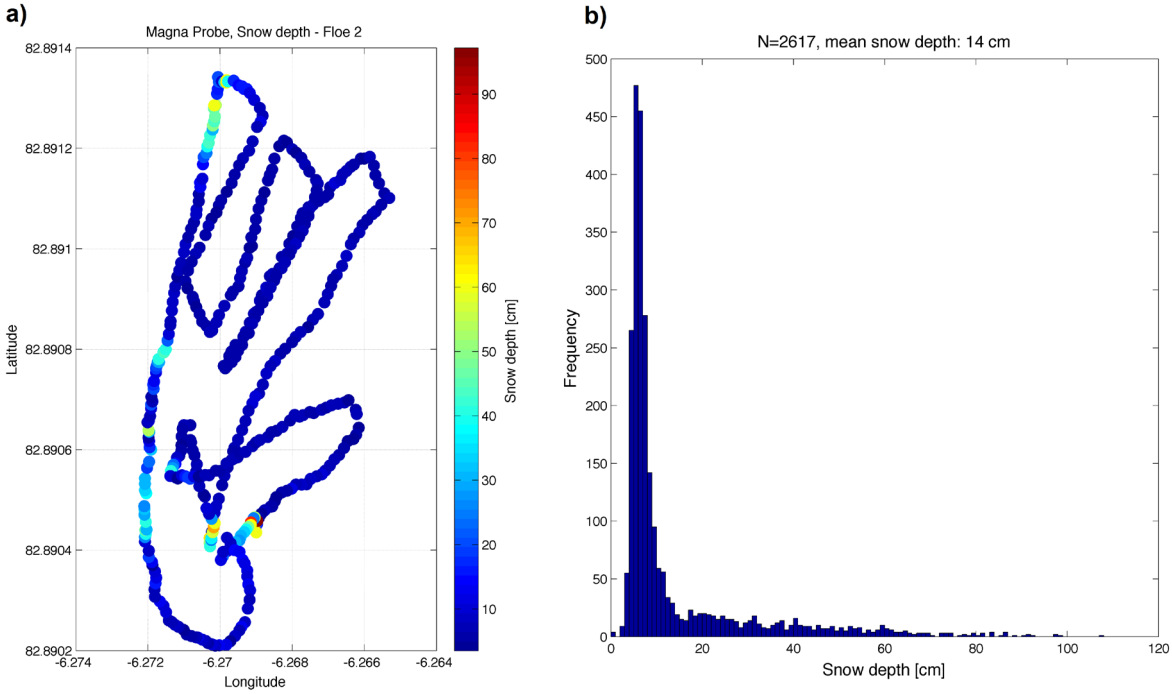

Fig. 9.3: a) Map of snow thickness distribution on an exemplary ice floe. b) Histogram of all snow-thickness measurements acquired with the magna probe.

The continuous observations of the sea ice conditions during the cruise were made using the ASSIST 2.0 software. Observers were trained at the beginning of the cruise. On the northward voyage *Polarstern* travelled in the mostly open waters in the polynya on the Greenland side of Fram strait. The exceptionally large opening of the polynya enabled the ship to make up for some of the time losses that occurred at the start of the voyage. Only about 40 miles before the target area at the Aurora vent field the ice concentration increased significantly to 70-80 %. During the time at the Aurora vent field a high number of large open water ponds occurred in the area. Nearly all sea ice encountered on this voyage was old multiyear sea-ice with a level ice thickness around 2-2.5 m with significant snow cover. While the stage of early melt pond formation could be observed during the first few days, ponds consolidated to mostly discrete ponds surrounded by water saturated snow. Most of the ice exhibited strong signs of deformation with ridge sail heights above 3 m.

In the first half of the cruise, three SAMS type ice mass balance buoys where deployed by helicopter after initial testing on board. Difficult flight weather conditions inhibited long distance flights on many days. The buoys were deployed on level ice with a thickness between 2.16 m and 2.42 m with a mean distance to each other of 50 nm. All buoys are reporting measurements successfully via iridium satellite.

Fig. 9.4: (left) One of the three SAMS type IMB buoys deployed during the cruise. (right) Map of deployment positions and drift tracks of the deployed buoys.

ARGOS position data of the drifting seismometer array (see Chapter 4) were retrieved and plotted to assist station planning with sea-ice drift information. After an initial phase of fast southerly drift, which could be explained by tidal and wind forcing, drift paths took a less predictable pattern. The sea-ice forecast obtained daily from the TOPAZ system proved to be only helpful for a very rough prediction of drift speed and a general drift direction, but not for the drift development of the upcoming hours needed for positioning of the ship to reach the deep sea positions of interest.

The basic WaMoS radar data provided useful material although no adjustments that could have resulted to a better image quality and wider range could be done. The stored radar image quicklooks can be used to survey ice conditions during the cruise and the georeferencing enables the generation of along route radar mosaics. In lower concentrations the geometry of floes and ridges on them is clearly visible. The clutter from waves that in the oceanic conditions obscures the images is mostly absent and ice free open water appears black.

Higher concentrations pose challenges for image interpretation (Fig. 9.5). Leads with small floes and fragmented ice have very high backscattering intensity (A). Narrow leads can be visually indiscernible from ridges, floe boundaries are obscured, and visual concentration estimates go astray. Image processing methods addressing these problems must be developed before automated algorithms estimating concentrations in all conditions are possible. Apart from this problem, Fig. 9.5 demonstrates that the retrieving of ridging is possible (B). The large melt ponds are seen (C), and generally the level ice intensity decreases with increasing melt pond coverage. The brighter round area close to the ship (D) has similar melt pond characteristics with the adjacent area (E) and other level ice areas of the image. This suggests older age. In the opposite corner, an instance of feature disappearing due to ridge shadowing (F) is seen. This is a case of range effects, which add to the general decrease of intensity with distance. Other comparisons between aerial photographs and radar images support these observations.

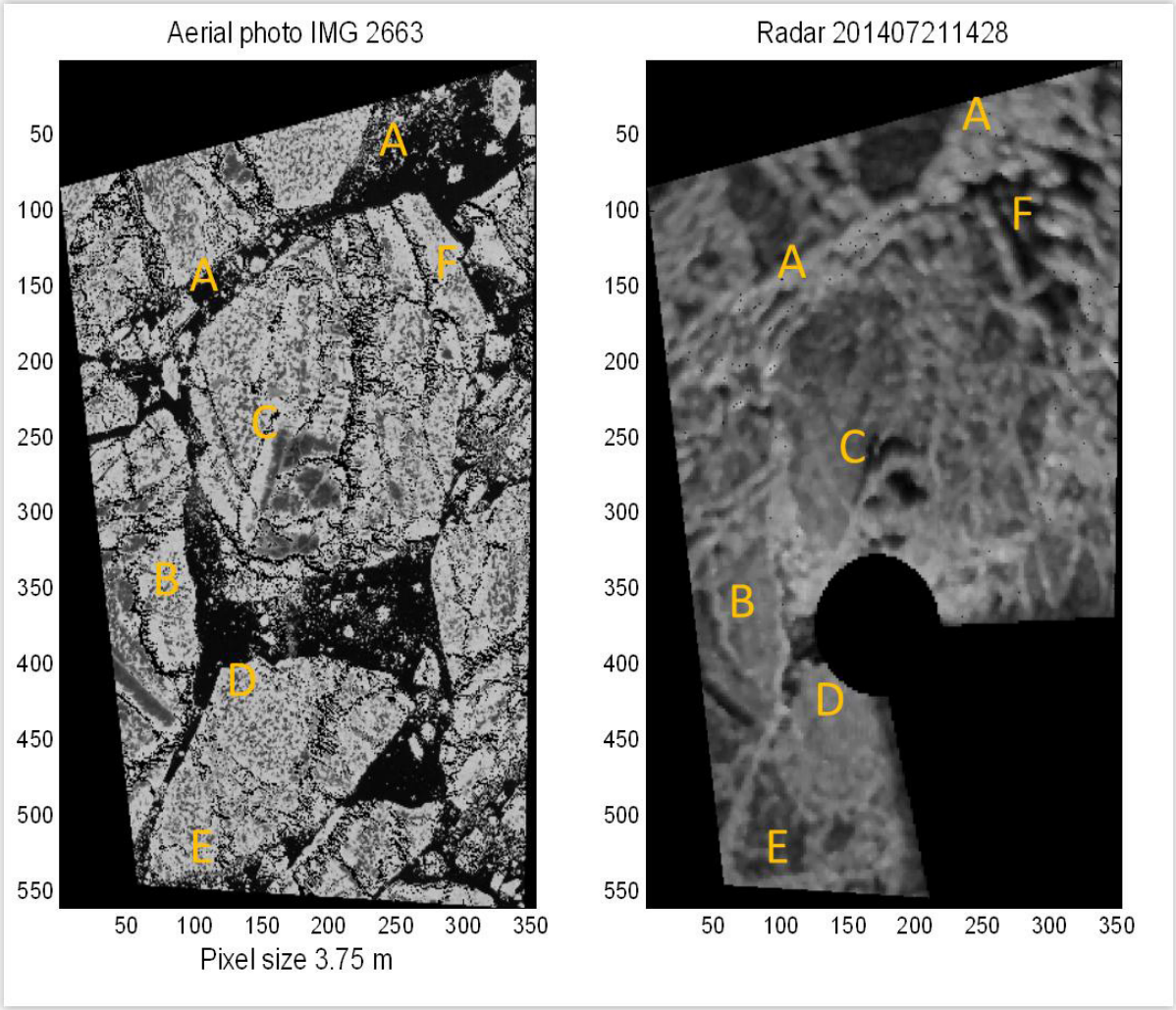

Fig. 9.5: Comparison of a WaMoS Radar image (right, resampled to 3.75 m resolution) with a co-registered aerial photograph (left). The image area is 1,300 m x 2,100 m. In the photograph the originally bright reflections from ridges are shown black. The grey spotted texture on the floes represents melt ponds.

Data management

All data from the radiation measurements require post-processing after the cruise. The data from AWI sensors will be made publically available in the PANGAEA database within one year. Visual sea ice observation data will be distributed by a standardized database at the International Arctic Research Center, University of Alaska, Fairbanks, and are already available through the PANGAEA repository (http://doi.pangaea.de/10.1594/PANGAEA.835578).

The WaMoS polar files are stored following the practices of the WaMoS data management. Georeferenced radar imagery (50GB) is available immediately after the cruise. Preliminary ice thickness and surface profile data are available after the cruise and more accurate data within one year. The imagery and the data are made available in PANGAEA within one year.

Snow thickness measurements are already available on PANGAEA (Table 9.1).

T**ab. 9.1:** PANGAEA links to the snow thickness datasets.

Sea Ice Station	PANGAEA Link
AURORA2014 HELI-25 MAGNA 1	http://doi.pangaea.de/10.1594/PANGAEA.835377
AURORA2014 HELI-25 MAGNA 2	http://doi.pangaea.de/10.1594/PANGAEA.835378
AURORA2014 HELI-25 MAGNA 3	http://doi.pangaea.de/10.1594/PANGAEA.835379
AURORA2014 HELI-25 MAGNA 4	http://doi.pangaea.de/10.1594/PANGAEA.835380
AURORA2014 HELI-25 MAGNA 5	http://doi.pangaea.de/10.1594/PANGAEA.835381
AURORA2014 HELI-28 MAGNA 1	http://doi.pangaea.de/10.1594/PANGAEA.835382
AURORA2014 HELI-28 MAGNA 2	http://doi.pangaea.de/10.1594/PANGAEA.835383
AURORA2014 HELI-28 MAGNA 3	http://doi.pangaea.de/10.1594/PANGAEA.835384
AURORA2014 HELI-28 MAGNA 4	http://doi.pangaea.de/10.1594/PANGAEA.835385
AURORA2014 HELI-28 MAGNA 5	http://doi.pangaea.de/10.1594/PANGAEA.835386
AURORA2014 HELI-29 MAGNA 1	http://doi.pangaea.de/10.1594/PANGAEA.835387
AURORA2014 HELI-29 MAGNA 2	http://doi.pangaea.de/10.1594/PANGAEA.835388
AURORA2014 HELI-29 MAGNA 3	http://doi.pangaea.de/10.1594/PANGAEA.835389
PS86/031-1	http://doi.pangaea.de/10.1594/PANGAEA.835390
PS86/071-1	http://doi.pangaea.de/10.1594/PANGAEA.835391
PS86/080-1	http://doi.pangaea.de/10.1594/PANGAEA.835392

References

Nicolaus M, Katlein C (2013) Mapping radiation transfer through sea ice using a remotely operated vehicle (ROV). The Cryosphere, 7, 763–777.

Nicolaus, M, Katlein C, Maslanik J, and Hendricks S (2012), Changes in Arctic sea ice result in increasing light transmittance and absorption, Geophys. Res. Lett., 39, L24501, doi:10.1029/2012GL053738.

10. TECHNOLOGY DEVELOPMENT: USE OF HROV NUI FOR UNDER ICE RESEARCH

Christopher R. German[1], Michael V. Jakuba[1], John Bailey[1], Stephen Elliott[1], Christopher Judge[1], Christopher McFarland[1], Stefano Suman[1], Louis L. Whitcomb[1,2], and Samuel Laney[1] (not on board)

[1]WHOI
[2]JHU

Objectives

We utilized a newly developed hybrid remotely operated vehicle (HROV) system, Nereid Under Ice (*NUI*), Fig. 10.1, to attempt the first detailed *in-situ* characterization of photosynthetically-driven biological communities reliant on the penetration of sunlight through the overlying ice within the uppermost 100 m of the Arctic Ocean including the ice/ocean interface itself. Real-time pilot control, closed-loop semi-autonomous behaviors, along with the sensor suite and sampling paradigm together with a horizontal standoff capability of up to 20 km from *Polarstern* will, we believe, enable us to profile precisely the parameters critical to supporting photosynthetically-based ecosystems in an undisturbed water column, far from the mixed wake of an ice breaker. To date, the standoff distances achieved for similar studies have been limited to a few hundred meters and/or utilized less comprehensive sensor suites. This is the first research expedition to take advantage of the new *NUI* vehicle, purpose-built for studying the ice-ocean interface under both glacial and sea-ice, thus we are pursuing both engineering and science objectives.

Fig. 10.1: Nereid Under-Ice (NUI) in the Polarstern Geolab

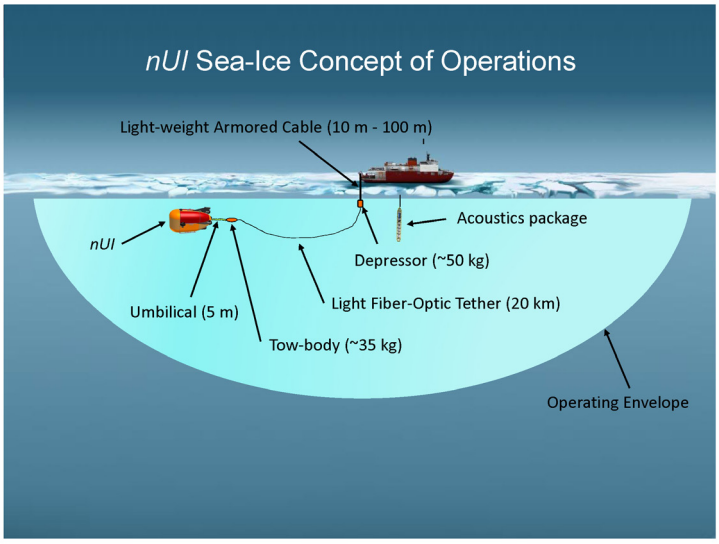

Fig. 10.2: Nereid Under-Ice (NUI) Concept or Operations

The key technology behind the hybrid ROV Nereid Under Ice (*NUI*) is a light-weight (250 µm diameter) communications-only fiber-optic tether technology originally developed for the *Nereus* 11,000 m full-ocean-depth capable vehicle (Bowen et al., 2009), as depicted in Fig. 10.2. This tether enables operation by a pilot with high-bandwidth real-time streaming of all data feeds including HD video back to the ship, at horizontal stand-off distances up to 20 km from the host ship. Our overarching engineering objective is to demonstrate the viability of the tethering technology and of *NUI*, Fig. 10.1, in general to conduct operations from an ice breaker through permanent ice cover.

Specific engineering milestones we expected to achieve included:

- Establish the overall usability of *NUI* in conditions likely to occur in Polar regions, including the viability of launch and recovery procedures through sea ice, protocols for minimizing time on deck and mitigating the impacts of sub-zero temperatures on vehicle systems and scientific payloads, adequacy of pilot situational awareness, recovery aids, and tempo of operations.
- Demonstrate the viability of the tethering system for real-time piloted control at various distances from the ship. We did not plan to exercise the ultimate limit of 20 km on this expedition.
- Demonstrate piloted, semi-autonomous, and autonomous „come-home“ behaviors designed to return the vehicle to a location within 100 m of the ship for recovery under a variety of scenarios and (simulated) failure modes, most prominently loss of tether and loss of acoustic communication.
- Demonstrate under-ice navigation, both in ice-relative and geo-referenced coordinate frames, at minimum under a single contiguous floe with *Polarstern* rigidly moored to that floe, and ideally within a field composed of multiple floes in motion relative to one another and the ship.
- Demonstrate the ability of the vehicle to operate as essentially an inverted ROV – in particular to land on the underside of the ice and to hold station relative to overlying ice and execute other motions under closed-loop control.

Work at sea

We planned to conduct 4 to 6 dives over the course of the cruise to evaluate and improve the engineering development of *NUI*'s overall functioning and its individual subsystems including energy storage, propulsion, ice-relative underwater navigation, fiber-optic tether, underwater acoustic telemetry, radio-frequency (RF) telemetry, command and control, acoustically controlled semi-autonomous operation, buoyancy, emergency localization, and launch/recovery operations. We also planned to conduct *NUI*'s first science operations including targeted high-resolution vertical profiling; constant distance from ice or constant depth survey, primarily for ir/radiance measurements and electronic still camera imaging, multibeam under-ice topography mapping, high-definition optical imaging of water column and under-ice biology and under-ice topography.

For this cruise *NUI* was equipped with dual up/down 300 kHz ADCP/DVLs, a SeaBird FastCAT49 CTD, a WetLabs Chl/NTU fluorometer, a forward-looking BlueView imaging sonar, and an internal pan/tilt/zoom HD video camera capable of looking upward with supporting dedicated lights. For this expedition we equipped the vehicle with additional stand-alone sensors: an upward-looking Imagenex Delta-T multibeam sonar, a high bit-depth machine vision still camera, and radiometers mounted along the dorsal „spine" of the vehicle to monitor incident radiation penetrating through the ice. A water-sampling snorkel delivered water to an integrated suite of *in-situ* sensors in the principal payload space at the front of the vehicle: additional fluorometers, a SUNA *in-situ* nitrate sensor and an FRRF (Fast Repetition Rate Fluorometer with integrated IC PAR irradiance sensor). Two TriOS RAMSES spectrophotometers (1 Radiance ARC and 1 Irradiance ACC Sensor) measured light penetrating through the sea-ice to determine the energy fluxes available to drive photosynthesis. Measures of the light field will include intensity, color and geometry of the ice-cover. The FRRF, Fluorometers, and SUNA were coupled to a SeaBird25+ unit to pump water from the snorkel to the sensor package: the FRRF to measure photosynthetic performance and a WetLabs Eco-Triplet fluorometer that combines chlorophyll with backscatter and CDOM measurements to investigate algal, particulate and dissolved organic matter concentrations. By adding the SUNA *in-situ* nitrate sensor to this sample suite we can replicate, *in-situ*, the full suite of measurements reported by Arrigo et al. (2012).

Fig. 10.3: NUI dive 2 launch on July 21, 2014, showing NUI being deployed tethered to the orange tow-body which is mated to the grey depressor during the first part of the launch sequence.

Preliminary Results

We conducted four dives during the PS86 cruise as listed in Table 10.1. Dive locations are listed in the station-list Appendix. Fig 10.3 shows *NUI* dive 2 launch on July 21, 2014, showing *NUI* being deployed tethered to the orange tow-body, which is mated to the grey depressor during the first part of the launch sequence.

Tab. 10.1: Overview of *NUI* deployments

Station	Date	Launch Time (UTC)	Recovery Time (UTC)	Dive Duration
PS86/0053-1	7/21/2014	11:44	16:52	5:08
PS86/0060-1	7/23/2014	11:03	16:08	5:05
PS86/0070-1	7/26/2014	6:43	11:44	5:01
PS86/0080-1	7/28/2014	12:29	17:49	5:20

Tab. 10.2: Overview of *NUI* Sensors and Systems for PS86 Deployments

System/Sensor	**Dive 1** 7/18/14	**Dive 2** 7/21/14	**Dive 3** 7/23/14	**Dive 4** 7/26/14
Batteries	100 %	100 %	100 %	100 %
Propulsion	100 %	100 %	100 %	100 %
Control System	100 %	100 %	100 %	100 %
Towbody depressor release	0 %	100 %	100 %	100 %
Semi-Autonomous Return	50 %	75 %	100 %	100 %
Upward Doppler DVL/ADCP	100 %	100 %	100 %	100 %
Downward Doppler ADCP	100 %	100 %	100 %	100 %
Paro Pressure Depth Sensor	100 %	100 %	100 %	100 %
Phins Gyrocompass	100 %	100 %	100 %	100 %
Blueview Fwd-looking Multibeam Sonar	100 %	100 %	100 %	100 %
Imagenix Upward Multibeam – under-ice topography	0 %	0 %	100 %	100 %
High-Def. Forward Camera	100 %	100 %	100 %	100 %
Utility cameras (3)	100 %	100 %	100 %	100 %
Upward Digital Still Camera	0 %	0 %	100 %	100 %
RAMSES Radiance ARC	0 %	50 %	100 %	100 %
RAMSES Irradiance ACC	0 %	50 %	100 %	100 %
Seabird SBE49 CTD	100 %	100 %	100 %	100 %
Seabird SBE25+ CTD	100 %	100 %	100 %	100 %
SUNA nitrate sensor	100 %	100 %	100 %	100 %
FRRF: fluorometer, PAR sensor, pressure sensor	0 %	0 %	100 %	100 %
Eco-Triplet fluorometer	100 %	100 %	100 %	100 %
Light fiber-optic tether	100 %	100 %	100 %	100 %
RF surface telemetry	10 %	100 %	100 %	100 %
10 kHz acoustic telemetry	100 %	100 %	100 %	100 %
3.5 kHz acoustic telemetry	100 %	100 %	replaced	replaced
10 kHz alternate acoustic telemetry (replaces 3.5 kHz)	N/A	N/A	100 %	100 %
9 kHz transponder system	100 %	100 %	100 %	100 %

Dive 1: Engineering Synopsis

Dive 1 commenced with deployment of the acoustic telemetry and ranging package from the *Polarstern*'s moon pool, followed by a normal deployment of *NUI* and its mated tow-body/depressor from *Polarstern*'s starboard deck just aft of the CTD station. After preliminary checkout of *NUI* on the surface, *NUI* was commanded to dive to 25 m depth while the depressor was lowered to about 22 m depth. A full checkout of all *NUI* systems at 25 m depth was completed at 14:10 with the tow-body still mated to the depressor. All systems that checked-out during

pre-dive checks were determined to be functioning, including checkouts of auto-heading and auto-depth control. Remote-controlled release of the tow-body from the depressor was attempted and failed. *NUI* was piloted back to the surface, and the mated tow-body/depressor package was raised clear of the free surface. Examination of the depressor from a small-boat revealed the release mechanism to be jammed, whereupon the tow-body was released manually at 14:50, and *NUI* was piloted to 4 m depth as the depressor was lowered back to depth. *NUI* was operating in a mostly open pool of water with many independently-moving floes. Remotely piloted by a pilot on the *Polarstern*, *NUI* navigated under a moving floe and the upward-looking Doppler sonar was tested verified to obtain reliable Doppler-lock on the overhead ice floe. The control and navigation system was tested to verify functionality of auto-XY closed-loop control to hold station under the moving ice and to execute ice-relative motion in XYZ and heading. Landing *NUI* on the underside of an ice floe was attempted and proved to be practical, with the vehicle's positive buoyancy holding *NUI* to the ice floe. An attempt was then made to pilot *NUI* under a larger floe of rafted ice at 4 m depth. The fiber-optic tether severed at 15:42. Although semi-autonomous return had been tested in simulation prior to the dive, loss of the tether forced the use of this system without the benefit of high bandwidth pilot oversight as was planned for the end of the dive. *NUI* autonomously dove to a safe depth of 30 m upon loss of fiber-optic telemetry and was then commanded via acoustic telemetry to return to ship via a series of short-duration operator-directed maneuvers designed to allow the autonomous system to fall back into a safe state if it perceives loss of acoustic telemetry. When the vehicle's upward-looking Doppler sonar indicated open water above the vehicle, *NUI* was acoustically commanded to surface in the open pool near *Polarstern.* RF surface telemetry was intermittent, so the small boat towed *NUI* back for recovery on *Polarstern*. The depressor was recovered. *NUI* was recovered at 16:52. The ship-board acoustic modem transducers were then recovered.

Forensic analysis of dive 1 showed that *NUI* had been piloted without sufficient situational awareness regarding the location of its fiber-optic tether, the paid-out portion of which behaves more or less like a string of lagrangian drifters. *NUI* had been inadvertently piloted over its own tether (despite careful navigation of the vehicle so as to not cross its own path in a ship-fixed frame) as well as use of the ship's ADCP to judge currents and the likely evolution in the position of the fiber. These measures proved inadequate to predict fiber location near the surface and in the strong currents generated by *Polarstern*'s propulsion system while engaged in actively managing ice around the ship. A visualization of the tether location relative to *NUI* based on modeled vehicle dynamics was added to the suite of situational awareness tools available to the pilot and navigators to reduce the chance of a similar failure on subsequent dives.

Dive 1: Science Synopsis

Although *NUI* Dive 1 was an engineering dive, it also allowed for important scientific progress to be made – notably to test/confirm the data pipelines from the vehicle to the data-logging computers aboard ship for the various scientific sensor suites. Importantly, it was discovered that dedicating sufficient bandwidth from the vehicle fiber-optic telemetry to facilitate ship-wide public viewing of the video feed via subsea encoding of the HD-SDI video stream interfered with *NUI*'s ability to relay data for the RAMSES sensors, the bio-sensor suite and the digital still camera, none of which were able to collect data routinely during this dive – a problem that will be remedied before *NUI*'s next cruise. The HD Video Camera functioned well and was able to collect first examples of high quality imagery from beneath an ice-floe and revealed a high abundance of biological productivity (Fig. 10.4).

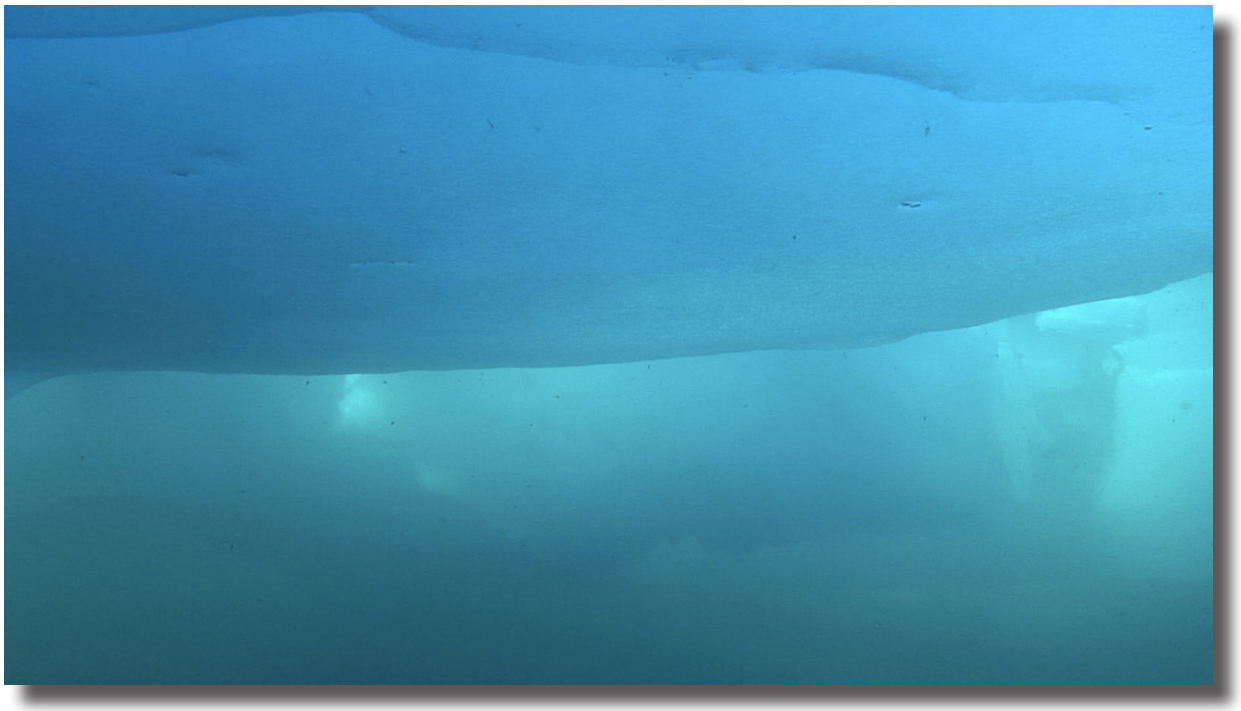

Fig. 10.4: NUI dive 1 provided a first opportunity to test the HDTV camera and reveal the complexity of the under-ice landscape and numerous copepods.

Dive 2: Engineering Synopsis

Dive 2 commenced with deployment of the acoustic telemetry and ranging package from the *Polarstern*'s moon pool, followed by a normal deployment of *NUI* and its mated tow-body/ depressor from *Polarstern*'s starboard deck just aft of the CTD station. After preliminary checkout of *NUI* on the surface, *NUI* was piloted to 25 m depth while the depressor was lowered to about 22 m depth. A full checkout of all *NUI* systems at 25 m depth was completed with the tow-body still mated to the depressor. Remote-controlled release of the tow-body from the depressor was completed successfully at 11:55 UTC. *NUI* was piloted under a series of broken floes up-current and aft of ship. Acoustic ranging to the vehicle proved intermittent, so the decision was made to surface *NUI* in an open lead while under pilot control with fiber-optic telemetry intact in order to avoid a potentially long recovery process complicated by poor acoustic telemetry. *NUI* was piloted to the surface in an open lead about 500 m aft of the ship and located visually. *NUI* was piloted on the surface along a series of open leads back toward *Polarstern*. A final floe blocking the path back to *Polarstern* forced the pilot to submerge *NUI* before surfacing in the open pool adjacent to the ship. The tether remained intact and the decision was made to continue the dive despite the paid out fiber now lying upstream of *NUI*'s location.

Polarstern had been set up against a large floe on the starboard bow for the duration of the dive. This afforded the opportunity to trial the combination of ice-relative dead-reckoning augmented by acoustic ranging, all in a frame affixed to the ship, as opposed to a series of independently moving floes where ice-relative dead-reckoning proved confusing and operators had been forced to rely entirely on acoustic ranging methods. At the risk of a more lengthy recovery under the significantly thicker ice off the starboard bow should acoustic telemetry to the vehicle fail, *NUI* was piloted under the ice with the intention of remaining within 200 m of *Polarstern*.

Ice-relative dead-reckoning proved an effective complement to acoustic ranging, and operators were able to direct *NUI* to a series of specific ice features visible in a photograph taken from *Polarstern*'s bridge. The pilots tested the sensor suite, performing a series of ir/radiance survey transects at a constant depth of 10 m. The fiber position prediction tool developed after dive 1 indicated no further ice available within 200 m that would not have risked the tether so *NUI* was piloted back into the pool along *Polarstern*'s starboard side to attempt vertical profiles under a medium detached floe despite the known risk to the fiber. One profile from 30 m to the under-ice surface was completed successfully, but ultimately the fiber-optic tether failed at 15:15. The depressor was recovered while *NUI* autonomously held station under the floe. *NUI*'s proximity to the ship allowed for a rapid recovery; the vehicle was commanded acoustically to emerge from the floe at shallow depth and, upon visual confirmation that the vehicle was in open water, to return to surface. The pilot took control over the RF link and drove the vehicle over to the recovery point without the need for a small boat. *NUI* was back on deck at 16:08. The ship-board acoustic modem transducers were then recovered.

Dive 2: Science Synopsis

Two important science goals were met during the course of Dive 2. First, using the RAMSES radiance sensor, a constant-depth survey was conducted beneath varying ice cover under an ice-floe to which the ship was rigidly attached off the starboard bow. By combining under-ice navigation with photography of the upper ice surface from above the ship's bridge and operating with no artificial lighting provided by the *NUI* vehicle (except when navigating beneath a particularly deep ridge ice-keel), a first coherent approach to investigating ice-penetrating solar radiation using the *NUI* vehicle was attempted (See Chapter 9).

Following the success of that operation, a second scientific operation was attempted, diving beneath a second floe, off the starboard beam of the ship to conduct a first controlled ascent from 30 m depth. Although only a subset of the bio-sensor suite was operational on Dive 2 (See Table 10.2), this work allowed us to test the vehicle's ability to rise slowly and at a fixed rate under auto-XY control, holding station beneath a fixed point on the overlying (continuously moving) ice-floe at rates of no greater than 3 m/minute (5 cm/s) to provide extremely high resolution vertical profile data. Key outcomes from this operation were the collection of first calibration data for the RAMSES irradiance sensor (only one RAMSES instrument could be operated at a time during this dive; see Chapter 9) and our ability to begin to reveal the complex interplay of local hydrography and biology under the ice (Fig. 10.5).

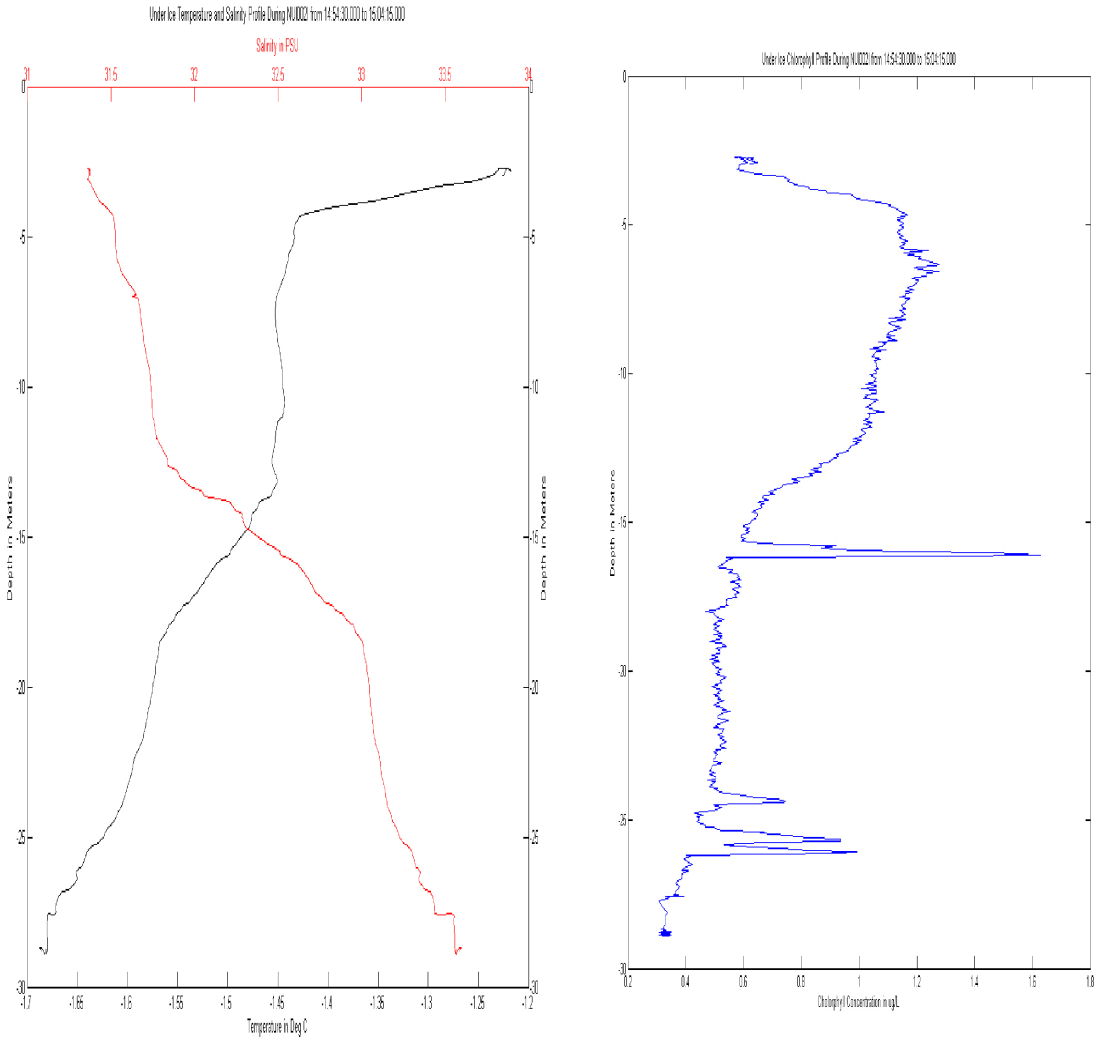

Fig. 10.5: NUI Dive 2 profile from ~30 m revealed a strong halocline at ~15 m with much higher abundances of chlorophyll evident in the upper (relatively warm and fresh) layer (Data courtesy of WHOI NUI Science Team)

Dive 3: Engineering Synopsis

Dive 3 commenced with deployment of the acoustic telemetry and ranging package from the *Polarstern*'s moon pool, followed by a normal deployment of *NUI* and its mated tow-body/ depressor from *Polarstern*'s starboard deck just aft of the CTD station. After preliminary checkout of *NUI* on the surface, *NUI* was piloted to 25 m depth while the depressor was lowered to about 22 m depth. A full checkout of all *NUI* systems at 25 m depth was completed with the tow-body still mated to the depressor. Remote-controlled release of the tow-body from the depressor was completed successfully at 07:17. *Polarstern* was set up as on dive

2 with the starboard bow pressed into a vast floe. *NUI* was piloted down-current at 40 m depth under this floe, both to gather a multibeam transect of under-ice topography and to set up for working slowly back upstream toward the ship at a shallower depth. Dead-reckoning (Doppler/north-seeking gyrocompass), complemented by acoustic ranging, provided excellent navigation throughout the dive. After the initial down-stream multibeam run *NUI* was piloted along a series of interlaced ir/radiance/multibeam transects at constant depth interlaced with vertical profiles and ending with engineering tests of the upward-looking digital still camera in an area rich with algal material. The fiber-optic tether remained intact throughout the dive. *NUI* was piloted via fiber-optic tether to the surface in the open pool on *Polarstern*'s starboard side, and control was successfully transferred to the RF link before deliberately severing the fiber and recovering the depressor. *NUI* was recovered back onto deck at 11:44. The ship-board acoustic modem transducers were then recovered.

Dive 3 was the first full trial of new navigation software designed to visualize Doppler and range-based acoustic navigation. A ship-centered perspective provided operators with visualizations of all available navigation sources and handles to assess their consistency and to adjust the deck-reckoned solution to accommodate drift. Time series plots of range data were also displayed to aid in vehicle navigation during time periods when acoustic range data was infrequently available. This software aided operators in evaluating which sources of navigation data were providing the most accurate understanding of vehicle position.

Dive 3: Science Synopsis

NUI Dive 3 was the first dive dedicated principally to scientific operations and much success was achieved. Operating entirely without use of artificial lighting, a series of 8 constant-depth under-ice transects were conducted at 10 m nominal depth in a loose square-wave formation (Fig. 10.6, Fig. 10.7). At the ends of the first 5 of these transects, *NUI* dived to 30 m to also collect vertical profiles for the bio-sensor suite and the RAMSES ARC and ACC sensors (the latter two were operating continuously in parallel by the start of Dive 3) to test spatial variability of both hydrographic and biological parameters over the region investigated (Fig. 10.8). Following the 5th profile, concern was raised over the proximity of successive survey transects to one another and so, erring on the side of caution with respect to vehicle fiber-optic tether integrity, it was decided to discontinue vertical profiling and continue for 3 further lateral constant depth transects before ending the dive with a series of tests of the upward looking digital still camera starting at 3 m altitude and then varying in depths between 1 m and 5 m separation from the overlying ice. While conducting these calibration tests for the digital still camera, the opportunity was also taken to conduct extensive video imaging of algal material living immediately beneath the overlying ice (Fig. 10.9). An important additional test conducted during this dive was that the Delta-T multibeam system loaned by Ted Maksym (WHOI) for the cruise was mounted on the vehicle for the first time and data was acquired during the initial deep run out to the work area from the ship at 40 m and throughout the rest of the dive.

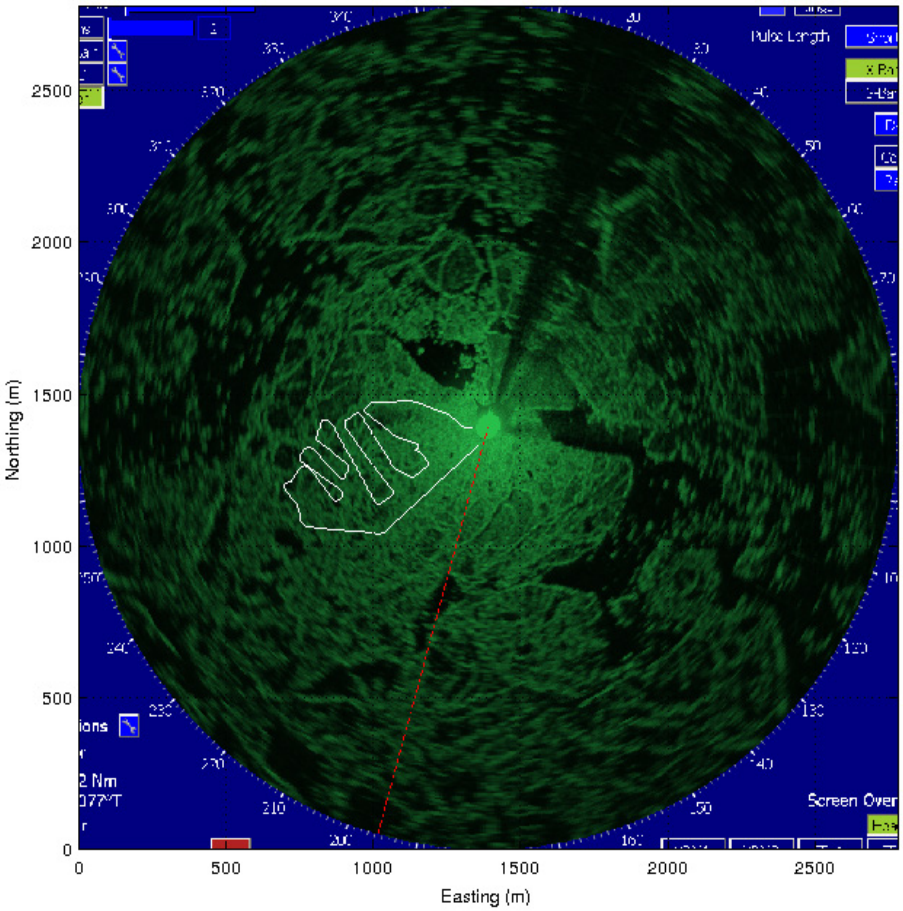

Fig. 10.6: NUI Dive 3 commenced with a long deep run (including data collection for the Delta-T multibeam system) followed by a loose square wave survey pattern that combined constant depth (10 m, lights out) sensor surveys interleaved with vertical profiles from 30 m up to landing on the underside of the ice at the ends of the first 5 of these transects (Fig. 10.7). Final operations included extensive testing of the digital still camera immediately beneath the ice (1-5 m separation) in parallel with extensive video-imaging of the abundant biological activity present throughout the survey (Fig. 10.8).

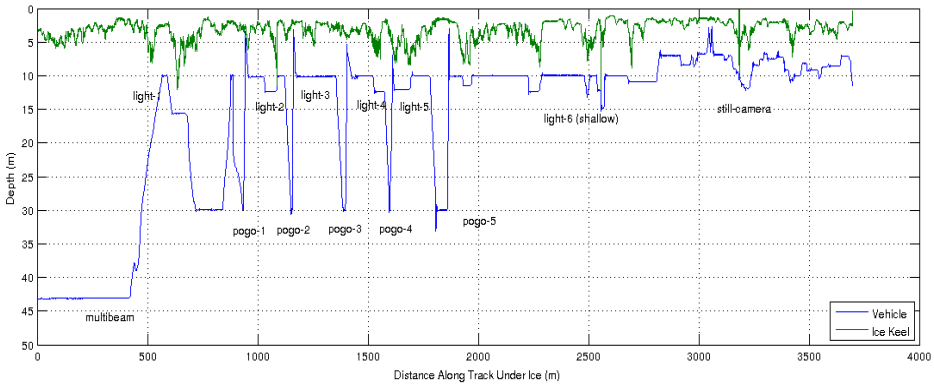

Fig. 10.7: Synopsis of dive activities versus distance under ice for dive 3. The portion labeled „light-5“ represents 4 separate transects for a total of 8 ir/radiance transects.

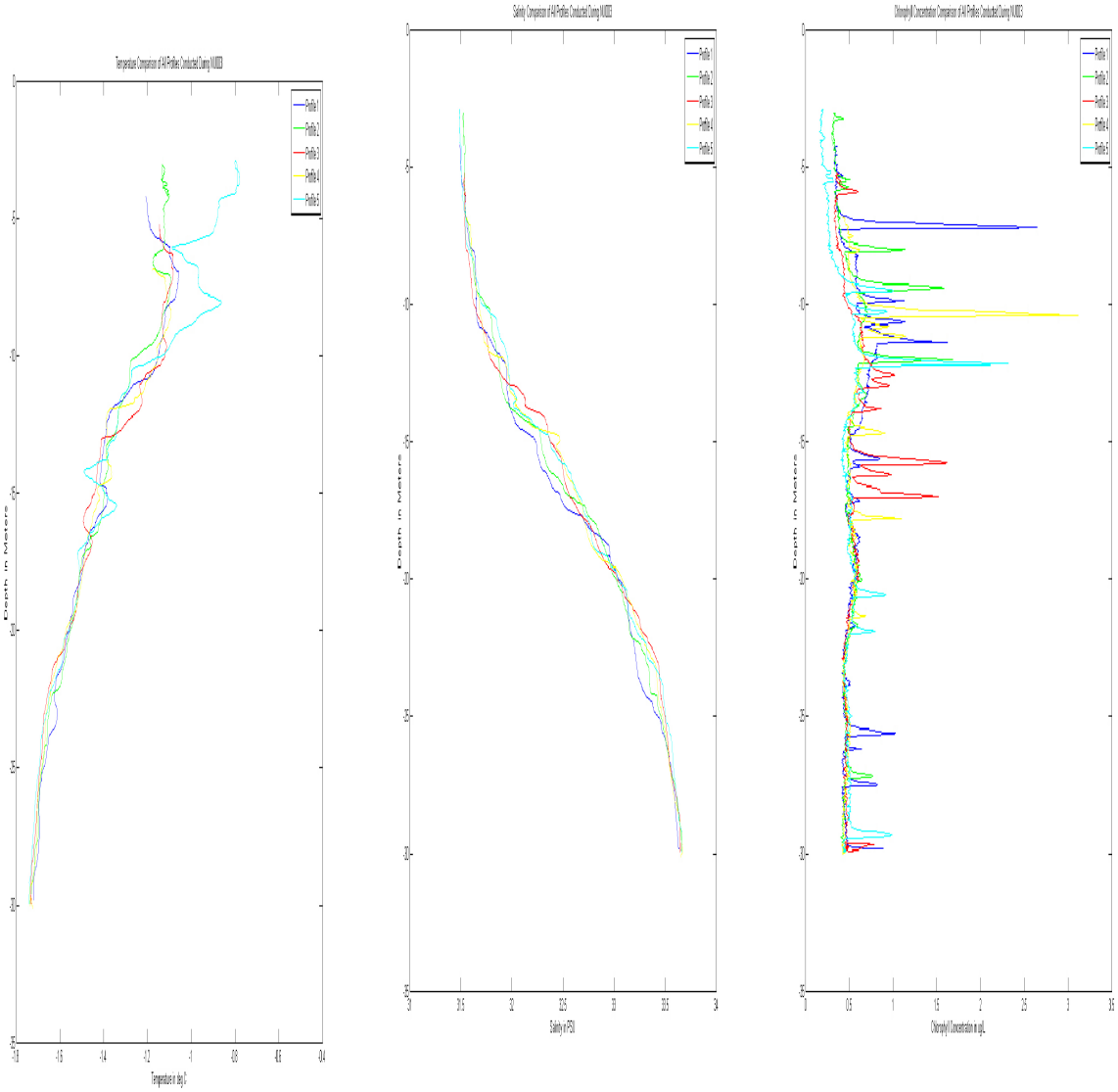

Fig. 10.8: NUI Dive 3 collected five vertical profiles from 30 m up to the underside of the ice at the ends of the first five constant-depth lateral transects to investigate spatial variability in terms of both hydrography and co-registered bio-sensor data. The results reveal that while salinity remains relatively uniformly distributed with depth across the study area there is significant spatial variability in both temperature and chlorophyll.

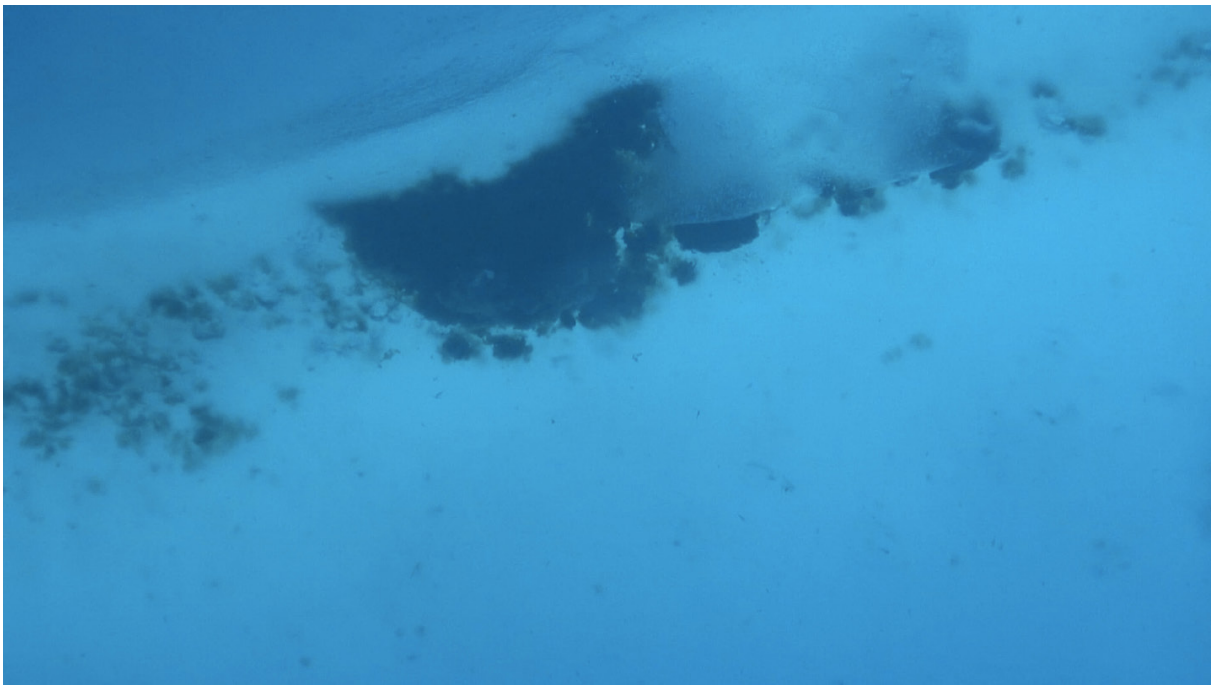

Fig. 10.9: Zoom-in image of large algal concentrations immediately beneath the ice cover toward the end of NUI Dive 003 captured by HD Video camera at <5 m separation.

Dive 4: Engineering Synopsis

Dive 4 commenced with deployment of the acoustic telemetry and ranging package from the *Polarstern*'s moon pool, followed by a normal deployment of *NUI* and its mated tow-body/depressor from *Polarstern*'s starboard deck just aft of the CTD station. After preliminary checkout of *NUI* on the surface, *NUI* was commanded to dive to 25 m depth while the depressor was lowered to about 22 m depth. A full checkout of all *NUI* systems at 25 m depth was completed with the tow-body still mated to the depressor. Remote-controlled release of the tow-body from the depressor was achieved successfully at 12:55. *Polarstern* was set up against a very large flow to its port side to permit ice station work to be carried out in parallel with the dive. Current, wind and ice drift were stronger, more variable, and relatively less aligned than the previous 3 dives. *NUI* was piloted at 40 m depth around the bow of the ship before reaching the overlying ice on the port side where the primary objective was to perform a transect collocated with a surface ice characterization transect off *Polarstern*'s port bow. Dead-reckoned and acoustic range-based navigation were very good; and the navigation visualization software completed for dive 3 proved invaluable in accommodating the stronger drift as well as in locating the surface transect.

NUI was piloted down-stream at 40 m depth while performing a multibeam transect of under-ice topography, followed by two vertical profiles and a photo-survey of the underside of the ice with the upward-looking still camera at 3 m headroom after turning back up-stream toward the ship and the dive's primary objective (Fig. 10.10). Using the navigation visualization software to display the position of vertical through-floe poles placed by the Ice Physics team, *NUI* surveyed an 80 m line co-located with surface measurements by that team. With ice closing in on the depressor, the fiber-optic tether finally failed at 16:13 just after completing the transect. The depressor was recovered rapidly but without incident on account of the closing floe. The ship was then repositioned to a more favorable location while *NUI* held position at 40 m depth awaiting instructions.

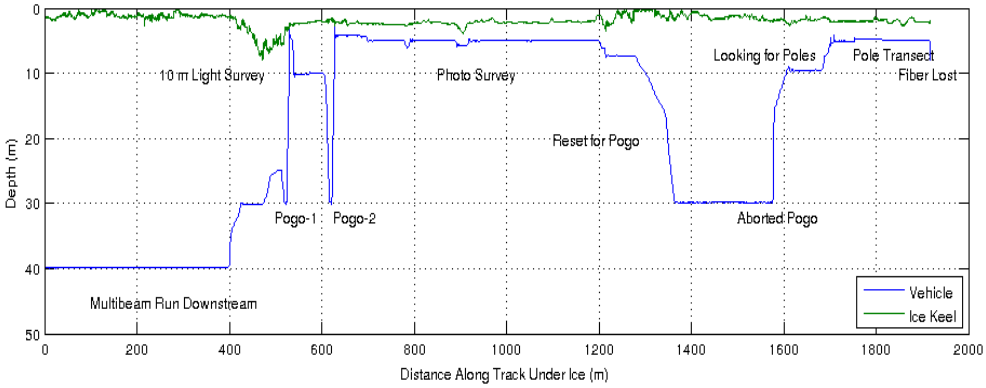

Fig. 10.10: Synopsis of dive activities versus distance under ice for dive 4.

NUI was then commanded acoustically in a series of short-duration maneuvers around the bow of *Polarstern* before surfacing in an open pool on *Polarstern*'s starboard side. Critical ice-cover information from the upward-looking ADCP/DVL contained in the acoustic telemetry from *NUI* to operators enabled operators to surface *NUI* in open water despite the rapidly evolving ice pack. *NUI* was recovered at 17:49. The ship-board acoustic modem transducers were then recovered.

Dive 4: Science Synopsis

Dive 4 provided the most complete testing of the *NUI* sensor-suite for scientific operations. Data displays at the start of the dive confirmed that the Delta-T multibeam system was operating well and acquiring data as required during the outbound 40 m transect to arrive in the designated work area. While our Ice Physics colleagues were busy deploying for co-registered on-ice work (Chapter 9) the vehicle was next used to collect vertical profiles with a short snorkel, connected in-line with the bio-sensor suite for the first time on this dive. Rising up from 30 m depth to the ice-water interface, the value of the addition of the snorkel was immediately apparent because, for the first time, we were able to profile to within 2-4 cm beneath the ice-water interface, revealing a distinct low-salinity (presumed melt-water) horizon immediately beneath the ice cover (Fig. 10.11).

Two further important observations were made from this vertical profile. First, there was very good agreement with the user-provided SBE25+ CTD provided by the WHOI Science Team and the lower-specification SBE49 CTD that is provided as standard with *NUI* (Fig. 10.12). Additionally, an offset between the vertical profiles for Temperature and Salinity when plotted versus recorded depth of the CTD sensors (mounted side by side in *NUI*'s forward instrument bay) reveal that introducing the extensive inlet tubing required to implement the snorkel had also introduced a determinable time delay between water intake at the snorkel inlet and detection of that water at the instrument bay which will need to be corrected for, both for our CTD data and co-registered bio-sensor suite prior to scientific publication. Other key sensors deployed as part of the bio-sensor suite for the profiling operations on Dive 4 (and also Dive 3) included the ECO-Triplet fluoromoeter system, a Fast Repetition Rate Fluorometer (FRRF) and a SUNA *in-situ* nitrate analyser. Post-cruise calibration of data for the latter will be conducted in collaboration with Rafael Stiens and Prof. Dr. Antje Boetius (AWI) who collected water samples specifically for this purpose.

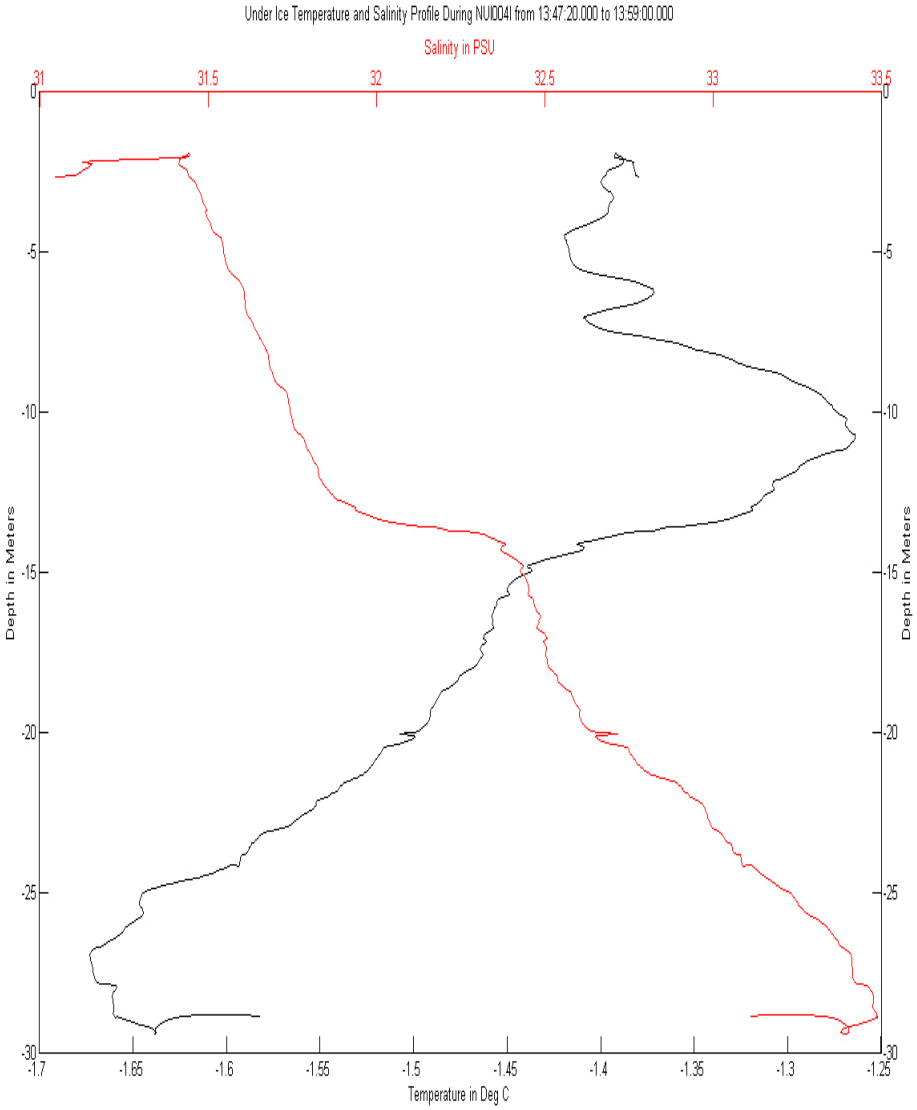

Fig. 10.11: Vertical profiles of Temperature and Salinity as detected from the bio-sensor suite following implementation of the snorkel for Dive 4 which allowed water to be sampled and measured in-situ from just 2-4 cm below the ice-water interface. Note the anomalously low-salinity upper water, interpreted to reflect fresh meltwater input.

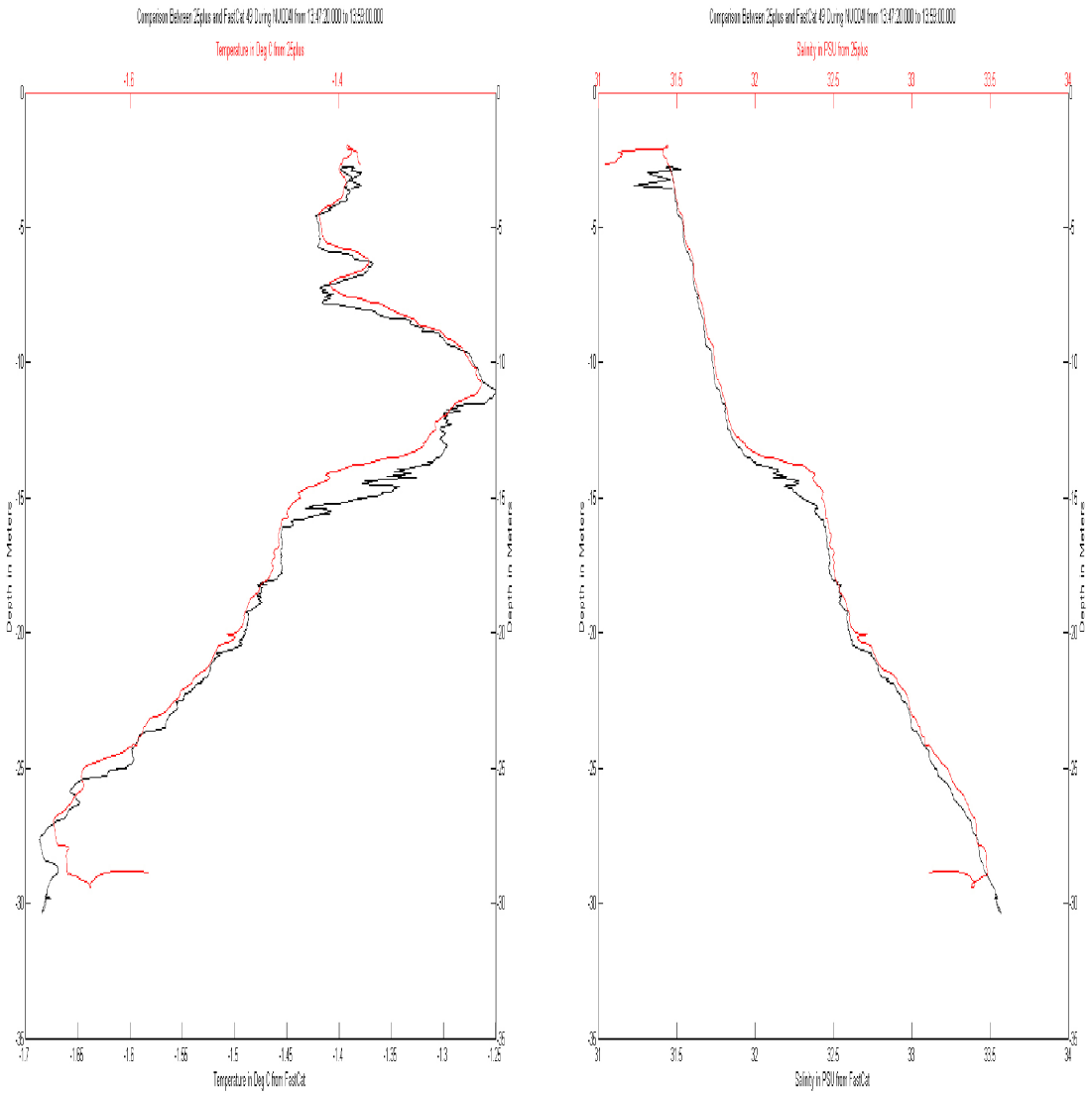

Fig. 10.12: Vertical profiles of Temperature and Salinity as determined from the NUI SBE49 CTD and the co-located SBE25+ equipped with a snorkel inlet for NUI Dive 4. Note both the good inter-correlation between the two sensor systems and, in detail, an offset in depth during the upcast reflecting a time-lag between data acquisition from any given depth between the free-flooded SBE49 sensors (black trace) and the pumped SBE25+ system connected in-line with the bio-sensor suite (red trace).

During the second of the vertical profiles conducted on Dive 4, a region of varying, high and low algal concentrations was observed immediately against the underside of an area of relatively regular and flat-bottomed ice cover immediately ahead of the vehicle. Taking advantage of the favourable orientation of the vehicle to the area of interest, coupled with adjustments that had

been made to the upward-looking still camera's aperture following Dive 3 to improve depth-of-field, a dedicated transect was conducted at 5 m depth, passing directly beneath the algal bloom material. An example of the quality of imaging achieved is shown in Fig. 10.13.

Fig. 10.13: Digital still color image (1360x1024) from upward-looking camera showing algae on the underside of the ice, taken at 3 m range during the under-ice optical survey conducted on NUI dive 4.

The final scientific operation conducted during *NUI* Dive 004 involved locating, subsurface, a series of survey poles that had been deployed by the Ice Physics team (Chapter 9) so that a detailed under-ice survey could be conducted by *NUI* that could be co-registered with on-ice and above-ice (helicopter photo-surveys) in a common geographic/navigational context. The final scientific activity for *NUI* on *Polarstern* Cruise PS86 was to conduct a constant-depth 5 m RAMSES sensor survey along the length of these poles, located using a combination of acoustic ranging and dead-reckoning, with near-field localization reliant on the BlueView imaging sonar (Fig. 10.14) and visual reconnaissance from the HD video camera (Fig. 10.15) while simultaneously collecting co-registered upward-looking digital still camera photographs typically 2-3 m distant from the underside of the ice, Delta-T upward-looking multibeam under-ice topography, CTD and biosensor data.

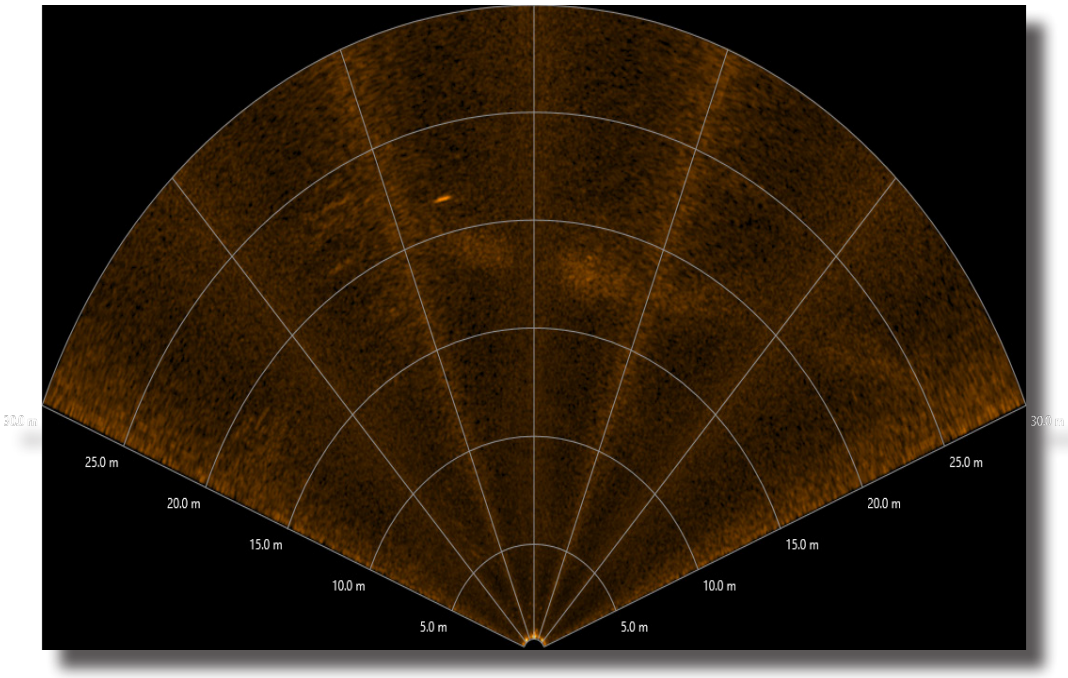

Fig. 10.14: Sonar Image from the forward-looking BlueView imaging sonar showing an ice-survey through-ice pole at a range of 22 m just left of the center of the image.

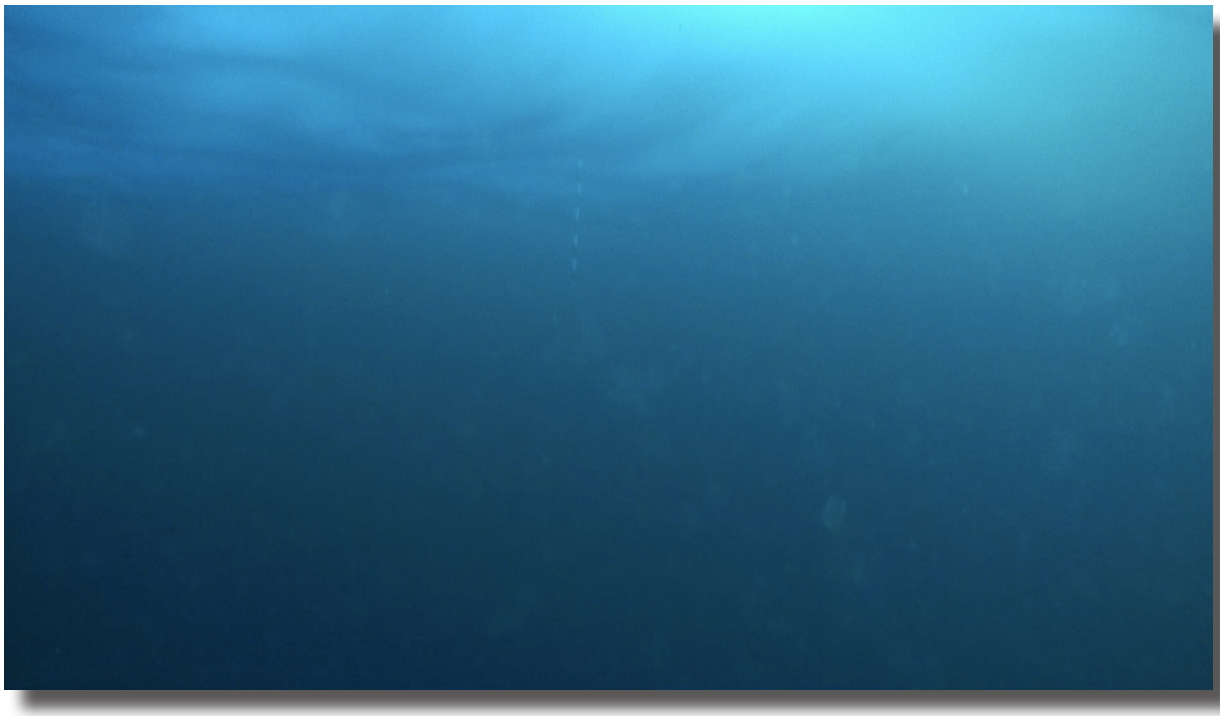

Fig. 10.15: HD video frame of one of the poles deployed by the Ice Physics group for NUI dive 4. With visibility reduced to no greater than 10 m because of the abundance of biological activity in the upper water column, precise location of the Pole Survey relied primarily on the BlueView sonar with HD video imaging providing visual confirmation of proximity to the poles.

Data management

Data arising from the *NUI* operations is similar to those obtained by other ROVs designed and operated by WHOI including the *Nereus* hybrid ROV/AUV and, more pertinent to this section, *Jason* which is part of the US National Deep Submergence Facility. Standard data products from this cruise will include: navigation data, topographic multibeam ice-draft data, time-stamped *in-situ* (physical and biogeochemical) water-column data, and HD video and still imagery of the sea-ice interface. A summary of which sensors were operational and, hence, which archived data are to be expected, is listed in Table 10.3. Per WHOI institutional policy, these data will be duplicated for long term storage, conservancy, and public accessibility at the WHOI Digital Library and Archives http://dla.whoi.edu/dla. The data will be made available to researchers at the discretion of Group Lead German until 2 years after the conclusion of PS86-3, after which the data will become publicly available for scientific use. However, as per UNOLS/DESSC policy, WHOI will retain copyright for all video and still imagery for any commercial (e.g. TV broadcast) purposes.

Tables 10.3 and 10.4 list the sensors, for which *NUI* data was archived on PS86.

Tab. 10.3: WHOI/NUI Provided Sensor Suite

Dive #	BlueView Imaging Sonar	HD Video	Digital Still Camera	CTD (SBE49)	Fluorometer (Chl/NTU)	Delta-T multibeam
001	√	√	x[1]	√	x[2]	x
002	√	√	x	√	x[2]	x
003	√	√	√	√	x[2]	√
004	√	√	√	√	x[2]	√

Tab. 10.4: User-Provided Sensor Suite

Dive #	Rameses ARC	Rameses ACC	CTD (SBE25+)	SUNA	ECO Fluorometer	FRRF
001	x[3]	x[3]	√	√	√	x
002	0.5[3]	0.5[3]	√	√	√	x
003	√	√	√	√	√	√
004	√	√	√[4]	√[4]	√[4]	√[4]

Notes:

[1]*Worked intermittently on Dive 001 but was found to have leaked upon recovery and was removed from vehicle for repair on Dive 002. Worked on Dive 003 and Dive 004 with aperture changes made between final 2 dives to improve focus closer to the ice via increased depth-of-field based on science-user feedback.*

[2]*Disabled to avoid using a suspect power supply that had originally been intended to be used to support the Laney Lab bio-sensor suite.*

[3]*Ice Physics group (Group Leader: Christian Katlein, AWI) could only connect to their sensors intermittently during Dive 001 and could only interrogate their radiance and irradiance sensors sequentially on Dive 002 rather than in parallel.*

[4]*FRRF failed electronically at sea but was repaired by NUI engineering team in time for data to be acquired on NUI dives 003 and 004. Snorkel was installed for Dive 4 only.*

Acknowledgements

We at WHOI and Johns Hopkins University have a great many people to thank for this opportunity. The US National Science Foundation (NSF) Office of Polar Programmes provided the primary vehicle development funding, with additional funding from the James Family Foundation, the George Frederick Jewett Foundation East, the Woods Hole Oceanographic Institution, NSF OCE and the Office of Naval Research. The US National Oceanic and Atmospheric Administration (NOAA) provided the support for our participation in these trials, with the Alfred Wegener Institute (AWI) for Polar and Marine Research and Chief Scientist Antje Boetius for PS/86-3 generously providing the ship-time aboard AWI's FS *Polarstern*. Many colleagues from around WHOI and other institutions have provided critical advice on operating in ice.

References

Bowen A, D Yoerger, C Taylor, R McCabe, J Howland, D Gomez-Ibanez, J Kinsey, M Heintz, G McDonald, D Peters, C Young, J Buescher, B Fletcher, LL Whitcomb, SC Martin, S E Webster and MV Jakuba (2009). The Nereus hybrid underwater robotic vehicle. International Journal of the Society for Underwater Technology, v. 28, no. 3, p. 79–89, doi: http://dx.doi.org/10.3723/ut.28.079.

Arrigo KR, Perovich, D.K. et al. (2012). Massive phytoplankton blooms under Arctic sea ice. Science, v. 336, p. 1408, doi: 10.1126/science.1215065.

11. SEABIRDS AND MARINE MAMMALS AT SEA DISTRIBUTION

Diederick D'Hert[1], Michel Watelet[1], Claude Joiris[1] [1]PolE
(not on board)

Objectives

Our long-term study on upper trophic level species (i.e. seabirds and marine mammals) in polar marine ecosystems aims to deepen the understanding of the basic mechanisms influencing their at-sea distribution.

Studies on the distribution at sea of the upper trophic levels often reflect the existence of limited zones with very high aggregations: they allow us to localise areas of high biological production, even in ecosystems characterized by very low biodiversity such as the polar ones, because these predators depend on high local prey availability.

The integration of the data into a time series running since 1973 could unravel possible changes in numbers and distribution that might be connected to global changes such as increasing water temperature and reduction in ice coverage over the last 30-35 years.

Work at sea

Depending on light and visibility conditions allowing seabird and marine mammal transect counts were carried out on a continuous basis while *Polarstern* was moving. Transect counting method without width limitation was applied from the bridge, lasting half-an-hour each and covering a 90° angle from the bow to one side (starboard or portside), the bridge being too broad for allowing simultaneous counting on both sides by one observer. The animals were detected with the naked eye and observations confirmed and complemented with binoculars (Swarovison and Leica Ultravid 10 X 42). Results are presented as basic unmodified data, i.e. numbers encountered per half-an-hour transect count. Density can be calculated as well, the surface covered during each count being evaluated on the basis of specific detection distances (Joiris 2007, 2011b; Joiris and Falck 2010) and mean ship's speed in the different zones.

When *Polarstern* was not sailing (on station or drifting), additional sightings were done to contribute to the knowledge of the presence of the higher tropic levels in remote arctic areas. Digital cameras were used to facilitate identification and to document the presence of rarities.

Statistical significance of noted geographical differences and correlation with hydrological parameters will be tested later on.

Preliminary (expected) results

During the transit from Tromsø to the Aurora Vent field, a total of 233 periods of data recording (each consisting of 30 minutes) were conducted (totalling 115,5 h). However, only very low numbers of seabirds (see Table 11.1) and marine mammals (see Table 11.2) were detected. These low numbers can be explained by the extremely poor visibility conditions (75 % of time less than 2 km) due to intense fog/low clouds; hence, the numbers probably do not reflect the true abundance of the species. The mean number of seabirds (4 per count) is far less than previous campaigns (generally between 20 and 35).

The species composition on the other hand, seems to be similar to – as expected – previous campaigns: northern fulmar (*Fulmarus glacialis*) and black-legged kittiwake (*Rissa tridactyla*) were, once at sea, the most numerous ones. The number of ivory gull (*Pagophila eburnea*) (Fig. 11.1) – a species rarely seen once out of the ice - was quite high, but reflects the great proportion of time spent in the pack ice and the vicinity of a breeding population on Greenland. The number of glaucous gull (*Larus hyperboreus*) and little auk (*Alle alle*) was surprisingly low, but this might be due to the lack of any breeding population nearby.

Due to the reduced visibility, detection of whales and dolphins was very hard, if not impossible, for most of the time. Therefore, the low numbers should not be compared with numbers of previous campaigns.

Tab. 11.1: Number of observations of different bird species during 233 recording periods while sailing from Tromsø to the Aurora Vent field

Species	Scientific name	German	Total
northern fulmar	*Fulmarus glacialis*	*Eissturmvogel*	527
northern gannet	*Morus bassanus*	*Baßtölpel*	1
eurasian curlew	*Numenius arquata*	*Groer Brachvogel*	2
black-legged kittiwake	*Rissa tridactyla*	*Dreizehenmöwe*	69
ivory gull	*Pagophila eburnea*	*Elfenbeinmöwe*	122
great black-backed gull	*Larus marinus*	*Mantelmöwe*	13
glaucous gull	*Larus hyperboreus*	*Eismöwe*	2
European herring gull	*Larus argentatus*	*Silbermöwe*	5
lesser black-backed gull	*Larus fuscus*	*Heringsmöwe*	2
arctic tern	*Sterna paradisaea*	*Küstenseeschwalbe*	7
great skua	*Stercorarius skua*	*Skua*	3
pomarine skua	*Stercorarius pomarinus*	*Spatelraubmöwe*	1
parasitic Jaeger	*Stercorarius parasiticus*	*Schmarotzerraubmöwe*	5
long-tailed Jaeger	*Stercorarius longicaudus*	*Falkenraubmöwe*	8
little auk	*Alle alle*	*Krabbentaucher*	10
thick-billed murre	*Uria lomvia*	*Dickschnabellumme*	23
common murre	*Uria aalge*	*Trottellumme*	5
black guillemot	*Cepphus grylle*	*Gryllteiste*	3
Atlantic puffin	*Fratercula arctica*	*Papageitaucher*	157

Tab. 11.2: Number of observations of different marine mammals during 233 recording periods while sailing from Tromsø to the Aurora Vent field

Species	Scientific name	German	Total
humpback whale	*Megaptera novaeangliae*	*Buckelwal*	5
fin whale	*Balaenoptera physalus*	*Finnwal*	4
whale sp.	*/*	*Wal sp.*	5
killer whale	*Orcinus orca*	*Schwertwal*	9
white-beaked dolphin	*Lagenorhynchus albirostris*	*Weißschauzendelfin*	8
dolphin sp.	*/*	*Delfin sp.*	3
hooded seal	*Cystophora cristata*	*Klappmütze*	19
bearded seal	*Erignathus barbatus*	*Bartrobbe*	5
ringed seal	*Pusa hispida*	*Ringelrobbe*	7
seal sp.	*/*	*Robbe sp.*	28
polar bear	*Ursus maritimus*	*Eisbär*	1

Fig. 11.1: The ivory gull is a species typical for the pack ice, and seldom seen when no pack-ice in the vicinity

On station (or drifting) in the pack ice, an additional total of 125 hours of observation were done. The numbers and composition of bird species (see Table 11.3) reflect what could be expected: Northern fulmar, kittiwake and ivory gull being the most abundant species. The high abundance of lower food chains (copepods, algae, jellyfish) detected under the ice by other groups, was not reflected in high densities of the higher tropic levels, meaning that their abundance is at least strongly influenced by other factors. Very low numbers of seals (Table 11.4) were observed, with hooded seal (*Cystophora cristata*) outnumbering harp seal *(Pagophilus groenlandicus)* – which was not the case on previous campaigns, but might indicate that hooded seal is better adapted to pack-ice.

Only 4 sightings of polar bear *(Ursus maritimus)* – the top predator of the Arctic - were achieved (twice a single individual and twice a mother with 2 large cubs), despite diligent efforts (additional 50+ hours searching for this species exclusively).

Tab. 11.3: Number of observations of different marine mammals during 125 observation hours while on station or drifting on the Aurora Vent field.

Species	Scientific name	German	Total
northern fulmar	*Fulmarus glacialis*	*Eissturmvogel*	114
black-legged kittiwake	*Rissa tridactyla*	*Dreizehenmöwe*	259
ivory gull	*Pagophila eburnea*	*Elfenbeinmöwe*	179
Sabine's gull	*Xema sabini*	*Schwalbenmöwe*	1
glaucous gull	*Larus hyperboreus*	*Eismöwe*	3
arctic tern	*Sterna paradisaea*	*Küstenseeschwalbe*	2
long-tailed Jaeger	*Stercorarius longicaudus*	*Falkenraubmöwe*	24
little auk	*Alle alle*	*Krabbentaucher*	4
thick-billed murre	*Uria lomvia*	*Dickschnabellumme*	18
black guillemot	*Cepphus grylle*	*Gryllteiste*	7

Tab. 11.4: Numbers of observed marine mammals during 125 hours of observation while on station or drifting on the Aurora Vent field.

Species	Scientific name	German	Total
hooded seal	*Cystophora cristata*	*Klappmütze*	10
harp seal	*Pagophilus groenlandicus*	*Sattelrobbe*	1
ringed seal	*Pusa hispida*	*Ringelrobbe*	10
seal sp.	/	*Robbe sp.*	29
polar bear	*Ursus maritimus*	*Eisbär*	8

Data Management

All data will be included in our PolE data set, available by contacting coordinator Claude R. Joiris (crjoiris@gmail.com) and later proposed to PANGAEA data set. Publication in international journals is foreseen within one, maximum two years.

References

Joiris, C.R. (1992). Summer distribution and ecological role of seabirds and marine mammals in the Norwegian and Greenland seas (June 1988). J Mar Syst v. 3, no. 1-2, 73-89.

Joiris, C.R. (2007). At-sea distribution of seabirds and marine mammals in the Greenland and Norwegian seas: impact of extremely low ice coverage. Symposium European Research on Polar Environment and Climate, Brussels, 5–6 Mar 2007.

Joiris, C.R. (2011a). A major feeding ground for cetaceans and seabirds in the south-western Greenland Sea. Polar Biology, v. 34, no. 10, 1597-1607.

Joiris, C.R. (2011b). Possible impact of decreasing Arctic pack ice on the higher trophic levels – seabirds and marine mammals. Advances in Environmental Research, v. 23, 207-221.

Joiris, C.R., Dochy, O. (2013). A major autumn feeding ground for fin whales, southern fulmars and grey-headed albatrosses around the South Shetland Islands, Antarctica. Polar Biology, v. 36, no. 11, 1649-1658.

Joiris, C.R., Falck, E. (2010). Summer at-sea distribution of little auks Alle alle and harp seals Pagophilus (Phoca) groenlandica in the Greenland Sea: impact of small-scale hydrological events. Polar Biology, v. 34, no. 4, 541–548.

Joiris, C.R., Tahon, J. (1992). Distribution and food intake of seabirds and marine mammals in the Norwegian and Greenland seas (July 1988). Royal Acad Overseas Sci (Brussels), 113-133.

APPENDIX

A.1 PARTICIPATING INSTITUTIONS

A.2 CRUISE PARTICIPANTS

A.3 SHIP'S CREW

A.4 STATION LIST

A.5 SCIENTIFIC APPENDIX

A.1 TEILNEHMENDE INSTITUTE/PARTICIPATING INSTITUTIONS

	Address
AWI	Alfred Wegener Institute Helmholtz Centre for Polar and Marine Research Am Handelshafen 12 27515 Bremerhaven Germany
DWD	Deutscher Wetterdienst Geschäftsbereich Wettervorhersage Seeschifffahrtsberatung Bernhard Nocht Str. 76 20359 Hamburg Germany
FIELAX	FIELAX Gesellschaft für wissenschaftliche Datenverarbeitung mbH Schleusenstr. 14 D-27568 Bremerhaven Germany
FMI	Finnish Meteorological Institute Erik Palménin aukio 1 FI-00560 Helsinki Finland
HeliService	HeliService international GmbH Am Luneort 15 27572 Bremerhaven Germany
HGF MPG	HGF MPG Research Group on Deep Sea Ecology and Technology Alfred Wegener Institute Helmholtz Centre for Polar and Marine Research Am Handelshafen 12 27515 Bremerhaven Germany
iSiTEC	iSiTEC GmbH Bussestr. 27 27570 Bremerhaven Germany
JHU	Johns Hopkins University 123 Latrobe Hall 3400 N. Charles Street Baltimore, MD 21218 USA

	Address
MARUM	MARUM Center for Marine Environmental Research University Bremen Leobener Str. D-28359 Bremen Germany
MPI-Bremen	Max-Planck-Institut für Marine Mikrobiologie Celsiusstr. 1 28359 Bremen Germany
PolE	Laboratory for Polar Ecology 502 chemin de Ribian F-26130 Saint-Restitut France
Reederei Laeisz	Reederei F. Laeisz GmbH Trostbrücke 1 20457 Hamburg Germany
UHB-GEO	Fachbereich 5 Geowissenschaften der Universität Bremen GEO Gebäude Klagenfurter Straße 28359 Bremen Germany
UHB-IUP	Universität Bremen Institut für Umweltphysik/ Sektion Ozeanographie Otto Hahn Allee 1; Gebäude: NW1 28359 Bremen Germany
WHOI	Woods Hole Oceanographic Institution 86 Water St. Woods Hole, MA 02543-1050 USA

A.2 FAHRTTEILNEHMER / CRUISE PARTICIPANTS

Name/ Last name	Vorname/ First name	Beruf/ Profession
Albrecht	Sebastian	Technician, bathymetry / data management
Arndt	Stefanie	Scientist, sea ice
Bachmann	Denise	Student, petrology/fluid chemistry
Bailey	John	Engineer, *nUI* ROV
Boetius	Antje	Chief scientist, deep-sea ecology
Borowski	Christian	Scientist, symbiosis
D'Hert	Diederick	Scientist, mammal and seabird distribution
Diehl	Alexander	Student, petrology/fluid chemistry
Doll	Mechthild	Student, heat flow
Elliott	Stephen	Technician, *nUI* ROV
German	Christopher	Group leader, *nUI* ROV
Heesemann	Bernd	Technician, heat flow
Hempelt	Juliane	Meteorologist
Jakuba	Mike	Engineer, *nUI* ROV
Jechlitschek	Hendrik	Student, heat flow
Judge	Christopher	Engineer, *nUI* ROV
Katlein	Christian	Group leader, sea ice
Kaul	Norbert	Group leader, heat flow
Kirk	Henning	Technician, seismology
Köhler	Janna	Scientist, oceanography
Lee	Tammy Sabrina	Student, oceanography
Lensu	Mikko	Scientist, sea ice
Marcon	Yann	Scientist, videomapping
McFarland	Christopher	Engineer, *nUI* ROV
Meiners	Mirja	Technician, biogeochemistry
Mertens	Christian	Group leader, oceanography
Miller	Max	Meteorologist
Molari	Massimiliano	Scientist, microbiology
Nordhausen	Axel	Technician, TV grab
Nowak	Christopher	Student, oceanography
Pliet	Johannes	Technician, bathymetry / data management

Name/ Last name	Vorname/ First name	Beruf/ Profession
Rieper	Norbert	Engineer, videomapping
Schlindwein	Vera	Group leader, seismology
Schmid	Florian	Scientist, seismology
Schramm	Fabian	Technician, TV MUC
Sorgenicht	Alexandra	Outreach/TV
Stiens	Rafael	Technician, microsensor
Suman	Stefano	Engineer, *nUI* ROV
Türke	Andreas	Scientist, petrology/fluid chemistry
Vogt	Martin	Scientist, oceanography
Wagner	Louise	Student, petrology/fluid chemistry
Watelet	Michel	Scientist, mammal and seabird distribution
Wegener	Gunter	Scientist, biogeochemistry
Whitcomb	Louis	Engineer, *nUI* ROV
NN		Helicopter
NN		Helicopter
NN		Helicopter
NN		Helicopter

A.3 SCHIFFSBESATZUNG / SHIP'S CREW

No.	Name	Rank
01.	Schwarze, Stefan	Master
02.	Grundmann, Uwe	1. Offc.
03.	Heuck, Hinnerk	Ch. Eng.
04.	Fallei, Holger	2. Offc.
05.	Langhinrichs, Moritz	2. Offc.
06.	Stolze, Henrik	2. Offc.
07.	Spilok, Norbert	Doctor
08.	Fröb, Martin	R. Offc.
09.	Grafe, Jens	2. Eng.
10.	Minzlaff, Hans-Ulrich	2. Eng.
11.	Holst, Wolfgang	3. Eng.
12.	Scholz, Manfred	Elec. Eng.
13.	Christian, Boris	ELO
14.	Hüttebräucker, Olaf	ELO
15.	Nasis, Ilias	ELO
16.	Himmel, Frank	ELO
17.	Loidl, Reiner	Boatsw.
18.	Reise, Lutz	Carpenter
19.	Scheel, Sebastian	A.B.
20.	Brickmann, Peter	A.B.
21.	Winkler, Michael	A.B.
22.	Hagemann, Manfred	A.B.
23.	Schmidt, Uwe	A.B.
24.	NN	A.B.
25.	Wende, Uwe	A.B.
26.	Bäcker, Andreas	A.B.
27.	Guse, Hartmut	A.B.
28.	Preußner, Jörg	Storek.
29.	Teichert, Uwe	Mot-man
30.	Schütt, Norbert	Mot-man
31.	Elsner, Klaus	Mot-man
32.	Voy, Bernd	Mot-man
33.	Pinske, Lutz	Mot-man
34.	Müller-Homburg, Ralf-Dieter	Cook
35.	Silinski, Frank	Cooksmate
36.	Martens, Michael	Cooksmate
37.	Czyborra, Bärbel	1. Stwdess
38.	Wöckener, Martina	Stwdess/KS.
39.	Dibenau, Torsten	2. Steward
40.	Silinski, Carmen	2. Stwdess
41.	Arendt, Rene	2. Steward
42.	Möller, Wolfgang	2. Steward
43.	Sun, Yong Shen	2. Steward
44.	Yu, Kwok Yuen	Laundrym.
45.	Wittek, Sönke	Appr.
46.	Fachini, Simon	Appr.

A.4 STATIONSLISTE / STATION LIST PS 86

Gear abbrevations:

CTD	CTD
HF	Heat Flow Lance
HS_PS	Hydrosweep/Parasound
ICE	Ice Station
GC	Gravity Corer
OBS	Ocean Bottom Seismometer
OFOS	Ocean Floor Observation System
REL	Releaser Test
RO	Rosette water sampler
ROV	ROV
TVMUC	TV-Multicorer
XCTD	Expendable CTD

In the following list all position and depth information marked from position sensor SHIP are based on GPS positions and multibeam echosounder's center beam depth. Position and depth information from position sensor USBL are based on the acoustic underwater positioning system Posidonia. The depth then is the gear's/ transponder depth.

Station	Date	Time	Position Lat	Position Lon	Depth [m]	Gear	Action	Pos.-Sensor
PS86/0001-1	11.07.2014	08:01	81° 17.24' N	8° 59.91' W	303.0	XCTD	on ground/max depth	Ship
PS86/0002-1	11.07.2014	09:03	81° 24.35' N	9° 4.26' W	751.9	XCTD	on ground/max depth	Ship
PS86/0003-1	11.07.2014	10:00	81° 30.43' N	9° 18.38' W	1483.3	XCTD	on ground/max depth	Ship
PS86/0004-1	11.07.2014	10:45	81° 35.54' N	9° 14.61' W	1869.6	XCTD	on ground/max depth	Ship
PS86/0005-1	11.07.2014	11:28	81° 40.59' N	8° 52.52' W	2358.4	XCTD	on ground/max depth	Ship
PS86/0006-1	11.07.2014	13:12	81° 40.97' N	8° 47.15' W	2446.3	REL	on ground/max depth	Ship
PS86/0007-1	11.07.2014	15:38	81° 44.93' N	9° 7.19' W	2005.9	XCTD	on ground/max depth	Ship
PS86/0008-1	11.07.2014	16:24	81° 49.93' N	9° 29.84' W	2193.7	XCTD	on ground/max depth	Ship
PS86/0009-1	11.07.2014	16:58	81° 54.89' N	9° 31.40' W	2456.5	XCTD	on ground/max depth	Ship
PS86/0010-1	11.07.2014	17:29	81° 59.97' N	9° 44.33' W	2578.3	XCTD	on ground/max depth	Ship
PS86/0011-1	11.07.2014	17:59	82° 5.07' N	9° 47.98' W	2645.0	XCTD	on ground/max depth	Ship
PS86/0012-1	11.07.2014	18:34	82° 10.22' N	9° 48.08' W	2722.8	XCTD	on ground/max depth	Ship
PS86/0013-1	11.07.2014	19:21	82° 15.20' N	9° 22.91' W	2897.5	XCTD	on ground/max depth	Ship
PS86/0015-1	11.07.2014	21:32	82° 26.21' N	8° 12.00' W	2921.4	XCTD	on ground/max depth	Ship
PS86/0016-1	11.07.2014	23:53	82° 35.50' N	7° 20.92' W	3930.4	XCTD	on ground/max depth	Ship
PS86/0017-1	12.07.2014	03:49	82° 45.03' N	6° 43.24' W	4282.4	XCTD	on ground/max depth	Ship
PS86/0018-1	12.07.2014	07:18	82° 54.47' N	6° 20.08' W	4099.3	CTD/RO	in the water	Ship
PS86/0018-1	12.07.2014	10:05	82° 53.34' N	6° 25.69' W	4221.3	CTD/RO	on deck	Ship
PS86/0019-1	12.07.2014	15:15	82° 54.04' N	6° 22.65' W	4227.4	OFOS	in the water	Ship
PS86/0019-1	12.07.2014	19:52	82° 51.58' N	6° 21.43' W	4501.3	OFOS	on deck	Ship
PS86/0020-1	12.07.2014	21:38	82° 51.02' N	6° 24.32' W	4562.0	TVMUC	on ground/max depth	Ship
PS86/0020-1	12.07.2014	21:53	82° 50.98' N	6° 24.53' W	4613.0	TVMUC	information	Ship
PS86/0021-1	13.07.2014	01:44	82° 56.54' N	6° 6.10' W	4272.5	CTD/RO	in the water	Ship
PS86/0021-1	13.07.2014	07:03	82° 54.42' N	5° 58.51' W	3954.1	CTD/RO	on deck	Ship
PS86/0022-1	13.07.2014	10:29	82° 55.37' N	6° 12.23' W	4082.9	HF	on ground/max depth	Ship
PS86/0022-2	13.07.2014	11:08	82° 55.31' N	6° 11.74' W	4084.9	HF	on ground/max depth	Ship
PS86/0022-3	13.07.2014	12:02	82° 55.20' N	6° 10.12' W	4080.6	HF	on ground/max depth	Ship

Station	Date	Time	Position Lat	Position Lon	Depth [m]	Gear	Action	Pos.-Sensor
PS86/0022-4	13.07.2014	12:53	82° 55.10' N	6° 9.13' W	4050.8	HF	on ground/max depth	Ship
PS86/0022-5	13.07.2014	13:36	82° 54.99' N	6° 7.59' W	4006.1	HF	on ground/max depth	Ship
PS86/0023-1	13.07.2014	16:19	82° 54.75' N	6° 15.85' W	4063.5	CTD/RO	in the water	Ship
PS86/0023-1	13.07.2014	19:56	82° 53.27' N	6° 15.34' W	4113.7	CTD	on deck	Ship
PS86/0024-1	13.07.2014	21:04	82° 54.79' N	6° 15.18' W	4065.2	OFOS	in the water	Ship
PS86/0024-1	14.07.2014	02:55	82° 53.81' N	6° 9.56' W	4001.5	OFOS	on deck	Ship
PS86/0025-1	14.07.2014	10:03	82° 54.49' N	6° 13.81' W	3979.6	HF	on ground/max depth	Ship
PS86/0025-2	14.07.2014	10:47	82° 54.43' N	6° 14.31' W	4034.8	HF	on ground/max depth	Ship
PS86/0025-3	14.07.2014	11:22	82° 54.36' N	6° 14.27' W	3956.6	HF	on ground/max depth	Ship
PS86/0026-1	14.07.2014	13:34	82° 54.14' N	6° 12.30' W	3916.9	OBS	on ground/max depth	Ship
PS86/0027-1	14.07.2014	16:34	82° 55.39' N	6° 11.91' W	4096.9	GC	on ground/max depth	Ship
PS86/0028-1	14.07.2014	20:42	82° 55.19' N	6° 16.91' W	4115.5	TVMUC	on ground/max depth	Ship
PS86/0029-1	14.07.2014	22:54	82° 54.31' N	6° 13.68' W	3912.8	CTD	in the water	Ship
PS86/0029-1	15.07.2014	06:42	82° 54.31' N	6° 5.59' W	3976.9	CTD	on deck	Ship
PS86/0030-1	15.07.2014	07:39	82° 54.26' N	6° 14.41' W	3902.3	OFOS	in the water	Ship
PS86/0030-1	15.07.2014	13:44	82° 54.06' N	6° 8.63' W	3999.0	OFOS	on deck	Ship
PS86/0031-1	15.07.2014	09:05	82° 54.00' N	6° 14.38' W	3871.5	ICE	information	Ship
PS86/0032-1	15.07.2014	17:08	82° 57.517' N	6° 16.191' W	4265.0	OBS	on ground/max depth	USBL
PS86/0033-1	15.07.2014	21:40	82° 53.99' N	6° 21.13' W	4110.9	CTD/RO	in the water	Ship
PS86/0033-1	16.07.2014	04:25	82° 53.60' N	6° 6.65' W	4091.0	CTD/RO	on deck	Ship
PS86/0034-1	16.07.2014	06:40	82° 53.37' N	6° 14.22' W	4097.8	HF	on ground/max depth	Ship
PS86/0034-2	16.07.2014	07:21	82° 53.29' N	6° 13.39' W	4112.8	HF	on ground/max depth	Ship
PS86/0034-3	16.07.2014	07:59	82° 53.34' N	6° 12.81' W	4094.8	HF	on ground/max depth	Ship
PS86/0034-4	16.07.2014	08:39	82° 53.32' N	6° 12.14' W	4093.7	HF	on ground/max depth	Ship
PS86/0034-5	16.07.2014	09:12	82° 53.25' N	6° 11.26' W	4106.4	HF	on ground/max depth	Ship
PS86/0035-1	16.07.2014	12:56	82° 54.14' N	6° 21.43' W	4120.1	OFOS	in the water	Ship
PS86/0035-1	16.07.2014	14:06	82° 54.04' N	6° 18.87' W	4023.2	OFOS	information	Ship

Station	Date	Time	Position Lat	Position Lon	Depth [m]	Gear	Action	Pos.-Sensor
PS86/0035-1	16.07.2014	20:51	82° 53.66' N	6° 12.27' W	4111.1	OFOS	on deck	Ship
PS86/0036-1	16.07.2014	21:33	82° 54.21' N	6° 15.23' W	3924	CTD/RO	in the water	Ship
PS86/0036-1	17.07.2014	04:11	82° 53.45' N	6° 12.83' W	4088	CTD/RO	on deck	Ship
PS86/0037-1	17.07.2014	06:21	82° 54.365' N	6° 16.050' W	4066	HF	on ground/max depth	USBL
PS86/0037-2	17.07.2014	07:56	82° 54.083' N	6° 13.907' W	3884	HF	on ground/max depth	USBL
PS86/0037-3	17.07.2014	08:55	82° 54.139' N	6° 12.510' W	3901	HF	on ground/max depth	USBL
PS86/0037-4	17.07.2014	09:31	82° 54.126' N	6° 11.577' W	3930	HF	on ground/max depth	USBL
PS86/0038-1	17.07.2014	12:26	82°54.159'N	6°13.680'W	3677.6	GC	on ground/max depth	USBL
PS86/0039-1	17.07.2014	17:19	82° 54.32' N	6° 16.43' W	4059.4	OFOS	in the water	Ship
PS86/0039-1	17.07.2014	21:57	82° 54.97' N	6° 23.27' W	4139	OFOS	on deck	Ship
PS86/0040-1	17.07.2014	22:16	82° 55.07' N	6° 22.80' W	4133.1	CTD/RO	in the water	Ship
PS86/0040-1	18.07.2014	06:19	82° 53.61' N	6° 6.41' W	4084.4	CTD/RO	on deck	Ship
PS86/0041-1	18.07.2014	07:29	82° 54.95' N	6° 22.58' W	4142.8	TVMUC	in the water	Ship
PS86/0041-1	18.07.2014	12:50	82° 53.41' N	6° 11.58' W	4077.1	TVMUC	on deck	Ship
PS86/0042-1	18.07.2014	13:45	82° 53.16' N	6° 10.89' W	4169.3	ROV	in the water	Ship
PS86/0042-1	18.07.2014	18:25	82° 52.33' N	6° 7.09' W	4458.3	ROV	on deck	Ship
PS86/0043-1	18.07.2014	21:16	82° 54.48' N	6° 13.89' W	3986.7	CTD/RO	in the water	Ship
PS86/0043-1	19.07.2014	03:24	82° 53.30' N	6° 12.06' W	4093.2	CTD/RO	on deck	Ship
PS86/0044-1	19.07.2014	06:20	82° 54.00' N	6° 12.29' W	3908.7	GC	on ground/max depth	Ship
PS86/0045-1	19.07.2014	09:44	82° 54.02' N	6° 13.61' W	3874.1	GC	on ground/max depth	Ship
PS86/0046-1	19.07.2014	11:57	82° 54.84' N	6° 18.93' W	4105.5	OFOS	in the water	Ship
PS86/0046-1	19.07.2014	17:14	82° 53.96' N	6° 7.41' W	4024.7	OFOS	on deck	Ship
PS86/0047-1	19.07.2014	18:29	82° 54.74' N	6° 13.83' W	4008.4	HS_PS	profile start	Ship
PS86/0047-1	20.07.2014	05:32	83° 6.91' N	5° 45.26' W	4268.4	HS_PS	profile end	Ship
PS86/0048-1	20.07.2014	07:20	83° 5.18' N	6° 0.49' W	3612.3	CTD/RO	in the water	Ship
PS86/0048-1	20.07.2014	10:31	83° 5.03' N	5° 58.31' W	3552.9	CTD/RO	on deck	Ship
PS86/0049-1	20.07.2014	11:52	83° 3.91' N	6° 6.40' W	3779.2	CTD/RO	in the water	Ship

Station	Date	Time	Position Lat	Position Lon	Depth [m]	Gear	Action	Pos.-Sensor
PS86/0049-1	20.07.2014	15:27	83° 3.37' N	6° 5.60' W	3990.9	CTD/RO	on deck	Ship
PS86/0050-1	20.07.2014	16:10	83° 4.84' N	6° 6.25' W	3520.2	OFOS	in the water	Ship
PS86/0050-1	20.07.2014	22:06	83° 3.85' N	6° 4.84' W	3812.7	OFOS	on deck	Ship
PS86/0051-1	21.07.2014	01:00	83° 6.56' N	5° 45.79' W	4270	HF	on ground/max depth	Ship
PS86/0051-2	21.07.2014	02:07	83° 6.30' N	5° 46.21' W	4232.3	HF	on ground/max depth	Ship
PS86/0051-3	21.07.2014	03:32	83° 6.10' N	5° 46.21' W	4176.7	HF	on ground/max depth	Ship
PS86/0052-1	21.07.2014	07:26	83° 0.81' N	6° 24.59' W	4060.5	CTD/RO	in the water	Ship
PS86/0052-1	21.07.2014	10:24	82° 59.92' N	6° 26.28' W	4026.9	CTD/RO	on deck	Ship
PS86/0053-1	21.07.2014	11:44	82° 59.69' N	6° 27.77' W	4085.1	ROV	in the water	Ship
PS86/0053-1	21.07.2014	16:52	82° 58.61' N	6° 36.18' W	4119.5	ROV	on deck	Ship
PS86/0054-1	21.07.2014	19:10	83° 1.24' N	6° 16.03' W	3992.9	OFOS	in the water	Ship
PS86/0054-1	21.07.2014	23:32	83° 1.39' N	6° 20.51' W	3970.6	OFOS	on deck	Ship
PS86/0055-1	22.07.2014	03:31	82° 53.99' N	6° 19.02' W	4028.8	CTD/RO	in the water	Ship
PS86/0055-1	22.07.2014	10:00	82° 54.86' N	6° 1.26' W	4040.4	CTD/RO	on deck	Ship
PS86/0056-1	22.07.2014	12:53	82° 53.82' N	6° 24.92' W	4197.8	OFOS	in the water	Ship
PS86/0056-1	22.07.2014	19:36	82° 53.96' N	6° 19.65' W	4053.9	OFOS	on deck	Ship
PS86/0057-1	22.07.2014	19:40	82° 53.96' N	6° 19.40' W	4047.5	CTD/RO	in the water	Ship
PS86/0057-1	22.07.2014	22:54	82° 53.65' N	6° 11.04' W	4034.6	CTD/RO	on deck	Ship
PS86/0058-1	23.07.2014	02:01	82° 54.219' N	6° 32.593' W	4101	HF	on ground/max depth	Ship
PS86/0058-2	23.07.2014	02:52	82° 54.078' N	6° 32.570' W	4113	HF	on ground/max depth	Ship
PS86/0058-3	23.07.2014	04:02	82° 53.919' N	6° 32.347' W	4171	HF	on ground/max depth	Ship
PS86/0059-1	23.07.2014	07:59	82° 54.45' N	6° 25.94' W	4163.2	GC	on ground/max depth	Ship
PS86/0060-1	23.07.2014	11:03	82° 53.89' N	6° 23.78' W	4188.1	ROV	in the water	Ship
PS86/0060-1	23.07.2014	16:08	82° 53.40' N	6° 24.35' W	4226.4	ROV	on deck	Ship
PS86/0061-1	23.07.2014	19:05	82° 54.04' N	6° 16.56' W	3998.2	TVMUC	in the water	Ship
PS86/0061-1	23.07.2014	22:50	82° 53.50' N	6° 15.52' W	4031.4	TVMUC	on deck	Ship
PS86/0062-1	24.07.2014	01:25	82° 55.63' N	6° 21.44' W	4113.2	HF	on ground/max depth	Ship

Station	Date	Time	Position Lat	Position Lon	Depth [m]	Gear	Action	Pos.-Sensor
PS86/0062-2	24.07.2014	02:21	82° 55.42' N	6° 23.88' W	4099.1	HF	on ground/max depth	Ship
PS86/0062-3	24.07.2014	02:55	82° 55.36' N	6° 25.53' W	4101.7	HF	on ground/max depth	Ship
PS86/0062-4	24.07.2014	03:50	82° 55.26' N	6° 28.29' W	4132.2	HF	on ground/max depth	Ship
PS86/0063-1	24.07.2014	07:12	82° 57.66' N	6° 11.74' W	4269.4	OBS	on ground/max depth	Ship
PS86/0063-1	24.07.2014	10:32	82° 57.34' N	6° 17.83' W	0	OBS	on deck	Ship
PS86/0064-1	24.07.2014	12:36	82° 55.33' N	6° 19.87' W	4129.4	GC	on ground/max depth	Ship
PS86/0065-1	24.07.2014	15:03	82° 54.84' N	6° 12.01' W	3988.8	OFOS	in the water	Ship
PS86/0065-1	24.07.2014	22:16	82° 53.04' N	6° 15.07' W	4178.1	OFOS	on deck	Ship
PS86/0066-1	24.07.2014	22:56	82° 54.73' N	6° 17.17' W	4076.7	CTD/RO	in the water	Ship
PS86/0066-1	25.07.2014	04:27	82° 53.17' N	6° 20.38' W	4167.4	CTD/RO	on deck	Ship
PS86/0067-1	25.07.2014	07:39	82° 53.82' N	6° 15.02' W	3906.8	GC	on ground/max depth	Ship
PS86/0068-1	25.07.2014	10:57	82° 54.57' N	6° 6.14' W	3948	OFOS	in the water	Ship
PS86/0068-1	25.07.2014	18:57	82° 53.66' N	6° 18.98' W	3992.7	OFOS	on deck	Ship
PS86/0069-1	25.07.2014	21:27	82° 54.23' N	6° 10.31' W	3959.3	CTD/RO	in the water	Ship
PS86/0069-1	26.07.2014	04:45	82° 53.74' N	6° 18.86' W	4003.9	CTD/RO	on deck	Ship
PS86/0070-1	26.07.2014	06:43	82° 53.00' N	6° 23.27' W	4186.4	ROV	in the water	Ship
PS86/0070-1	26.07.2014	11:44	82° 52.09' N	6° 22.77' W	4332.6	ROV	on deck	Ship
PS86/0071-1	26.07.2014	12:13	82° 52.00' N	6° 23.00' W	4369.8	ICE	on ground/max depth	Ship
PS86/0071-1	26.07.2014	13:08	82° 51.81' N	6° 23.57' W	4308	ICE	on deck	Ship
PS86/0072-1	26.07.2014	14:00	82° 53.63' N	6° 15.36' W	3985.5	HS_PS	profile start	Ship
PS86/0072-1	27.07.2014	01:00	83° 7.31' N	2° 31.12' W	2858.6	HS_PS	profile end	Ship
PS86/0073-1	27.07.2014	04:07	83° 6.68' N	2° 27.92' W	3042.2	HF	on ground/max depth	Ship
PS86/0073-2	27.07.2014	04:56	83° 6.59' N	2° 26.94' W	3070.6	HF	on ground/max depth	Ship
PS86/0074-1	27.07.2014	06:55	83° 6.39' N	2° 27.35' W	3033.7	CTD/RO	in the water	Ship
PS86/0074-1	27.07.2014	08:58	83° 6.31' N	2° 27.97' W	2953.7	CTD/RO	on deck	Ship
PS86/0075-1	27.07.2014	08:58	83° 6.31' N	2° 27.97' W	2953.7	HS_PS	profile start	Ship
PS86/0075-1	27.07.2014	17:00	82° 53.68' N	6° 12.91' W	4006	HS_PS	profile end	Ship

Station	Date	Time	Position Lat	Position Lon	Depth [m]	Gear	Action	Pos.-Sensor
PS86/0076-1	27.07.2014	17:41	82° 53.96' N	6° 12.97' W	3888.7	TVMUC	in the water	Ship
PS86/0076-1	27.07.2014	20:24	82° 53.41' N	6° 19.13' W	4088.7	TVMUC	on deck	Ship
PS86/0077-1	27.07.2014	22:24	82° 54.26' N	6° 12.89' W	3930.5	OFOS	in the water	Ship
PS86/0077-1	28.07.2014	02:20	82° 53.44' N	6° 20.11' W	4067.3	OFOS	on deck	Ship
PS86/0078-1	28.07.2014	05:14	82° 53.735' N	6° 15.955' W	3947	HF	on ground/max depth	USBL
PS86/0078-2	28.07.2014	05:26	82° 53.710' N	6° 16.338' W	3973	HF	on ground/max depth	USBL
PS86/0079-1	28.07.2014	09:27	82° 53.73' N	6° 13.41' W	3986.4	GC	on ground/max depth	Ship
PS86/0080-1	28.07.2014	12:01	82° 53.17' N	6° 18.43' W	4136.4	ICE	on ground/max depth	Ship
PS86/0081-1	28.07.2014	12:29	82° 53.01' N	6° 19.14' W	4196.7	ROV	in the water	Ship
PS86/0081-1	28.07.2014	17:51	82° 51.82' N	6° 28.28' W	4442.3	ROV	on deck	Ship
PS86/0082-1	28.07.2014	21:15	82° 54.43' N	6° 11.06' W	3991	OFOS	in the water	Ship
PS86/0082-1	29.07.2014	02:20	82° 53.47' N	6° 16.83' W	4039.8	OFOS	on deck	Ship
PS86/0083-1	29.07.2014	03:03	82° 54.82' N	6° 8.98' W	4007.6	CTD/RO	in the water	Ship
PS86/0083-1	29.07.2014	09:41	82° 53.45' N	6° 15.27' W	4060.7	CTD/RO	on deck	Ship
PS86/0084-1	29.07.2014	10:34	82° 54.63' N	6° 16.03' W	4057.6	OFOS	in the water	Ship
PS86/0084-1	29.07.2014	15:25	82° 53.71' N	6° 17.50' W	3982.3	OFOS	on deck	Ship
PS86/0085-1	29.07.2014	17:20	82° 54.13' N	6° 13.92' W	3877.6	OFOS	in the water	Ship
PS86/0085-1	29.07.2014	21:26	82° 53.32' N	6° 14.85' W	4080.7	OFOS	on deck	Ship
PS86/0086-1	29.07.2014	22:05	82° 54.36' N	6° 15.63' W	4020	OFOS	in the water	Ship
PS86/0086-1	30.07.2014	02:22	82° 52.91' N	6° 19.44' W	4199.4	OFOS	on deck	Ship
PS86/0087-1	02.08.2014	08:18	72° 0.29' N	14° 43.29' E	1236.6	HS_PS	HydroSweep/ ParaSound profile start	Ship
PS86/0087-1	02.08.2014	09:21	72° 0.03' N	14° 42.66' E	1245.4	HS_PS	HydroSweep/ ParaSound profile end	Ship

APPENDIX 5 MARINE GEOLOGY

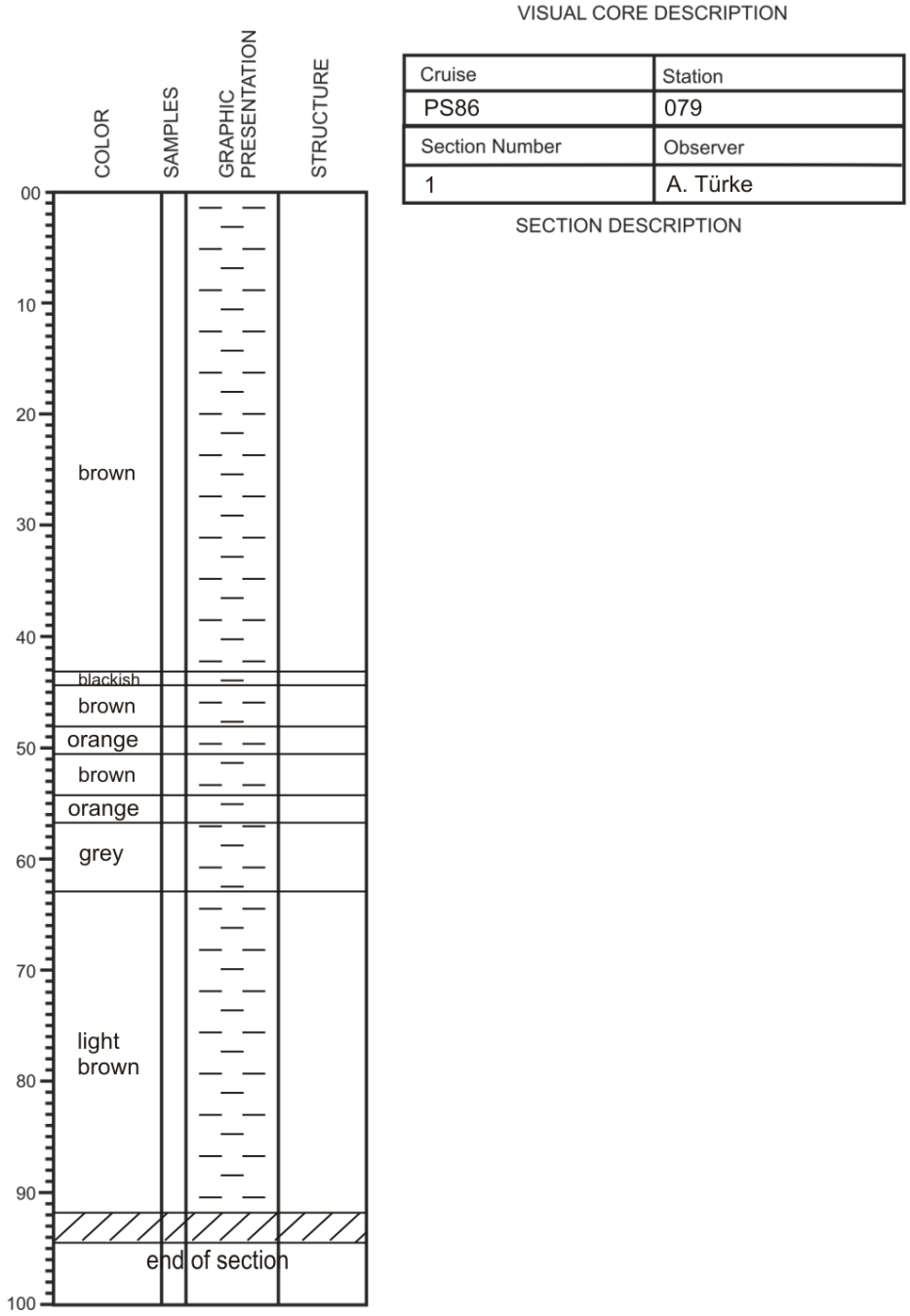

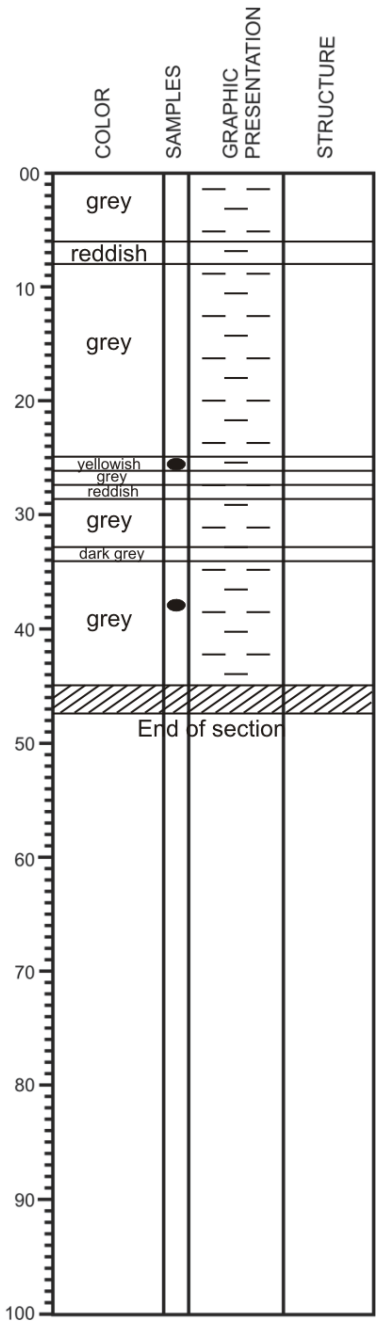

VISUAL CORE DESCRIPTION

Cruise	Station
PS86	027
Section Number	Observer
2	A. Türke / A. Diehl

SECTION DESCRIPTION

Macroscopic observations: homogeneous dark brown clay

Binocular: sulfide fragments and rounded black basalt(?) fragments (both accessory),

VISUAL CORE DESCRIPTION

Cruise	Station
PS86	027
Section Number	Observer
3	A. Türke / A. Diehl

SECTION DESCRIPTION

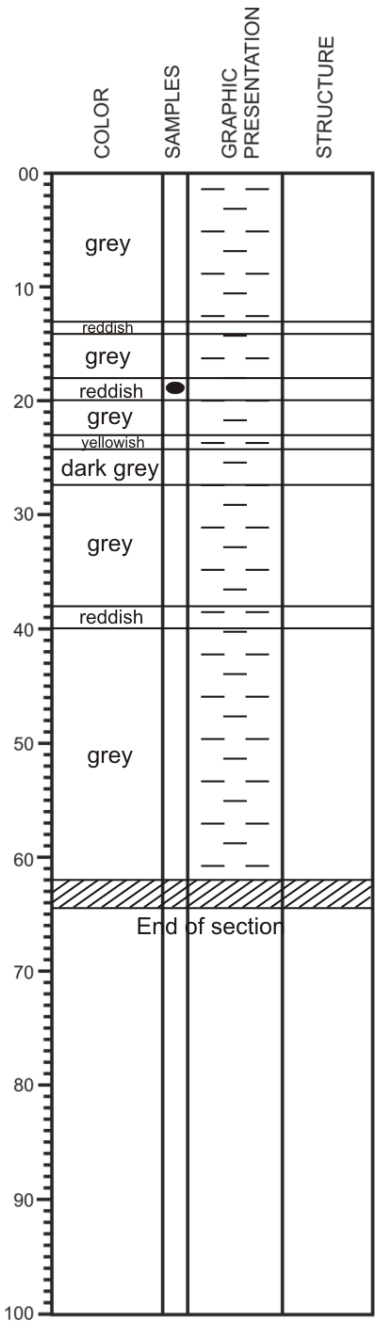

VISUAL CORE DESCRIPTION

Cruise	Station
PS86	045
Section Number	Observer
1	A. Diehl

SECTION DESCRIPTION

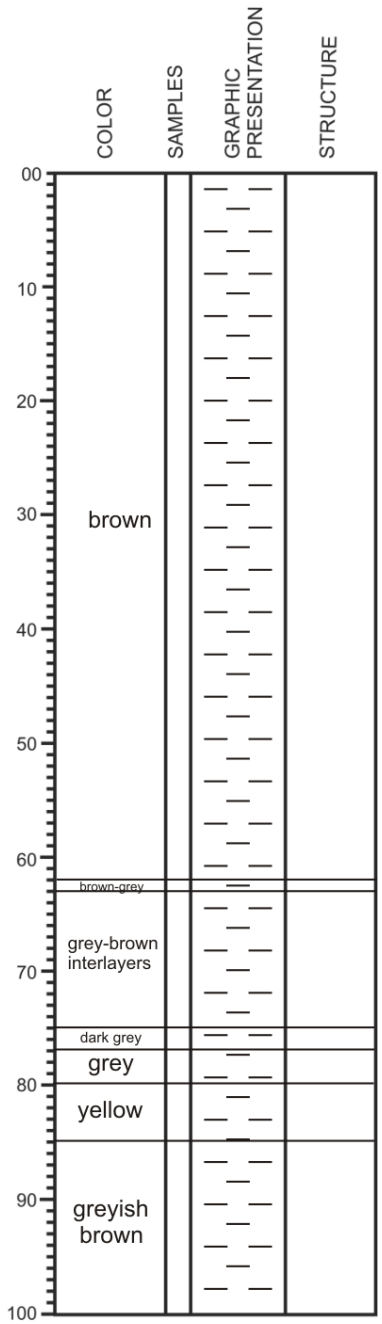

VISUAL CORE DESCRIPTION

Cruise	Station
PS86	045
Section Number	Observer
2	A. Diehl

SECTION DESCRIPTION

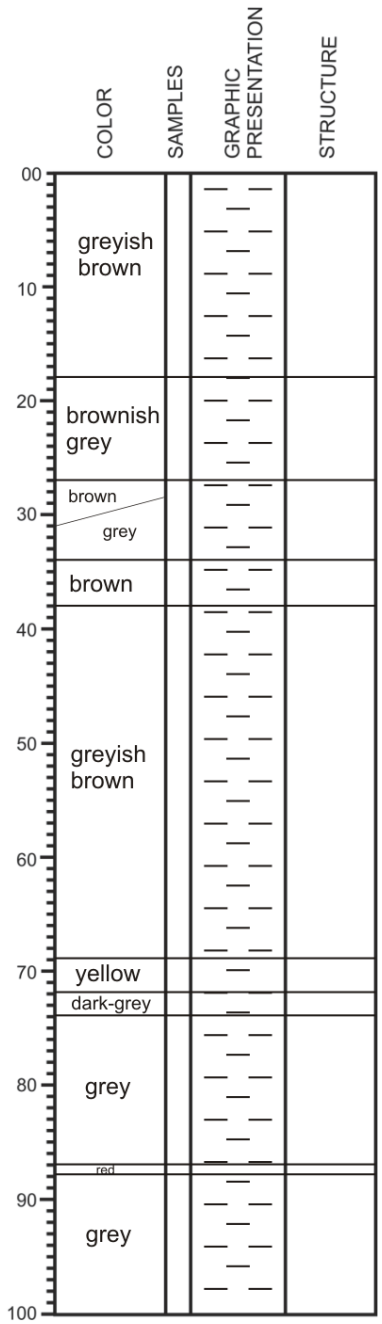

brown layers contain ferry-hydroxides (rusty particles)
(oxidized sulfides?)

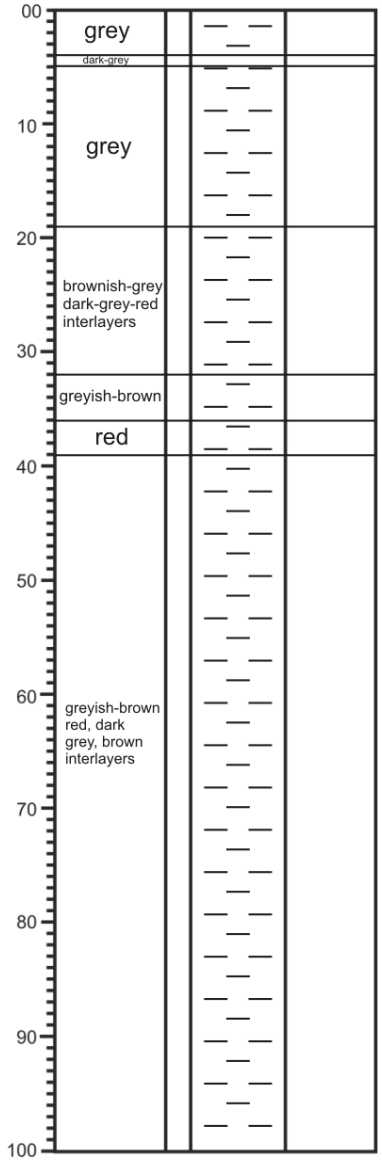

VISUAL CORE DESCRIPTION

Cruise	Station
PS86	045
Section Number	Observer
3	A. Diehl

SECTION DESCRIPTION

black particles (oxidized sulfides?)

VISUAL CORE DESCRIPTION

Cruise	Station
PS86	045
Section Number	Observer
4	A. Diehl

SECTION DESCRIPTION

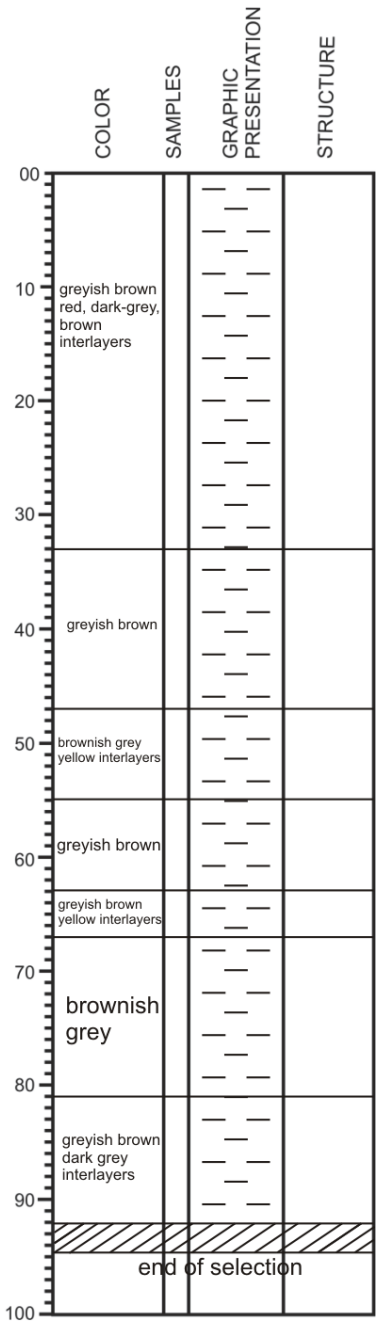

black particles (oxidized sulfides?)

VISUAL CORE DESCRIPTION

Cruise	Station
PS86	059
Section Number	Observer
5	A. Diehl

SECTION DESCRIPTION

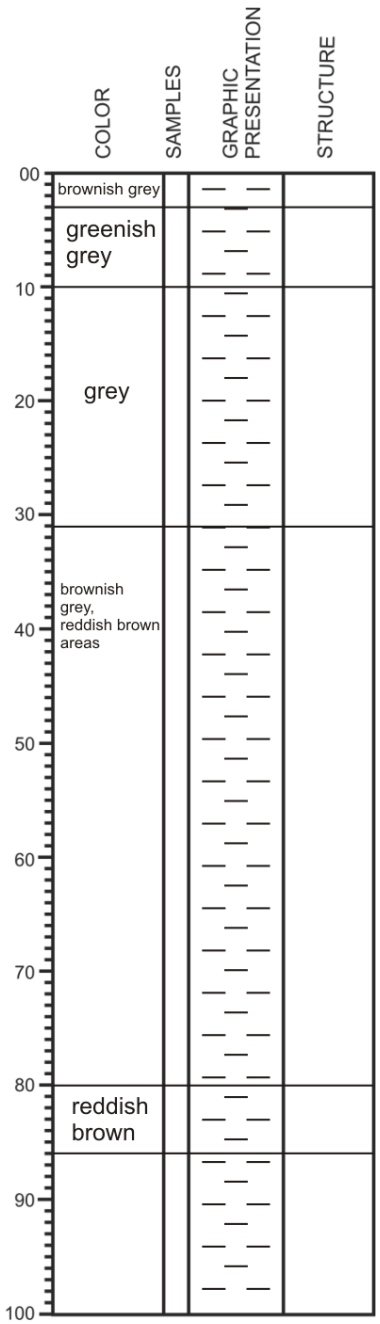

VISUAL CORE DESCRIPTION

Cruise	Station
PS86	059
Section Number	Observer
1	A. Diehl

SECTION DESCRIPTION

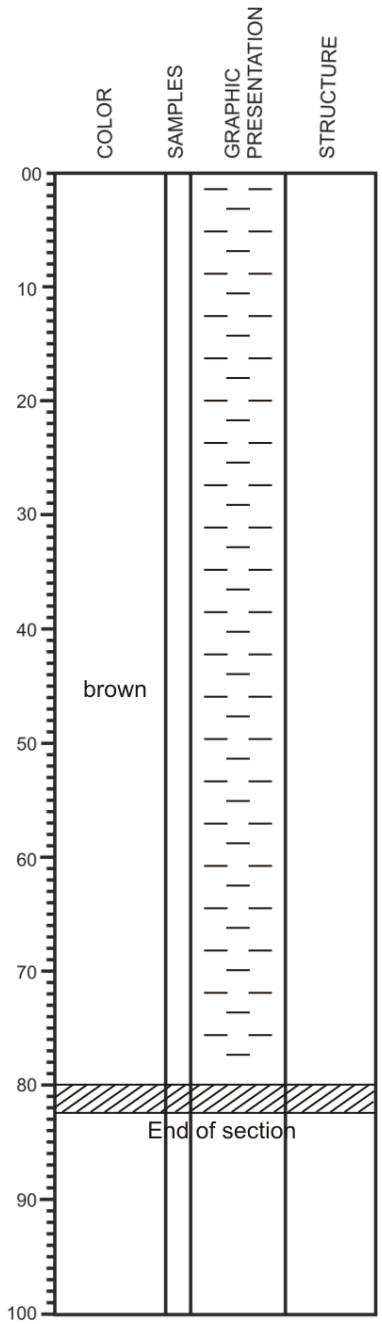

VISUAL CORE DESCRIPTION

Cruise	Station
PS86	059
Section Number	Observer
2	A. Diehl

SECTION DESCRIPTION

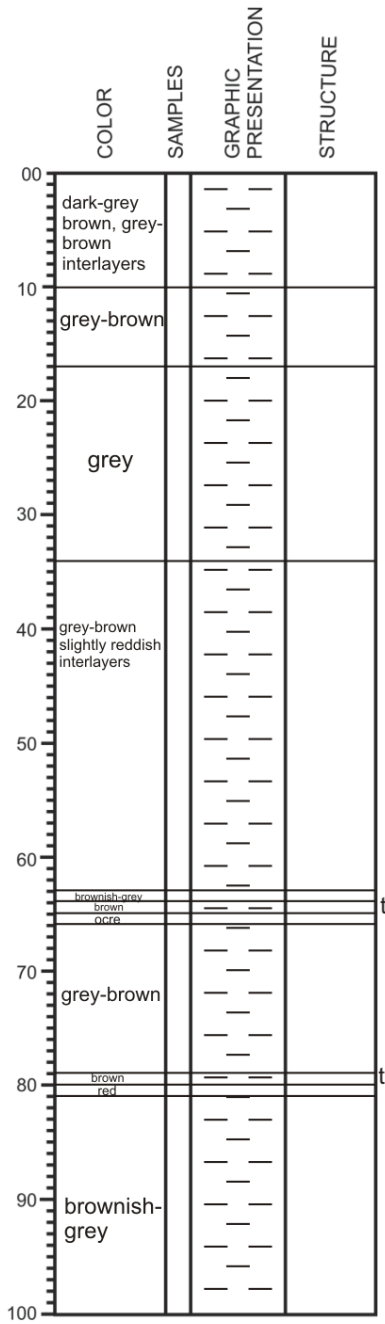

black particles (millimeter sized)

thickness 2 mm, sharp boundaries, grainy quality

thickness 1 mm, sharp boundaries, grainy quality

VISUAL CORE DESCRIPTION

Cruise	Station
PS86	059
Section Number	Observer
3	A. Diehl

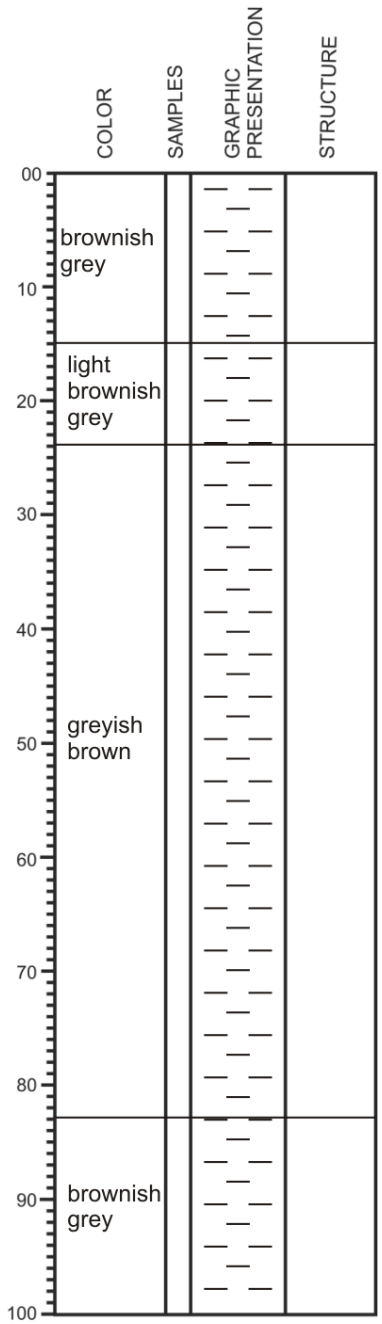

SECTION DESCRIPTION

black particles

dark grey and red interlayers

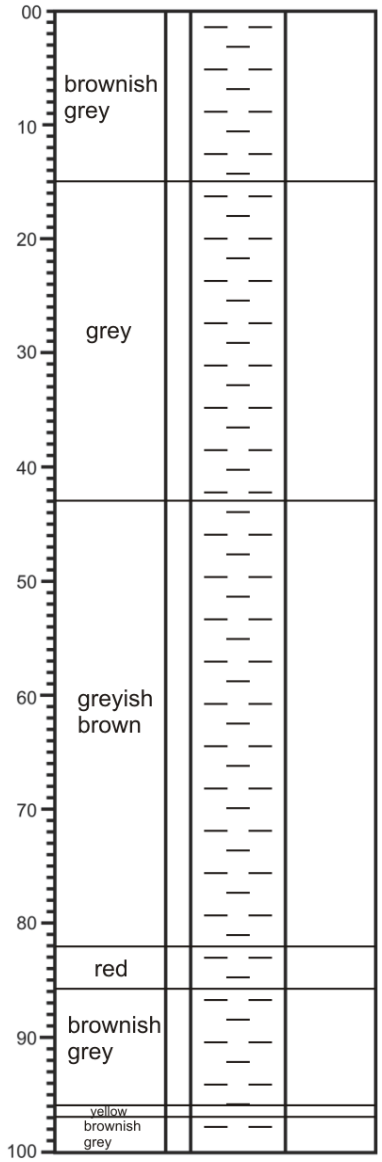

VISUAL CORE DESCRIPTION

Cruise	Station
PS86	059
Section Number	Observer
4	A. Diehl

SECTION DESCRIPTION

brownish interlayer

grey and brown-yellowish interlayers

corny interlayer

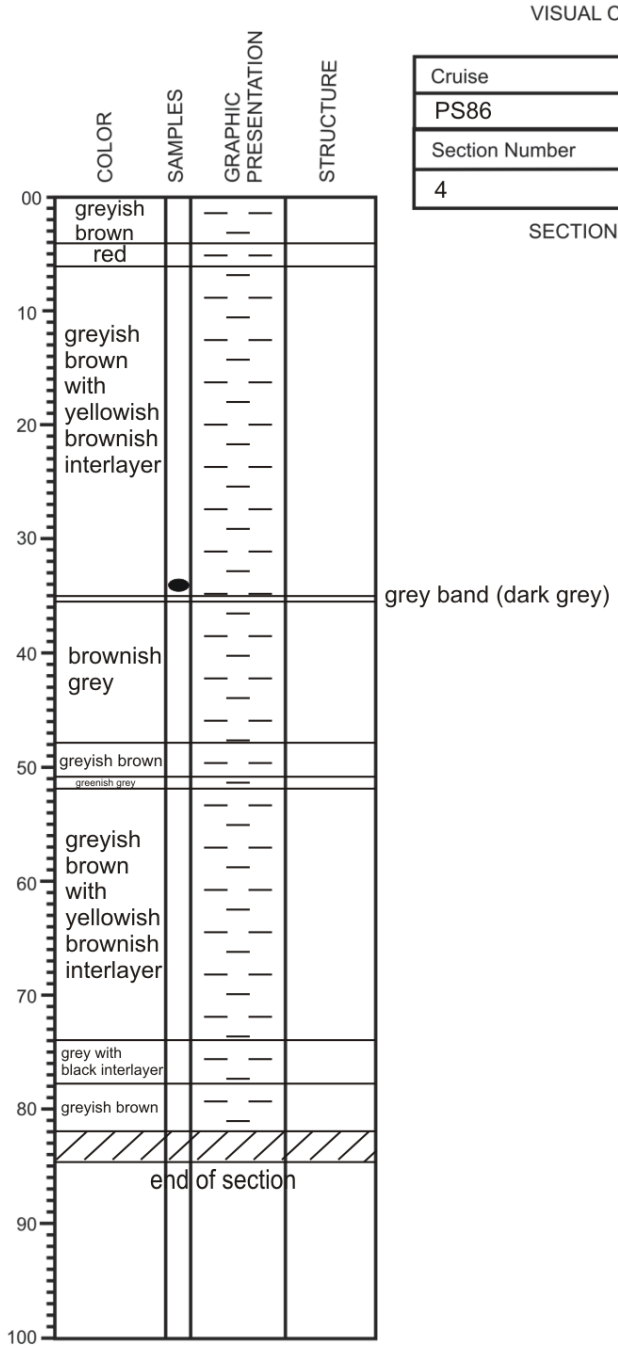
VISUAL CORE DESCRIPTION
Cruise
Station
PS86
064
Section Number
Observer
4
A. Diehl
SECTION DESCRIPTION
COLOR
SAMPLES
GRAPHIC PRESENTATION
STRUCTURE
00
10
20
30
40
50
60
70
80
90
100
greyish brown
red
greyish brown with yellowish brownish interlayer
grey band (dark grey)
brownish grey
greyish brown
greenish grey
greyish brown with yellowish brownish interlayer
grey with black interlayer
greyish brown
end of section

VISUAL CORE DESCRIPTION

Cruise	Station
PS86	064
Section Number	Observer
1	A. Diehl

SECTION DESCRIPTION

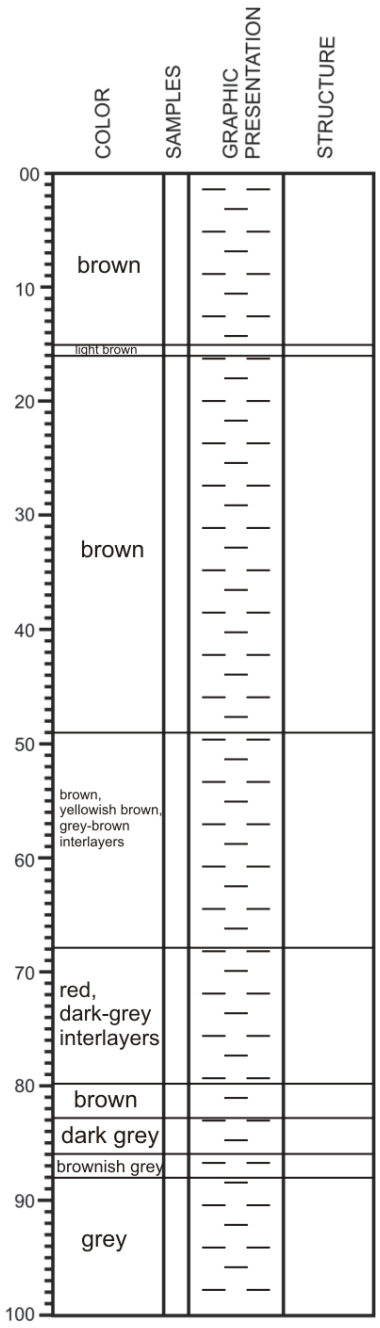

grainy quality

VISUAL CORE DESCRIPTION

Cruise	Station
PS86	064
Section Number	Observer
2	A. Diehl

SECTION DESCRIPTION

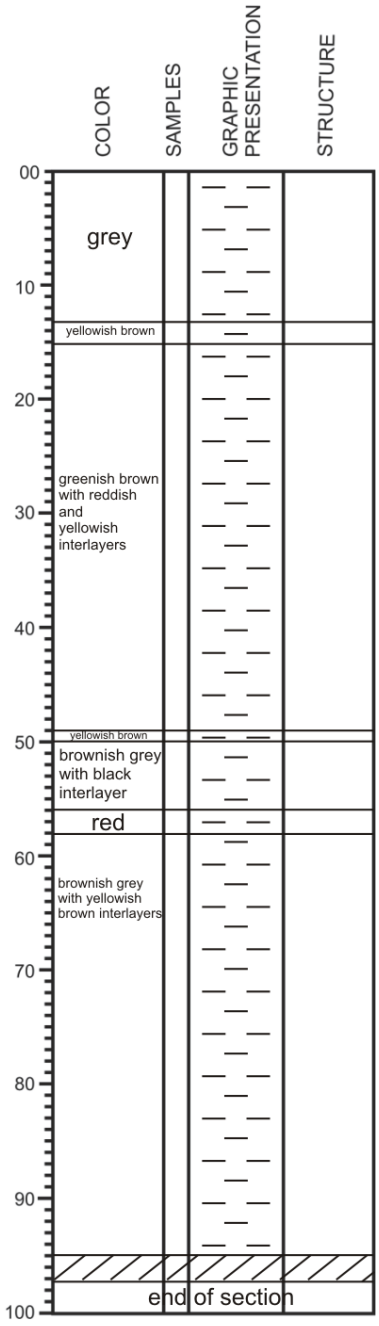

grainy appearance

VISUAL CORE DESCRIPTION

Cruise	Station
PS86	064
Section Number	Observer
3	A. Diehl

SECTION DESCRIPTION

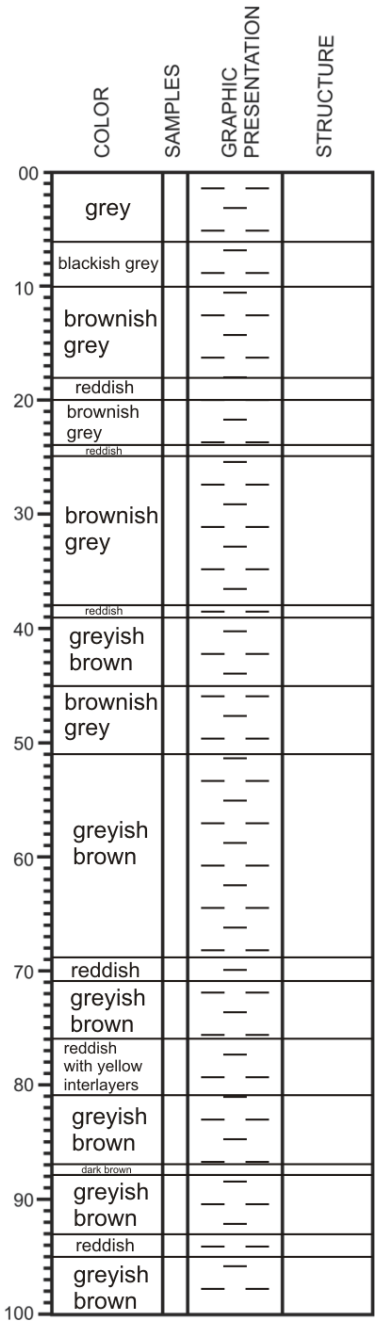

with yellowish interlayer

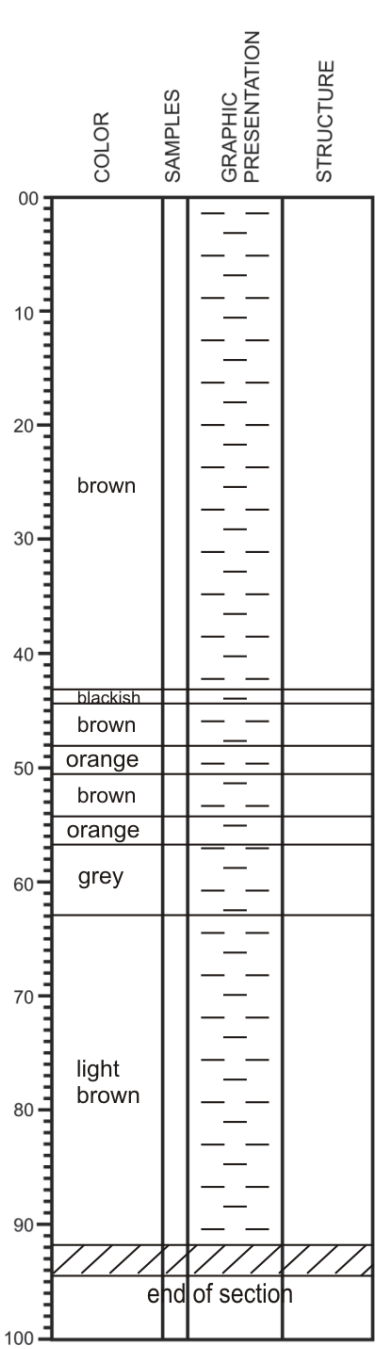

VISUAL CORE DESCRIPTION

Cruise	Station
PS86	079
Section Number	Observer
1	A. Türke

SECTION DESCRIPTION

Die **Berichte zur Polar- und Meeresforschung** (ISSN 1866-3192) werden beginnend mit dem Band 569 (2008) als Open-Access-Publikation herausgegeben. Ein Verzeichnis aller Bände einschließlich der Druckausgaben (ISSN 1618-3193, Band 377-568, von 2000 bis 2008) sowie der früheren **Berichte zur Polarforschung** (ISSN 0176-5027, Band 1-376, von 1981 bis 2000) befindet sich im electronic Publication Information Center **(ePIC)** des Alfred-Wegener-Instituts, Helmholtz-Zentrum für Polar- und Meeresforschung (AWI); see http://epic.awi.de. Durch Auswahl “Reports on Polar- and Marine Research“ (via “browse”/”type”) wird eine Liste der Publikationen, sortiert nach Bandnummer, innerhalb der absteigenden chronologischen Reihenfolge der Jahrgänge mit Verweis auf das jeweilige pdf-Symbol zum Herunterladen angezeigt.

The **Reports on Polar and Marine Research** (ISSN 1866-3192) are available as open access publications since 2008. A table of all volumes including the printed issues (ISSN 1618-3193, Vol. 1-376, from 2000 until 2008), as well as the earlier **Reports on Polar Research** (ISSN 0176-5027, Vol. 1-376, from 1981 until 2000) is provided by the electronic Publication Information Center **(ePIC)** of the Alfred Wegener Institute, Helmholtz Centre for Polar and Marine Research (AWI); see URL http://epic.awi.de. To generate a list of all Reports, use the URL http://epic.awi.de and select “browse”/ ”type” to browse ”Reports on Polar and Marine Research”. A chronological list in declining order will be presented, and pdf-icons displayed for downloading.

Zuletzt erschienene Ausgaben:

Recently published issues:

685 (2015) The Expedition PS86 of the Research Vessel POLARSTERN to the Arctic Ocean in 2014, edited by Antje Boetius

684 (2015) Russian-German Cooperation SYSTEM LAPTEV SEA: The Expedition Lena 2012, edited by Thomas Opel

683 (2014) The Expedition PS83 of the Research Vessel POLARSTERN to the Atlantic Ocean in 2014, edited by Hartwig Deneke

682 (2014) Handschriftliche Bemerkungen in Alfred Wegeners Exemplar von: Die Entstehung der Kontinente und Ozeane, 1. Auflage 1915, herausgegeben von Reinhard A. Krause

681 (2014) Und sie bewegen sich doch …Alfred Wegener (1880 – 1930): 100 Jahre Theorie der Kontinentverschiebung – eine Reflexion, von Reinhard A. Krause

680 (2014) The Expedition PS82 of the Research Vessel POLARSTERN to the southern Weddell Sea in 2013/2014, edited by Rainer Knust and Michael Schröder

679 (2014) The Expedition of the Research Vessel ‘Polarstern’ to the Antarctic in 2013 (ANT-XXIX/6), edited by Peter Lemke

678 (2014) Effects of cold glacier ice crystal anisotropy on seismic data, by Anja Diez

677 (2014) The Expedition of the Research Vessel “Sonne” to the Mozambique Ridge in 2014 (SO232), edited by Gabriele Uenzelmann-Neben

676 (2014) The Expedition of the Research Vessel “Sonne” to the Mozambique Basin in 2014 (SO230), edited by Wilfried Jokat

675 (2014) Polarforschung und Wissenschaftsutopien: Dargestellt und kommentiert am Beispiel von zehn Romanen aus der Zeit von 1831 bis 1934, von Reinhard A. Krause

ALFRED-WEGENER-INSTITUT
HELMHOLTZ-ZENTRUM FÜR POLAR-
UND MEERESFORSCHUNG

BREMERHAVEN

Am Handelshafen 12
27570 Bremerhaven
Telefon 0471 4831-0
Telefax 0471 4831-1149
www.awi.de

HELMHOLTZ
GEMEINSCHAFT